GEOLOGY AND METALLOGENY OF NORTH-CENTRAL NEWFOUNDLAND AND THE LITTLE DEER VMS DEPOSIT: AN INTRODUCTION AND OVERVIEW

HELENA CECILIA TOMAN

Abstract

The Little Deer deposit, Springdale Peninsula, north-central Newfoundland, is a Cyprus-type volcanogenic massive sulfide (VMS) deposit hosted by mafic volcanic rocks of the ophiolitic Late Cambrian (~505 Ma) Lushs Bight Group. The deposit has been a past-producer (Cu) and is currently the focus of extensive exploration, thereby providing a new opportunity to study the Little Deer deposit and to obtain a better understanding of ophiolite-hosted VMS mineralization in the northern Appalachians.

The Little Deer deposit consists of a stockwork that is composed primarily of disseminated and stringer-style mineralization with occasional semi-massive to massive sulfide horizons. Mineralization is dominated by chalcopyrite, pyrrhotite and pyrite with minor sphalerite and cobaltite. Native tellurium, bismuth/mercury/silver/nickel and lead tellurides, electrum, galena, selenium-bearing galena, and native arsenic are present as trace phases. The dominance of chalcopyrite-pyrrhotite-(± pyrite) mineralization throughout the deposit suggests that Little Deer formed from low pH (~2-4), low oxygen fugacity (~ -40 to -45), and high temperature (>300°C) fluids, typical of a mature VMS system.

The low abundance of trace phases at Little Deer and their textural association to the main sulfide components (which are void of enrichment in these trace phases), suggests that trace phases formed via annealing ("sweating") out of the main sulfides during post-VMS deformation and greenschist metamorphism.

On a global scale, the mineralogy, mineral assemblages and mineralization styles at Little Deer are similar to the massive sulfide deposits of Cyprus; the Italian Apennine deposits; and the Norwegian Caledonides. On a regional scale, *i.e.,* in

Newfoundland, Little Deer mineralization is similar to ophiolitic VMS deposits at Betts Cove, Tilt Cove, Colchester, Little Bay and Whalesback.

In situ sulfur isotope signatures for sulfide minerals at Little Deer range from $\delta^{34}S$ = -5.6‰ to +15.2‰, with values for chalcopyrite ranging from 0.6‰ to 10.5‰ (average: 3.8‰); pyrrhotite from -0.3‰ to +6.0‰ (average: 3.5‰); and pyrite from -5.6‰ to +15.2‰ (average: 4.3‰). A comparison between measured $\delta^{34}S$-values and calculated $\delta^{34}S$-values for thermochemical sulfate reduction of Late Cambrian seawater sulfate, suggests that Little Deer sulfur was primarily derived via thermochemical sulfate reduction, with or without an input of leached igneous sulfur from the surrounding basaltic/ultramafic rocks. Overall, the $\delta^{34}S$-values obtained for Little Deer are within ranges documented for Late Cambrian VMS deposits globally; this suggests that thermochemical sulfate reduction was an important global mechanism for the formation of reduced sulfur in Late Cambrian VMS deposits.

Acknowledgements

I thank my supervisor Dr. Stephen Piercey for offering me the opportunity of undertaking this MSc. Dr. Piercey's (and MUN's) policy of actively recruiting globally is in the best academic tradition. I am very appreciative of the opportunity he has afforded me of experiencing life in Newfoundland and of gaining insights into its mining industry. I found my supervisor to be a passionate geologist and a dedicated teacher.

Cornerstone Capital Resources, Thundermin Resources and an NSERC Collaborative Research and Development (CRD) grant (to Piercey) provided the funding for my study and I am glad to have this opportunity to record my gratitude to them. Additional funding was provided by an NSERC Discovery Grant and the NSERC-Altius Industrial Research Chair in Mineral Deposits (supported by NSERC, Altius Resources Inc., and the Research and Development Corporation of Newfoundland and Labrador) to Piercey.

Terry Brace, Andrew Hussey, Brad Dyke, Brent Thomas, and Steve Tsang are thanked for their discussions and logistical support. I should also like to record my gratitude to my thesis committee members: Dr. Graham Layne and Dr. Derek Wilton from whose edits this thesis has greatly benefited.

On a personal level I want to thank my family for their encouragement to 'grasp my chances' and for their love and support throughout. I will always be grateful to CYAN and MUNCC whose fellowship has been a social and emotional 'anchor' to me while undertaking my MSc. here in Newfoundland.

Table of Contents

List of Tables

Chapter 2

List of Figures

Chapter 1

Chapter 2

List of Abbreviations

AAT:	Annieopsquotch Accretionary Tract
apfu:	atoms per formula unit
Arg:	Argillite
BBL:	Baie Verte Brompton Line
BOI:	Bay of Islands
Boul:	Boulangerite
Bour:	Bournite
BVOT:	Baie Verte Oceanic Tract
Carb:	Carbonate
Ccp:	Chalcopyrite
CDT:	Canyon Diablo Troilite.
CF:	Cabot Fault
Chl:	Chlorite
CMB:	Central Mobile Belt
Cob:	Cobaltite
CP:	Coy Pond Complex
CREAIT-NETWORK:	Core Research Equipment and Instrument Training Network
DBL:	Dog Bay Line
Dom:	Dominated
EBSD:	Electron backscatter diffraction
EDX:	Energy dispersive X-ray spectrometry
EPMA:	Electron microprobe analyzer
EMW:	Elemental Molecular Weight

Flow:	Flow
GBF:	Green Bay Fault
Gn:	Galena
GRUB:	Gander River Ultramafic Belt
Hm:	Hematite
ICP-ES:	Inductively coupled plasma emission spectroscopy
ICP-MS:	Inductively coupled plasma mass spectroscopy
Int:	Intrusion
LBOT:	Lushs Bight Oceanic Tract
LCF:	Lobster Cove Fault
LR:	Long Range
LRF:	Lloyds River Fault
L. Tuff:	Lapilli Tuff
MDL:	Minimum Detection Limit
MF:	Mineral Formula
Mgt:	Magnetite
MLA:	Mineral liberation analysis
Mn:	Manganese
MP:	Molecular Proportions
MP (total):	Molecular Proportions Total
pH-fO_2-T:	pH-oxygen fugacity-temperature
Po:	Pyrrhotite
PP:	Pipestone Pond Complex
ppm:	parts per million

Py:	Pyrite
Py por:	Pyrite porphyroblasts
QA/QC:	Quality Assurance/Quality Control
Qtz:	Quartz
RIL:	Red Indian Line
SA:	St. Anthony
SEM:	Scanning electron microscopy
Seri:	Sericite
SIMS:	Secondary ion mass spectrometry
Sp:	Sphalerite
Sulf:	Massive sulfide
Tet:	Tetrahedrite
TP:	Tally Pond Belt;
TU:	Tulks Volcanic Belt
Tuff B.:	Tuff Breccia
VA:	Victoria Arc
VMS:	Volcanogenic massive sulfide
WB:	Wild Bight Group
wt (%):	weight percent

List of Appendices

Appendix A

Chapter 1

An Overview of the Geology and Metallogeny of north-central Newfoundland and the Little Deer VMS deposit.

[1.1] Introduction

Since its discovery in 1952, little modern documentation of the geology and mineralogy of the Little Deer volcanogenic massive sulfide (VMS) deposit of north-central Newfoundland has been undertaken. By utilizing field, petrographic, geochemical and isotopic data, this project attempts to provide a coherent understanding of the mineralogy, mineral assemblages, mineral textures, mineralization styles and metal zoning in the Little Deer VMS deposit. Sulfur isotopes are applied as isotopic tracers to provide clarification regarding sulfur sources at Little Deer. Using sulfur isotopes, together with bulk rock geochemical data and electron microprobe analysis (EPMA), this thesis provides information on the physicochemical controls (pH-$fO2$-T) and genesis of the Little Deer VMS system.

The overall objective of the project is to contribute to a better local and global understanding of the genesis of Cyprus-type (mafic-dominated) VMS systems.

[1.2] Geological Overview of Newfoundland

The Newfoundland Appalachians are separated into four tectono-stratigraphic zones and their associated subzones based on their differing stratigraphy, structure, fauna and metallogeny (Williams, 1979; Williams *et al.*, 1988; Swinden, 1991; Piercey, 2007). From west to east these are: the Humber; Dunnage (subzones: Notre Dame and Exploits); Gander; and Avalon (Williams, 1979, 1995; Williams *et al.*, 1988). Together these zones record a series of Early Paleozoic [600 – 300 Ma (Williams and Grant, 1988)] orogenic episodes (the Taconic, Penobscot, Salinic, Acadian and Neoacadian orogenies) that culminated in the formation of the Canadian Appalachians (Williams, 1979; van Staal, 2007; van Staal and Barr, in press). The development of the Appalachian Orogen records the opening and subsequent closure

of the Iapetus (Precambrian to Early Paleozoic) and Rheic (Early Ordovician) Oceans (van Staal, 2007; van Staal and Barr, in press).

[1.3] Geological Setting of the Little Deer VMS Deposit

The Little Deer VMS deposit is located within the Dunnage Zone (Figs. 1.1-1.3). Collectively, this zone preserves an assemblage of accreted late Cambrian – Middle Ordovician island arcs, extensional arc and back-arc terrains that formed at the margins of, and within, the Iapetus Ocean (Norman and Strong, 1975; Kidd, 1977; Williams *et al.*, 1988; Swinden, 1996; van Staal, 2007). The Dunnage Zone is further subdivided into the Notre Dame (peri-Laurentian) and Exploits (peri-Gondwanan) subzones (Fig. 1.1) (Williams *et al.*, 1988). The Little Deer VMS deposit lies within the Notre Dame subzone (Kean *et al.*, 1995).

The Notre Dame subzone is bound to the west by the Baie Verte-Bromton Line and to the east by the Red Indian Line (Fig. 1.1), and preserves three Cambrian-Middle Ordovician obducted oceanic terrains: 1) the Lushs Bight Oceanic Tract (LBOT, 510 – 501 Ma); 2) the Baie Verte Oceanic Tract (BVOT, ~489-477 Ma) and 3) the Annieopsquotch Accretionary Tract (~481–460 Ma), as well as the Notre Dame Arc (488–435 Ma) (Dunning and Krogh, 1985; Cawood *et al.*, 1996; van Staal, 2007; van Staal *et al.*, 2007; van Staal and Barr, in press). Together these document a protracted history of suprasubduction-zone formation, obduction, and subsequent magmatic overprinting occurring as a result of the onset of the Taconic Orogeny (van Staal, 2007; van Staal *et al.*, 2007).

Three principal VMS mineralization episodes have been identified within the Notre Dame subzone:

1) VMS mineralization within the highly chloritized, highly sheared, pillow lavas of the Late Cambrian Lushs Bight (associated with suprasubduction zone rifting) and Sleepy Cove (associated with arc rifting) groups. Examples of VMS occurrences associated with this mineralization event include: Whalesback, Little Bay and Little Deer (Swinden and Kean, 1988; Swinden, 1996; Kean *et al.*, 1995);

2) VMS mineralization in the volcanic sections of Lower Ordovician ophiolites - formed during suprasubduction zone rifting. Examples of VMS occurrences associated with this mineralization event include: Tilt Cove and the deposits of the Rambler Camp (Tuach and Kennedy, 1978; Tuach, 1988; Swinden, 1996); and

3) VMS mineralization associated with a mature Lower Ordovician island arc system. All VMS accumulations within this mineralization episode are hosted by rhyolite and/or calc alkalic lithologies. Examples of VMS occurrences associated with this mineralization event include: Buchans, Gullbridge and Pilley's Island (Swinden and Kean, 1988; Swinden, 1996).

The Little Deer VMS deposit is hosted in the Lushs Bight Group of the LBOT (Figs. 1.1 - 1.4). The Lushs Bight Group consists of an obducted island arc ophiolitic sequence containing pillow basalts, sheeted dykes, gabbro and ultramafic rocks (Kean *et al.*, 1995; van Staal, 2007) (Fig. 1.4). The deposit is situated within a chlorite-schist zone (trends 065°, dips 70 - 75 ° SE) hosted within island arc tholeiitic pillow lavas of the Lushs Bight Group; the chlorite-schist zone is 1050m in length and 60m in width (Papezik and Fleming, 1967; Fleming, 1970; West, 1972; Kean *et al.*, 1995). The basaltic host rocks for Little Deer have undergone varying degrees of chlorite and sericite alteration (West, 1972; Kean *et al.*, 1995). West (1972) suggested that the

Little Deer deposit lies on the southern limb of a major anticline, close to the axial hinge.

The Lushs Bight Group is host to numerous other VMS deposits (Fig. 1.4), such as the Whalesback, Colchester, McNeily, Little Bay, Lady Pond, and Miles Cove (Kean *et al.*, 1995; Swinden and Dunsworth, 1995 and van Staal, 2007). Mineralization is almost exclusively associated with chlorite-schist (shear) zones developed within tholeiitic pillow lavas (Kean and Evans, 1988; Kean *et al.*, 1995). It is interpreted that the intimate relationship between VMS mineralization and shear zones is the result of the chlorite alteration zones being remobilized as thrust faults during subsequent tectonism (Kean *et al.*, 1995).

[1.4] Classification of VMS Deposits

Volcanogenic massive sulfide deposits (VMS) form in extensional settings coinciding with elevated heat flow (e.g., ocean ridge spreading centers; fore-arc and back-arc environments) (Large 1977; Franklin *et al.*, 1981; Ohmoto *et al.*, 1983, Large, 1992; Ohmoto, 1996; Franklin 2005; Robb, 2005; Galley *et al.*, 2007). The presence of a heat source (e.g., subvolcanic intrusions; synvolcanic dyke swarms; upwelling asthenosphere, etc.) gives rise to cool (2°C), alkaline (pH~ 7-8), oxidizing, sulfate-rich (SO_4) and metal deficient seawater being convectively circulated through host lithology(ies) and subsequently transformed into hot (>300°C), acidic (pH ~4-6), reduced, H_2S-rich and metal-rich (Fe, Zn, Cu) hydrothermal fluids (Large 1977; Franklin *et al.*, 1981; Ohmoto *et al.*, 1983, Large, 1992; Ohmoto, 1996; Franklin 2005; Robb, 2005; Galley *et al.*, 2007). These hydrothermal fluids cool and mix with seawater resulting in the precipitation of mineralization at, or below the sea floor to form polymetallic (Zn, Cu, Pb, Ag, Au) massive sulfide lenses or sheets (Fig. 1.5)

(Franklin *et al.*, 1981, 2005; Lydon, 1988; Large, 1992, Ohmoto, 1996; Galley *et al.*, 2007).

Volcanogenic massive sulfide deposits have been divided into six types depending upon their lithology and tectonic setting (Fig. 1.5) (Barrie and Hannington, 1999; Franklin *et al.*, 2005; Galley *et al.*, 2007):

1) *Bimodal-mafic:* host rocks are ≥ 75% mafic rocks; however, there can be up to 25% of felsic lithologies present, often hosting the deposits. These deposits are typically Cu-Zn-(Au-Ag)-rich, and formed within incipient-rifted, intra-oceanic arcs (e.g., Rambler-Ming, Flin-Flon and Noranda);

2) *Mafic:* these deposits are hosted in basalt-dominated ophiolite-like assemblages. They are Cu-(Zn-Au)-rich and typically formed in fore-arc and back-arcs environments (e.g., Cyprus, Oman);

3) *Siliciclastic-mafic:* these deposits are hosted in a combination of mafic and/or ultramafic rocks and sedimentary rocks (e.g., terrigenous and/or volcaniclastic). They are Cu-(Zn,Co,Au)-rich and formed in mature back-arc, accreted-arc and juvenile-arc tectonic settings (e.g., Windy Craggy, Besshi);

4) *Bimodal-felsic:* these deposits are hosted in felsic volcanic dominated environments (35-70%) with lesser mafic (20-50%) and terrigenous sedimentary rocks (~10%). They are Zn-Pb-Cu-(Au-Ag)-rich and formed in continental margin arcs and back-arc environments (e.g., Kuroko, Hellyer, Buchans);

5) *Siliciclastic-felsic:* these deposits are hosted in siliciclastic-dominated strata (~80%) with lesser felsic (~25%) and mafic (~10%) rocks. They are Zn-Pb-Cu-(Ag,Au)-rich and formed within mature epicontinental back-arc environments (e.g., Bathurst, Wolverine); and

6) *High-sulfidation-bimodal-felsic:* these deposits are VMS-epithermal hybrids with characteristics of both bimodal-felsic VMS deposits (including bimodal assemblages: felsic, mafic and terrigenous sedimentary rocks and Zn-Pb-enrichments) and epithermal Au deposit characteristics [Hg-Bi-Sb-As-Au-Ag-rich; high sulfidation mineral assemblages (e.g., enargite, sulfosalt-rich) and aluminous alteration] (Sillitoe *et al.*, 1996; Hannington *et al.*, 1999; Dube *et al.*, 2007). They typically form(ed) in fore-arc, back-arc, primitive-rifted arc and successor magmatic-arc environments. These deposits are considered to have developed within shallower water (i.e., <1500m depth) compared to typical VMS systems (e.g., Eskay Creek; Bousquet-LaRonde) (Sillitoe *et al.*, 1996; Hannington *et al.*, 1999; Dube *et al.*, 2007).

The Little Deer deposit is hosted by ophiolitic mafic rocks and has a simple, Cu-dominated sulfide mineralogy (e.g., chalcopyrite, pyrrhotite and pyrite). It is a classic Appalachian mafic (Cyprus-type) VMS deposit that formed within a primitive arc environment (Figs. 1.5 - 1.6) (Kean *et al.*, 1995).

[1.5] Exploration History of Little Deer

The following discussion on the location, history and mineralization of the Little Deer deposit summarizes the findings and understandings of West (1972), Kean *et al.*, (1995), Pressacco (2009, 2010) and Putrich *et al.*, (2011).

Location and History: The Little Deer VMS deposit is located 10 kilometers north of the town of Springdale, north-central Newfoundland and was discovered in 1952 by Falconbridge Nickel Mines Ltd.

In 1955 the British Newfoundland Exploration Company (BRINEX) undertook preliminary soil geochemistry surveys. From 1960-1963, BRINEX proceeded with detailed geological mapping; geochemical, magnetic and

electromagnetic surveying and a drill program consisting of thirty seven holes. From 1970-1972 BRINEX mined the property for Cu via access from the Whalesback mine located to the north of the deposit.

From 1973-1974 the deposit was mined for Cu by the Green Bay Mining Company. Mining ceased in 1974 due to low Cu prices. By 1974 a non-National Instrument 43-101 (NI 43-101) compliant reserve of 210,200 t of ore with a grade of 1.53% Cu were estimated (for elevations 245m above sea level).

Exploration recommenced in 1998 with Mutapa Copper and Cobalt Inc. conducting further drilling (12 holes) on the property. Although significant Cu mineralization was discovered outside the scope of the previous mined area, by 2000 a depressed Cu market ceased additional interest.

From 2007 to present, Little Deer has been a 50:50 joint venture between Thundermin Resources Inc. and Cornerstone Capital Resources Inc. Drilling and exploration on the property has established an updated NI 43-101 resource with indicated resources of 1,150,500 t at an average grade of 2.8% Cu and inferred resources of 3,748,000 t at an average grade of 2.13% Cu (Putrich *et al.*, 2011). To date, Cu mineralization has been established to a vertical depth of 1000 meters (below sea level) and a strike length of ~1050 meters.

[1.6] Mineralization at Little Deer

The Little Deer VMS deposit consists of a stockwork that is composed of sulfide-rich stringers and disseminations with minor massive and semi-massive sulfide horizons. Sulfide mineralization is dominated by chalcopyrite, pyrrhotite and pyrite, with minor sphalerite and cobaltite. Pressacco (2010) suggested that mineralization at Little Deer occurs in an en-echelon manner. This observation can be linked to West's

(1972) interpretation for the formation of the chlorite-schist zone, which he attributed to en-echelon faulting occurring along the subsidiary Little Deer fault.

[1.7] Thesis Objectives

Since its discovery in 1952, Little Deer has had a brief history of production (ceased in 1974) and a sporadic history of exploration, which is ongoing. However, very little work, particularly in the last 15 years, has been undertaken to document the geology and mineralogy of the Little Deer deposit (West, 1972; Kean *et al.*, 1995).

The main objectives of this thesis are as follows:

1) To understand the major, minor and trace mineralogy, mineral assemblages, mineral textures, mineralization styles and metal zones in the Little Deer deposit;

2) To establish the source(s) of sulfur (e.g., biogenic and/or marine, and/or magmatic) for sulfides at Little Deer via the study of their sulfur isotopic signatures;

3) To discuss the roles that metamorphism and deformation may have had upon sulfide mineralization at Little Deer;

4) To combine the geometry of mineralization with assay data to evaluate the metal zoning of mineralization within Little Deer [3D model construction using Target for ArcGIS (Edition 10.0)]; and

5) To establish an overall paragenesis for the Little Deer deposit.

[1.8] Analytical Methods

[1.8.1] Field Work

This project utilizes the observations from fieldwork undertaken by the author in June - July 2011. During this field period, the mineralized horizons of 30 diamond drill cores (taken from across the Little Deer deposit) were graphically logged to

document the mineralogy, mineral assemblages, mineral textures, mineralization styles and metal zoning in the Little Deer deposit (see Appendix A.1).

A total of 145 representative samples of Little Deer mineralization (mineral assemblages, textures and styles) and alteration phases were collected from 30 diamond drill cores (see Appendix Table A.1).

[1.8.2] Petrography

Of the 145 representative samples (see 1.8.1 above), 97 samples (from 30 diamond drill cores) of Little Deer mineralization were sent, in July 2011, to Vancouver Petrographics Ltd. to be made into polished thin sections.

These samples were examined using standard transmitted and reflected light petrography. Sulfide and oxide assemblages were documented together with the silicate (and carbonate) gangue minerals. Standard transmitted and reflected light petrography established the major and minor sulfide mineralogy, mineral assemblages, their associations and textures, and a preliminary paragenesis. Standard transmitted and reflected light petrography was carried out using a Nikon LV100POL polarizing microscope at Memorial University.

Of the 97 samples analyzed, 43 samples from 22 diamond drill cores were chosen for scanning electron microscopy (SEM). Sulfide assemblages, associations and textures established via standard transmitted and reflected light petrography were confirmed through SEM analysis. Scanning electron microscopy also established and identified the trace phases present within Little Deer together with their siting within the sulfide phases. Scanning electron microscopy analysis was undertaken using the FEI Quanta 400 environmental SEM. This was equipped with an energy dispersive X-ray (EDX) analytical system from Roëntec; an electron backscatter diffraction

(EBSD) system from HKL; and mineral liberation analysis (MLA) software from JKTech (University of Queensland Australia). The SEM was undertaken at the Core Research Equipment and Instrument Training Network (CREAIT-NETWORK), Bruneau Innovation Centre, Memorial University of Newfoundland (http://www.mun.ca/research/ocp/creait/maf/SEM.php).

[1.8.3] Bulk Rock Assay Data

Of the 145 representative samples (see 1.8.1 above), 22 representative samples of Little Deer mineralization, from 15 diamond drill cores, were sent to ALS Minerals for assay. The following procedures were requested for each sample: 1) standard sample logging; 2) sample preparation; 3) 48 element analysis with a four acid digestion (analytes requested: Ag, Al, As, Ba, Be, Bi, Ca, Cd, Ce, Co, Cr, Cs, Cu, Fe, Ga, Ge, Hf, In, K, La, Li, Mg, Mn, Mo, Na, Nb, Ni, P, Pb, Rb, Re, S, Sb, Sc, Se, Sn, Sr, Ta, Te, Th, Ti, Tl, U, V, W, Y, Zn, Zr) followed by 4) analysis via inductively coupled plasma emission spectroscopy (ICP-ES) for major elements and finally, 5) inductively coupled plasma mass spectrometry (ICP-MS) for minor and trace elements. This obtained a full complement of metals for the whole rock sulfides allowing documentation of the metal and chemical compositions of the Little Deer ores.

[1.8.4] Mineral Chemistry

Of the 145 representative samples (see 1.8.1 above), 9 representative samples from 8 diamond drill cores were analyzed via electron microprobe analysis (EPMA) at the University of Toronto. This allowed documentation of the mineral chemistry and phases present at Little Deer. Analyses were undertaken using a Cameca SX50/51 equipped with 3 tunable wavelength dispersive spectrometers. The data were

processed using Analytical and Automation Software, the Enterprise version of 'Probe for Windows' written by J. Donovan and marketed by Advanced Microbeam.

[1.8.5] Sulfur Isotopes

Sulfur isotope compositions for chalcopyrite, pyrrhotite and pyrite in their various associations and assemblages were obtained for eight samples from 6 diamond drill holes in situ via the use of secondary ion mass spectroscopy (SIMS). The sulfur isotope signatures obtained have helped to indicate a likely source for the sulfur (e.g., biogenic and/or marine, and/or magmatic) within the Little Deer deposit. Secondary ion mass spectroscopy analysis was undertaken at the Core Research Equipment and Instrument Training Network (CREAIT-NETWORK), Bruneau Innovation Centre, Memorial University of Newfoundland (http://www.mun.ca/research/ocp/creait/maf/SIMS.php).

[1.9] Thesis Presentation

This thesis consists of an introductory chapter (Chapter 1), with Chapter 2 representing a journal article that will be submitted for a peer reviewed publication. Chapter 3 is a summary of the key results and conclusions established in Chapter 2 together with recommendations for further research. The appendices of the thesis lists all samples analyzed for Little Deer (standard transmitted and reflected light petrography and SEM analysis); all graphic logs for Little Deer; the conversion calculations and mineral formula calculations for microprobe results.

[1.10] Co-authorship Statement

The identification and design of this project was constructed by Dr. Stephen Piercey, Terry Brace, John Heslop, and Andrew Hussey. Practical research, including field work, standard transmitted and reflected light petrography, SEM, EPMA and

SIMS sample preparation were undertaken by the author. Secondary ion mass spectrometry analyses was conducted by Glenn Piercey; SIMS analytical methods are from Layne (unpublished). Data analysis and interpretation was undertaken by the author. The principle editor for this thesis is Dr. Stephen Piercey, with contributions from Dr. Graham Layne and Dr Derek Wilton.

[1.11] References

Barrie, C.T. and Hannington, M.D, 1999. Classification of volcanic-associated massive sulfide deposits based on host-rock compositions, Reviews in Economic Geology, v.8, p. 1-11.

Cawood, P.A., van Gool, J.A.M., and Dunning, G.R., 1996. Geological development of eastern Humber and western Dunnage zones; Corner Brook--Glover Island region, Newfoundland: Canadian Journal of Earth Sciences, v. 33, p. 182–198.

Dube, B., Gosselin, P., Mercier-Langevin, P., Hannington, M., Galley, A., 2007. Gold-rich volcanic massive sulphide deposits. In: Goodfellow, W.D. (Ed.), Mineral Deposits of Canada: A Synthesis of Major Deposit-Types. District Metallogeny, the Evolution of Geological Provinces and Exploration Methods: Geological Association of Canada, Mineral Deposits Division, Special Publication, v.5, p. 75–94.

Dunning, G.R., and Krogh, T.E., 1985. Geochronology of ophiolites of the Newfoundland Appalachians: Canadian Journal of Earth Sciences, v. 22, p. 1659–1670.

Fleming, J.M., 1970. Petrology of the volcanic rocks of the Whalesback area, Springdale Peninsula, Newfoundland. Unpublished M.Sc. thesis, Memorial University of Newfoundland, St. John's, p. 1-107.

Franklin, J.M., Lydon, J.W., and Sangster, D.F., 1981. Volcanic-associated massive sulphide deposits. Economic Geology, 75th Anniversary Volume, p. 485–627.

Franklin, J.M., Gibson, H.L., Jonasson, I.R., and Galley, A.G., 2005. Volcanogenic massive sulphide deposits. Economic Geology, 100th Anniversary Volume, p. 523–560.

Galley, A.G., Hannington, M., and Jonasson, I., 2007. Volcanogenic massive sulphide deposits, in Goodfellow, W. D., ed., Mineral Deposits of Canada: A Synthesis of Major Deposit types, District Metallogeny, the Evolution of Geological Provinces, and Exploration Methods, Special Publication 5, Mineral Deposits Division, Geological Association of Canada, p.141-161.

Hannington, M.D., Poulsen, K.H., Thompson, J.F.H., and Sillitoe, R.H., 1999. Volcanogenic gold in the massive sulfide environment, Reviews in Economic Geology, v.8, p. 324-356.

Hutchinson, R.W., and Searle, D.L., 1971. Stratabound pyrite deposits in Cyprus and relation to other sulfide ores. Mining Geology Society of Japan, Special Publication 3, p. 198-2005.

Kean, B. F., and Evans, D.T.W., 1988. Mineral deposits of the Lushs Bight Group, in Swinden, H.S., and Kean, B. F., eds., The Volcanogenic Sulphide Districts of Central Newfoundland, A guidebook and reference manual for volcanogenic sulphide deposits in the early Paleozoic oceanic volcanic

terranes of central Newfoundland: St. John's, NL, Canada, Mineral Deposits Division, Geological Association of Canada, p. 80-90.

Kean, B.F., Evans, D.T.W., and Jenner, G. A., 1995. Geology and Mineralization of the Lushs Bight Group, Report 95-02: St. John's, NL, Canada, Geological Survey of Newfoundland and Labrador, Newfoundland Department of Natural Resources, p. 1-204.

Kidd, W. S. F., 1977. The Baie Verte Lineament, Newfoundland: Ophiolite complex floor and mafic volcanic fill of a small Ordovician marginal basin. In Island arcs, deep sea trenches and back-arc basins. Edited by M. Talwani, and W. C. Pitman. American Geophysical Union, Maurice Ewing Series, v.1, p. 407-418.

Large, R.R., 1977. Chemical evolution and zonation of massive sulphide deposits in volcanic terrains: Economic Geology, v. 72, p. 549-572.

Large, R.R., 1992. Australian Volcanic-Hosted Massive Sulfide Deposits: Features, Styles, and Genetic Models. Economic Geology, v. 87, p. 471-510.

Lydon, J.W., 1984. Volcanogenic massive sulphide deposits Part 1: A descriptive model: Geoscience Canada, v. 11, p. 195-202.

Lydon, J. W., 1988. Ore deposit models #14: Volcanogenic massive sulfide deposits, Part 2: Genetic models. Geosci. Canada, v.15, p. 43–65.

Memorial University of Newfoundland. The Scanning Electron Microscope (SEM). [Online] Available at: http://www.mun.ca/research/ocp/creait/maf/SEM.php. [Accessed on: 26.03.2012]

Memorial University of Newfoundland. The Secondary Ion Mass Spectrometry (SIMS Laboratory). [Online] Available at:

http://www.mun.ca/research/ocp/creait/maf/SIMS.php [Accessed on: 26.03.2012]

Norman, R.E., and Strong, D.F., 1975. The geology and geochemistry of ophiolitic rocks exposed at Mings Bight, Newfoundland. Canadian Journal of Earth Sciences, v. 12, p. 777-797.

Ohmoto, H., Tanimura, S., Date, J., and Takahashi, T., 1983. Geologic setting of the kuroko deposits, Japan: Part I. Geologic history of the Green tuff region. Part II. Stratigraphy and structure of the Hokuroku district. Part III. Submarine calderas and kuroko genesis: Economic Geology Monograph 5, p. 9–54.

Ohmoto, H., 1996. Formation of volcanogenic massive sulfide deposits: The Kuroko perspective. Ore Geology Reviews, v. 10, p. 135-177.

Papezik, V.S., and Fleming, J.M., 1967. Basic volcanic rocks of the Whalesback area, Newfoundland. Geological Survey of Canada, Special Paper 4, p. 181-192

Piercey, S.J., 2007. Volcanic Massive Sulfide (VMS) of the Newfoundland Appalachains: An Overview of their Setting, Classification, Grade-Tonnage Data and Unresolved Questions, Newfoundland and Labrador Department of Natural Resources Geological Survey, Report 07-1, p.169-178.

Pressacco, R., 2009. Technical Report on the Initial Mineral Resource Estimate for the Little Deer Cu Deposit, Newfoundland, Canada for Thundermin Resources Inc. and Cornerstone Capital Resources Inc., National Instrument 43-101 Technical Report: Toronto, ON, Canada, National Instrument 43-101 Technical Report, p. 1-86.

Pressacco, R., 2010. Memorandum: Mineral Resource Update for the Little Deer Project undertaken by Scott Wilson Roscoe Postle Associates Inc. for

Thundermin Resources Inc. and Cornerstone Capital Resources Inc., National Instrument 43-101 Memorandum: Toronto, ON, Canada, p. 1-26.

Putrich, E., Ewert, W., Rodgers, K., Pearson, J. L., Orava, D., and Hayden, A., 2011. Technical Report and Preliminary Economic Assessment of the Little Deer Copper Deposit, Newfoundland, Canada for Cornerstone Capital Resources and Thundermin Resources, National Instrument 43-101 Technical Report: Toronto, ON, Canada, National Instrument 43-101 Technical Report, p. 86.

Robb, L., 2005. Introduction to ore-forming processes. Blackwell, Oxford, p. 180.

Sillitoe, R.H., Hannington, M.D., Thompson, J.F.H., 1996. High sulfidation deposits in the volcanogenic massive sulfide environment, Economic Geology, p. 91 - 204.

Swinden, H. S., and Kean, B. F., 1988. Eds. Volcanogenic sulphide districts of central Newfoundland: St. John's, Newfoundland, Geological Association of Canada, Mineral Deposits Division, (First Edition), p.1-238.

Swinden, H.S., and Dunsworth, S.M., 1995. Metallogeny, in Williams, H., ed., The Appalachian/Caledonian Orogen: Canada and Greenland: Geological Survey of Canada, Geology of Canada, No. 6, p. 681-814.

Swinden, H.S., 1996. The Application of Volcanic Geochemistry to the Metallogeny of Volcanic-Hosted Sulfide Deposits in Central Newfoundland In Wyman, D.A., ed., Trace Element Geochemistry of Volcanic Rocks: Applications for Massive Sulphide Exploration: Geological Association of Canada, Short Course Notes, v. 12, p. 329-358.

Tuach J., and Kennedy MJ., 1978. The geologic setting of the Ming and other sulfide deposits, Consolidated Rambler mines, northwest Newfoundland. Econ Geol. v.73, p.192-206.

Tuach, J., 1988. Geology and sulphide mineralization in the Pacquet Harbour Group, in Swinden, H. S., and Kean, B. F., eds., The volcanogenic sulphide districts of central Newfoundland, Geological Association of Canada, p.49-53.

University of Toronto. Microprobe Lab. [Online] Available at: http://www.geology.utoronto.ca/facilities/electron-probe-x-ray-microanalyzer-empa [Accessed 26.03.2012]

van Staal, C.R., Whalen, J.B., McNicoll, V.J., Pehrsson, S., Lissenberg, C.J., Zagorevski, A., van Breemen, O., and Jenner, G.A., 2007. The Notre Dame arc and the Taconic orogeny in Newfoundland, in Hatcher, R.D., Jr., Carlson, M.P., McBride, J.M., and Martínez Catalán, J.R., eds., 4-D Framework of Continental Crust: Geological Society of America Memoir 200, p. 511–552.

van Staal, C. R., 2007. Pre-Carboniferous tectonic evolution and metallogeny of the Canadian Appalachians, in Goodfellow, W. D., ed., Mineral Deposits of Canada: A Synthesis of Major Deposit-types, District Metallogeny, the Evolution of Geological Provinces, and Exploration Methods, Special Publication 5, Mineral Deposits Division, Geological Association of Canada, p. 793-818.

van Staal, C.R., and Barr, S.M. in press. Lithospheric architecture and tectonic evolution of the Canadian Appalachians. In Tectonic Styles in Canada Revisited: the LITHOPROBE perspective. Edited by J.A. Percival, F.A. Cook and R.M. Clowes. Geological Association of Canada, Special Paper 49.

West, J.M., 1972, Structure and ore-genesis; Little Deer Deposit, Whaleback Mine, Springdale, Newfoundland. Unpublished M.Sc. thesis, Queen's University, p.1-71

Williams, H., 1979. Appalachian Orogen in Canada. Canadian Journal of Earth Sciences, v. 16, p. 792-807.

Williams, H., Colman-Sadd, S.P., and Swinden H.S. 1988. Tectono-stratigraphic subdivisions of central Newfoundland. Geological Survey of Canada, Paper 88-1B, p. 91–98.

Williams, H., and Grant, A.C., 1998. Tectonic Assemblages, Atlantic Region, Canada: Geological Survey of Canada, Tectonic Assemblages, Atlantic Region, Canada, Open File 3657, scale: 1:3,000,000.

Williams, H., 1979. Appalachian Orogen in Canada. Canadian Journal of Earth Sciences, v. 16, p. 792-807.

Williams, H., 1995. Geology of the Appalachian-Caledonian Orogen in Canada and Greenland: Geological Survey of Canada, Geology of Canada No. 6, p. 944

Chapter 1 Figures

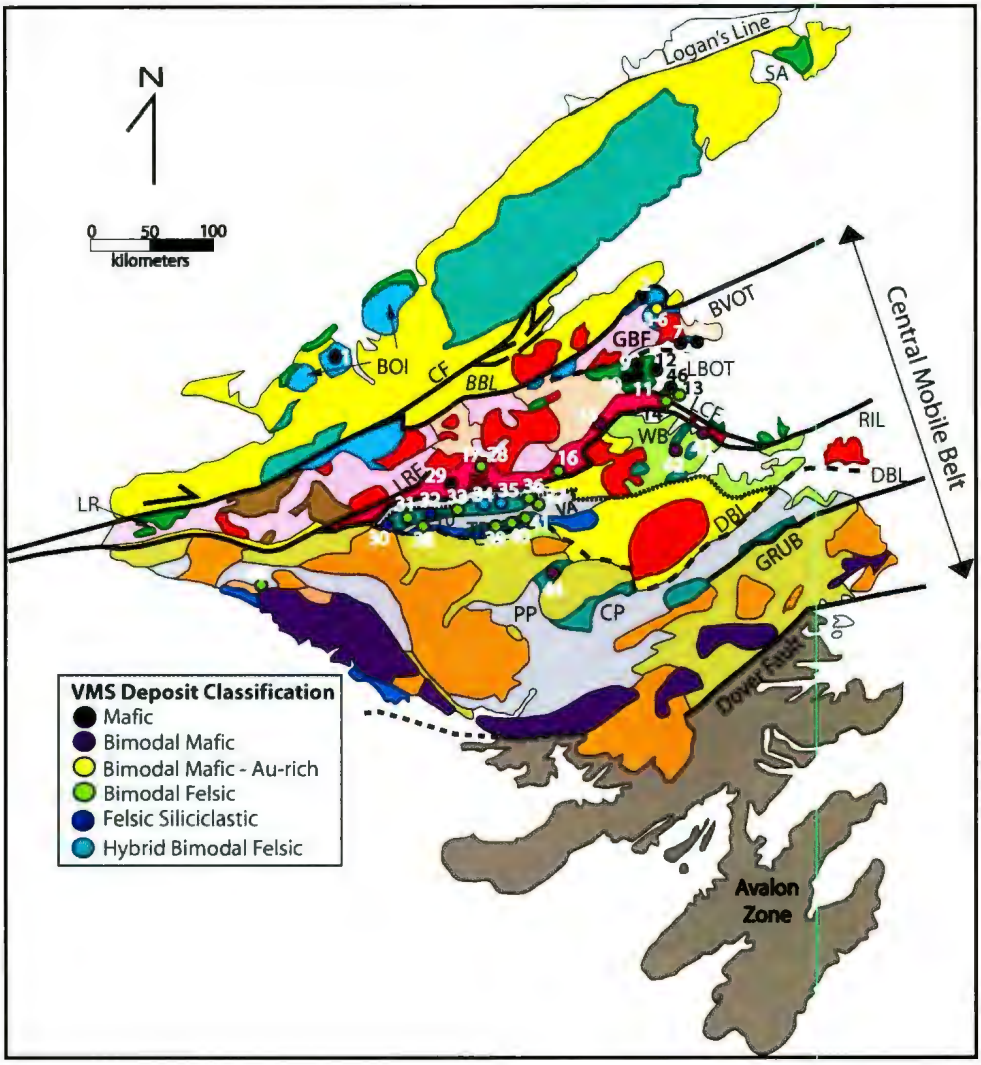

Figure 1.1: The tectonostratigraphic zones (and subzones), accretionary tracts and VMS deposits of the Newfoundland Appalachians. The Little Deer VMS deposit (# 10) is situated in the Notre Dame Subzone of the Dunnage Zone. Legend for map on page 22. Abbreviations: BBL - Baie Verte Brompton Line; BOI - Bay of Islands; BVOT - Baie Verte Oceanic Tract; CF - Cabot Fault; CP - Coy Pond Complex; DBL - Dog Bay Line; GBF - Green Bay Fault; GRUB - Gander River Ultramafic Belt; LBOT - Lushs Bight Oceanic Tract; LCF - Lobster Cove Fault; LR - Long Range; LRF - Lloyds River Fault; PP - Pipestone Pond Complex; RIL - Red Indian Line; SA - St. Anthony; TP - Tally Pond Belt; TU - Tulks Volcanic Belt; VA - Victoria Arc and WB - Wild Bight Group. Map Modified from van Staal (2007) and van Staal and Barr (in press). Volcanogenic massive sulfide (VMS) deposit classification from Piercey (2007), Hinchey (2011), and Piercey and Hinchey 2012).

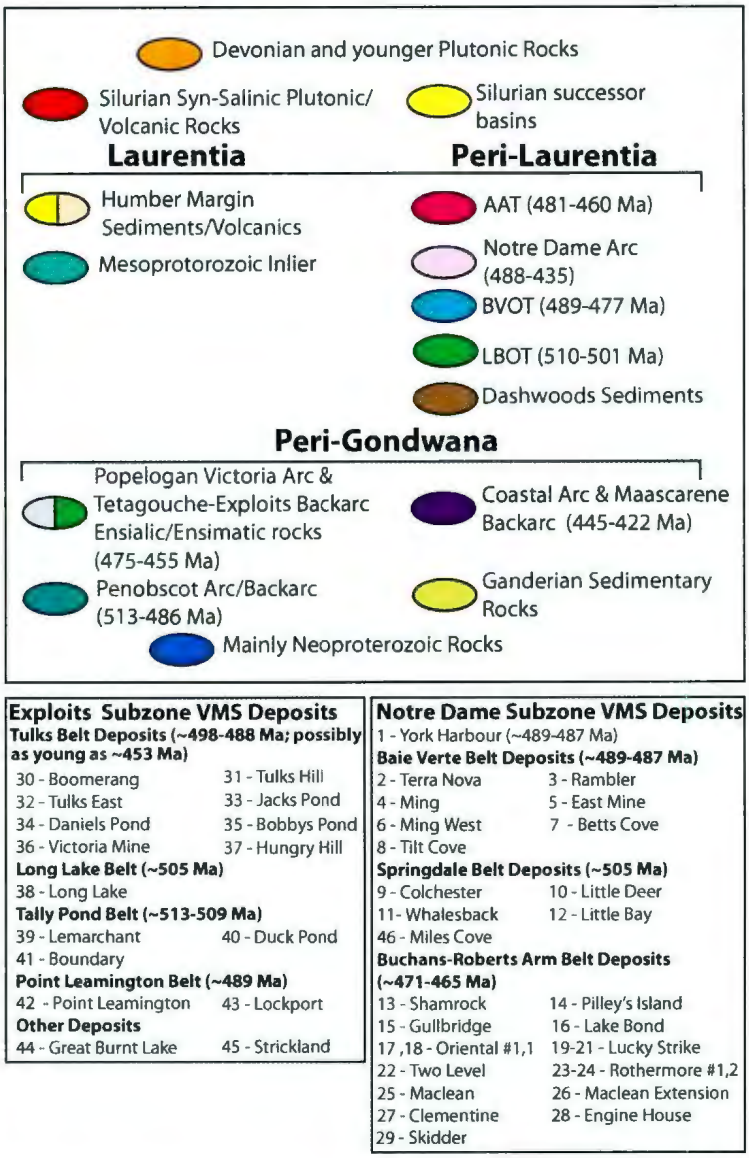

Exploits Subzone VMS Deposits

Tulks Belt Deposits (~498-488 Ma; possibly as young as ~453 Ma)

30 - Boomerang	31 - Tulks Hill
32 - Tulks East	33 - Jacks Pond
34 - Daniels Pond	35 - Bobbys Pond
36 - Victoria Mine	37 - Hungry Hill

Long Lake Belt (~505 Ma)

38 - Long Lake

Tally Pond Belt (~513-509 Ma)

39 - Lemarchant	40 - Duck Pond
41 - Boundary	

Point Leamington Belt (~489 Ma)

42 - Point Leamington	43 - Lockport

Other Deposits

44 - Great Burnt Lake	45 - Strickland

Notre Dame Subzone VMS Deposits

1 - York Harbour (~489-487 Ma)

Baie Verte Belt Deposits (~489-487 Ma)

2 - Terra Nova	3 - Rambler
4 - Ming	5 - East Mine
6 - Ming West	7 - Betts Cove
8 - Tilt Cove	

Springdale Belt Deposits (~505 Ma)

9 - Colchester	10 - Little Deer
11- Whalesback	12 - Little Bay
46 - Miles Cove	

Buchans-Roberts Arm Belt Deposits (~471-465 Ma)

13 - Shamrock	14 - Pilley's Island
15 - Gullbridge	16 - Lake Bond
17 ,18 - Oriental #1,1	19-21 - Lucky Strike
22 - Two Level	23-24 - Rothermore #1,2
25 - Maclean	26 - Maclean Extension
27 - Clementine	28 - Engine House
29 - Skidder	

Figure 1.1 cont: Legend for the tectonostratigraphic zones (and subzones), accretionary tracts and VMS deposits of the Newfoundland Appalachians. Volcanogenic massive sulfide (VMS) deposit classification from Piercey (2007), Hinchey (2011), and Piercey and Hinchey 2012).

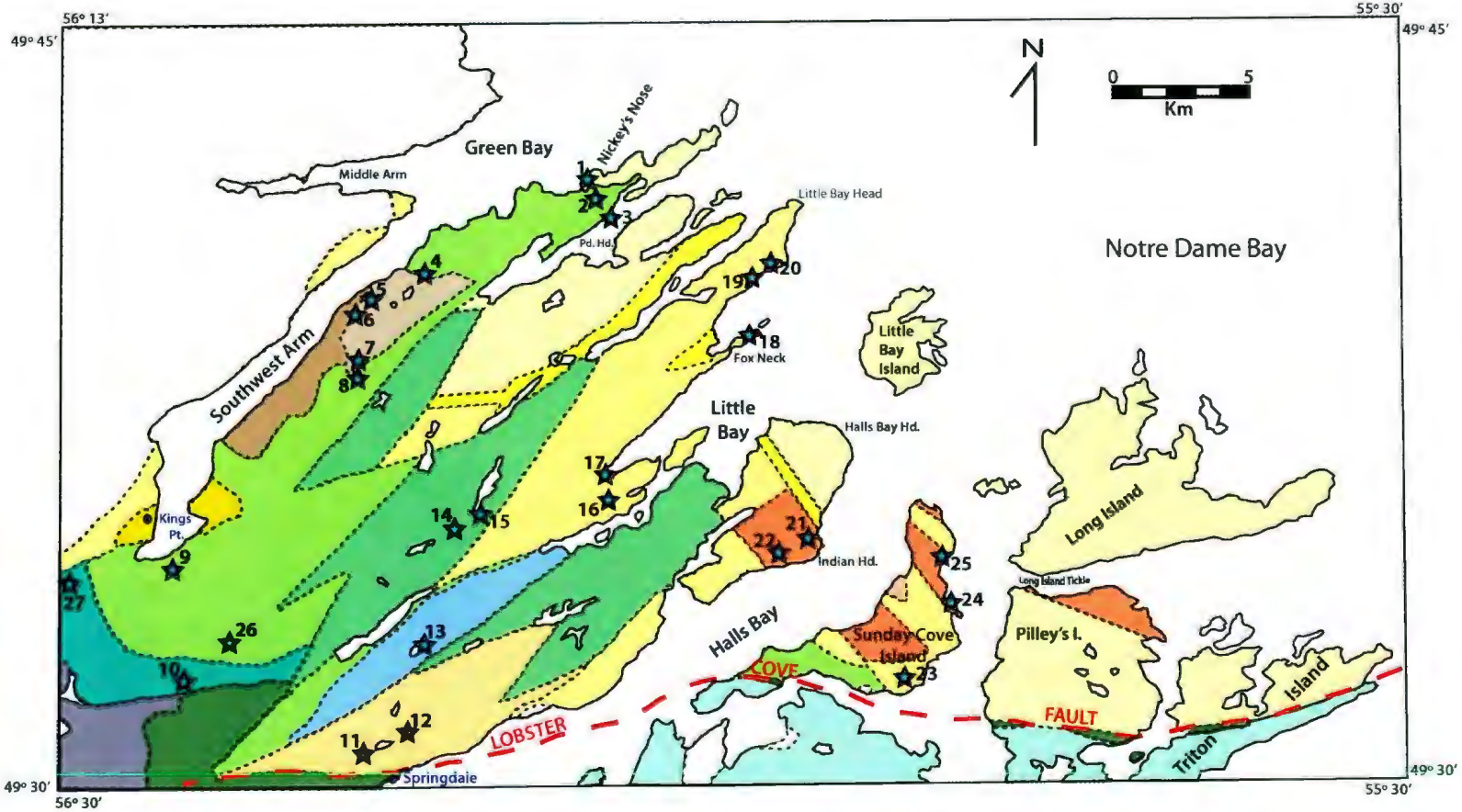

Figure 1.2 Geological map of the Springdale Peninsula together with VMS occurrences within the region (legend for map on page 24). From Kean *et al.* (1995).

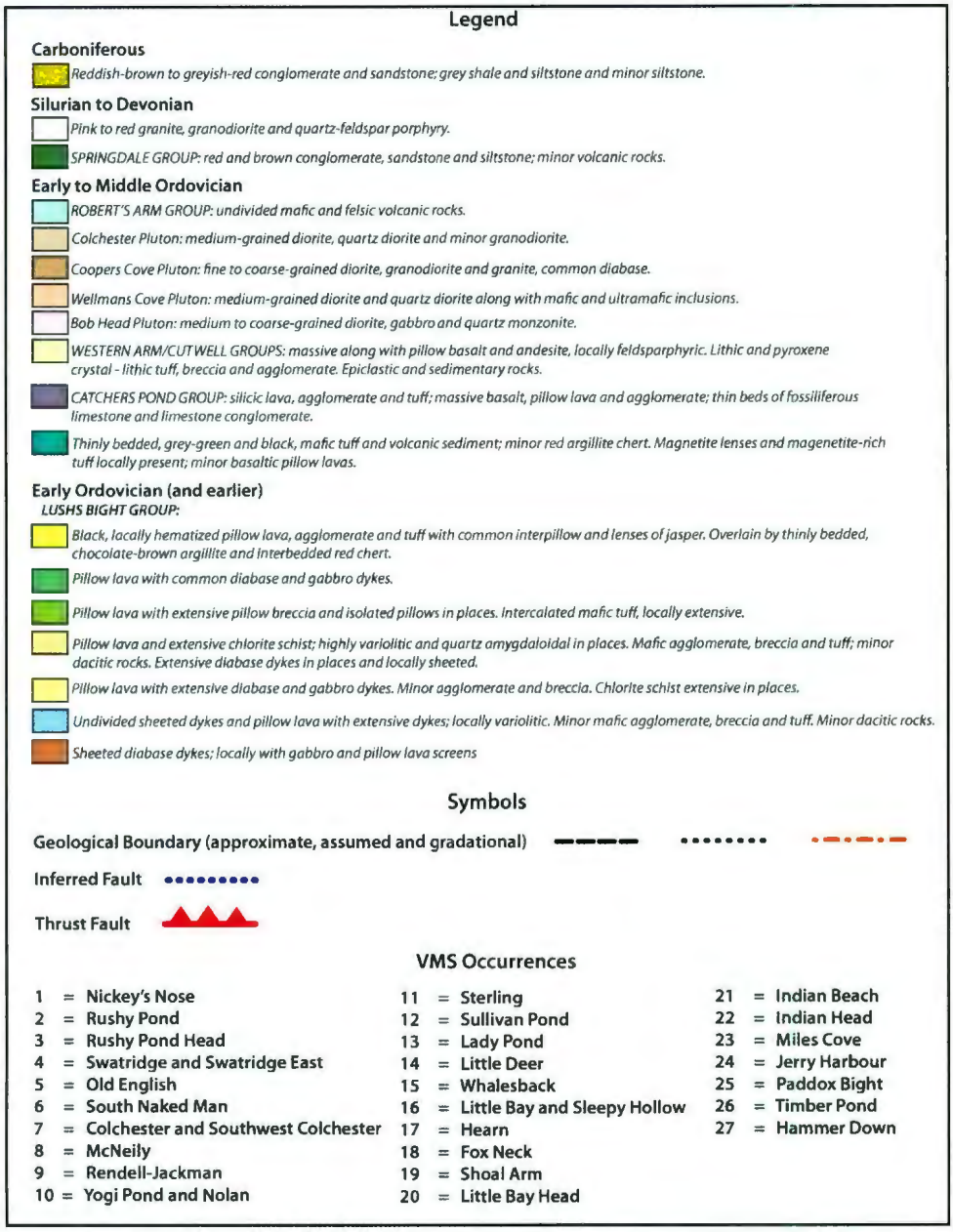

Figure 1.2 cont: Legend for the geological map of the Springdale Peninsula with VMS identification. From Kean *et al.* (1995).

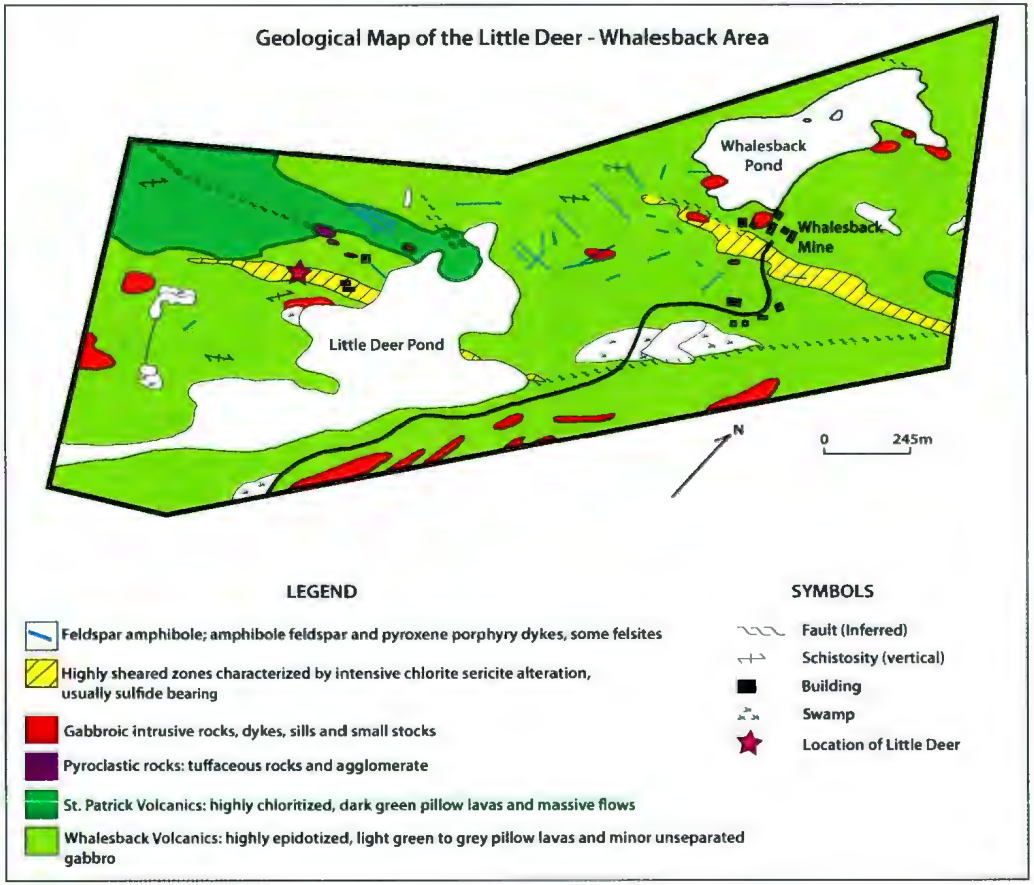

Figure 1.3 See page 26 for figure caption.

Figure 1.3 cont: Local geology of the Whalesback – Little Deer area. Based on their alteration facies, Papezik and Fleming (1967) and Fleming (1970) divided the Little Deer area into the 'Whalesback Volcanics' (highly epidotized tholeiitic pillow lavas) and the St. Patrick's Volcanics (highly chloritized tholeiitic pillow lavas). The Little Deer VMS deposit, according to this division, is located in a schist zone within the Whalesback Volcanics. From Papezik and Fleming (1967); Fleming (1970) and Kean *et al.* (1995) (coordinates for map not available on original map).

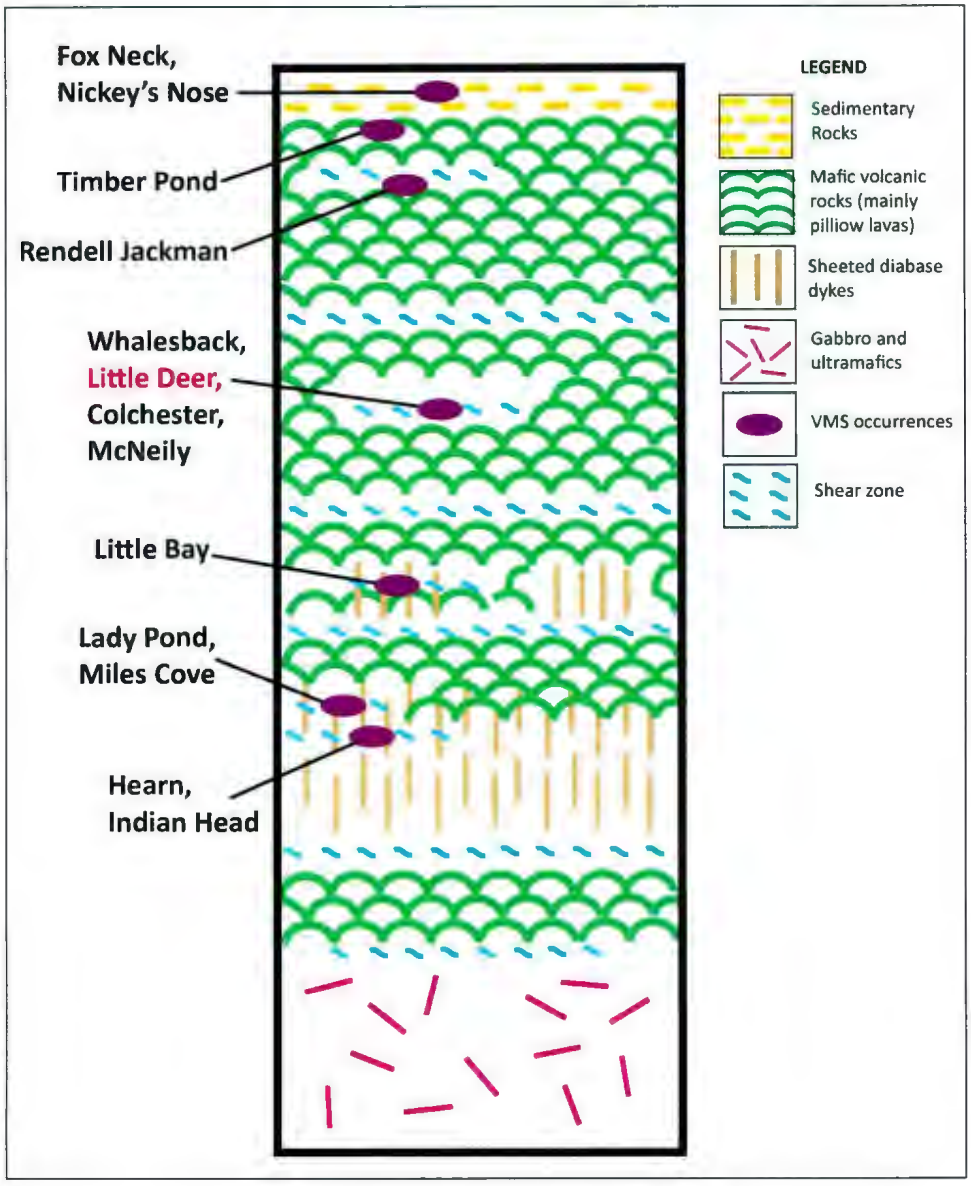

Figure 1.4 Stratigraphic setting for VMS occurrences within the Lushs Bight Group. Mineralization is almost exclusively associated with chlorite-schist zones developed within the pillow lava section of the ophiolite sequence. From Kean *et al.* (1995).

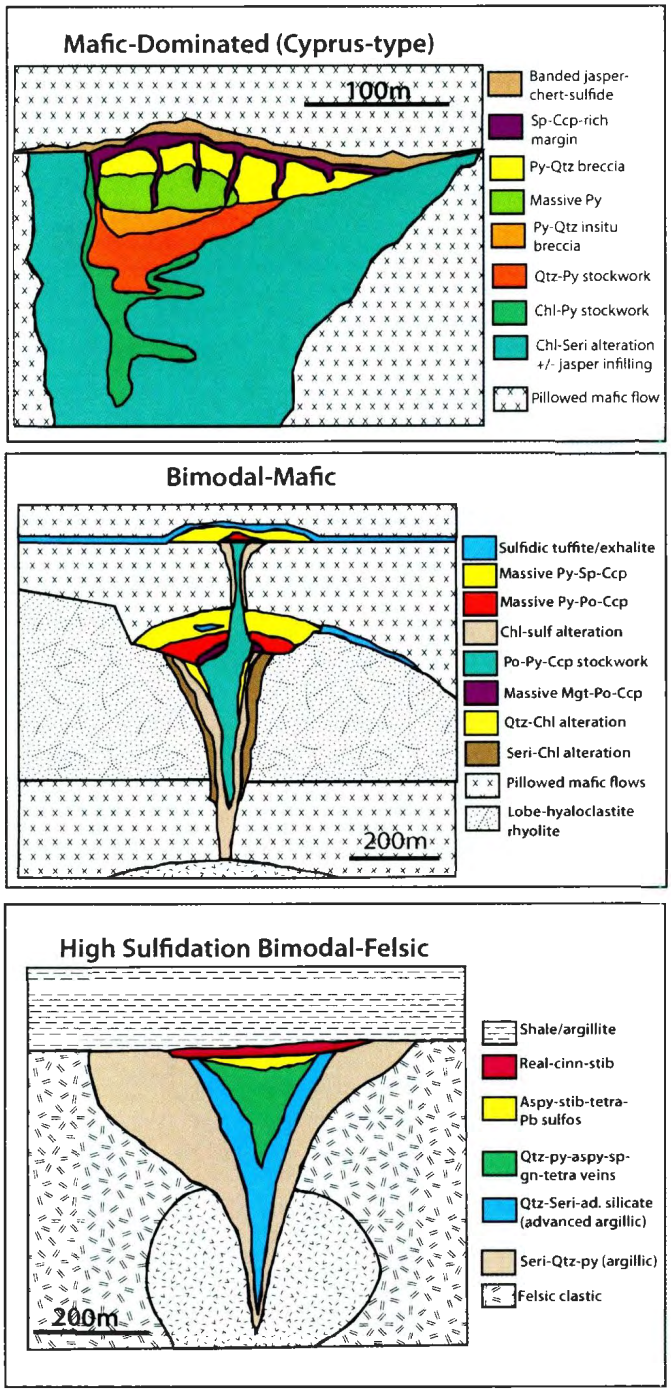

Figure 1.5 Formal classifications of VMS deposits based on lithology and tectonic setting. From Galley *et al.* (2007). The Little Deer VMS deposit has been classified as a 'mafic-dominated' system.

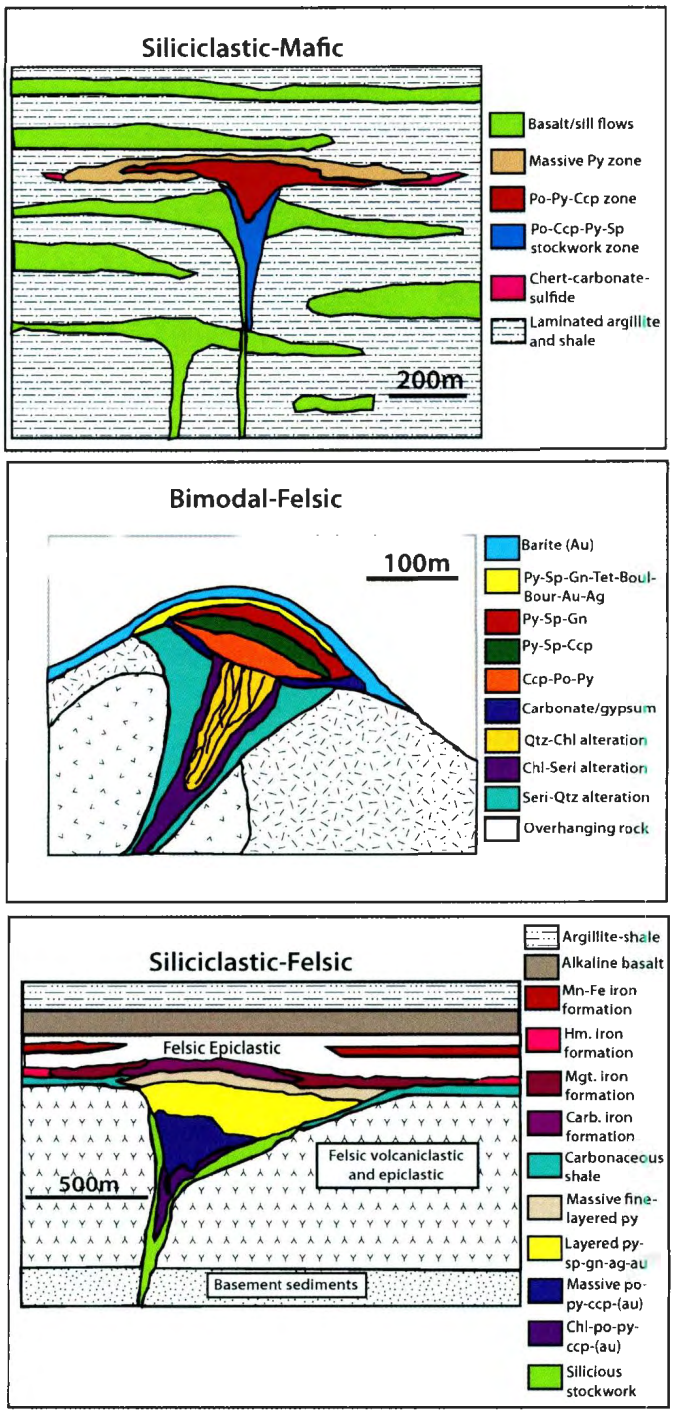

Figure 1.5 cont: Formal classifications of VMS deposits based on lithology and tectonic setting. From Galley *et al.* (2007).

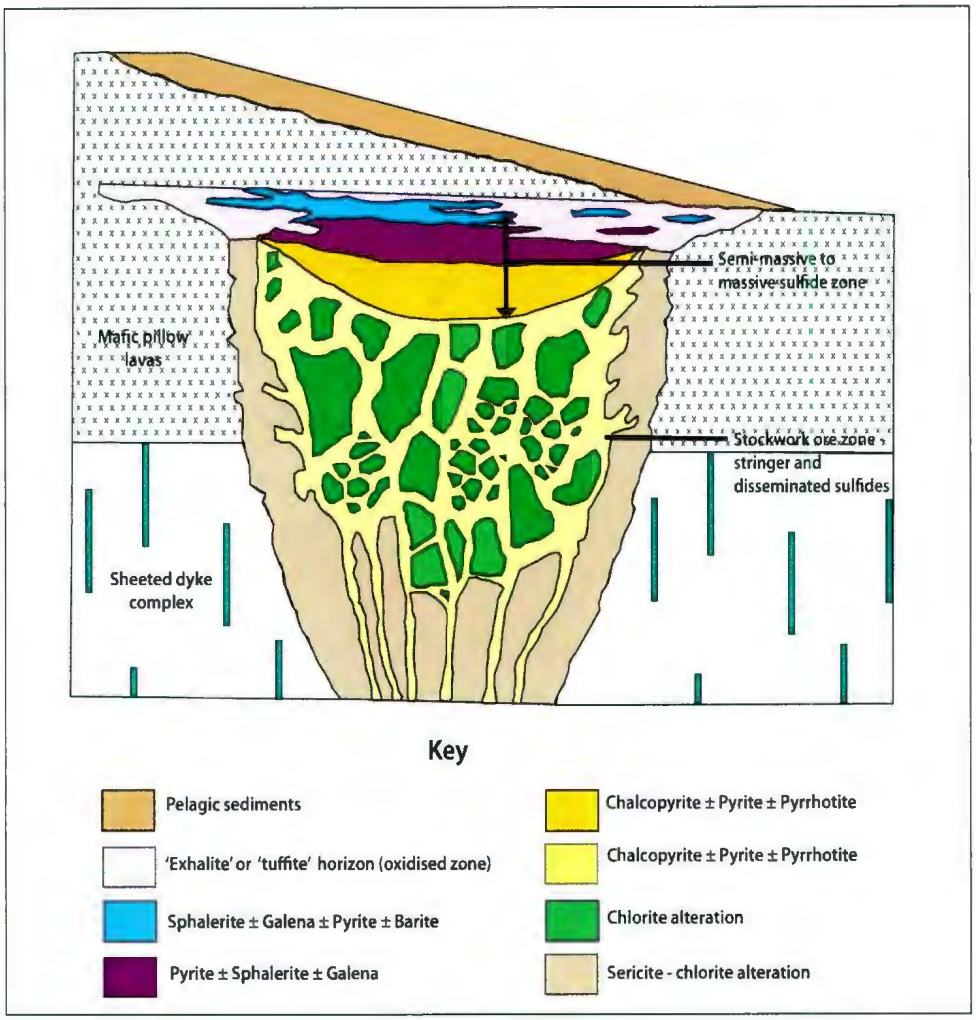

Figure 1.6 An idealized VMS model for mafic-(Cyprus)-type deposits - the likely environment of formation for the Little Deer deposit. From Hutchinson and Searle (1971) and Robb (2005). The Little Deer deposit consists of a stockwork that is comprised of sulfide rich stringers and disseminations that locally grade into massive and semi-massive sulfides. The massive sulfide lens is not present at Little Deer.

Chapter 2

Geology and Metallogeny of North-Central Newfoundland and the Little Deer VMS Deposit: An Introduction and Overview

[2.1] Abstract

The Little Deer deposit, Springdale Peninsula, north-central Newfoundland, is a mafic-type volcanogenic massive sulfide (VMS) deposit hosted in the ophiolitic Late Cambrian (~505 Ma) Lushs Bight Group. The deposit has been a past-producer (Cu) and is currently the focus of extensive exploration, thereby providing a new opportunity to study the Little Deer deposit and obtain a better understanding of ophiolite-hosted VMS mineralization in the northern Appalachians.

The Little Deer deposit consists of a stockwork that is comprised primarily of disseminated and stringer-style mineralization with occasional semi-massive to massive sulfide horizons. Mineralization is dominated by chalcopyrite, pyrrhotite and pyrite with minor sphalerite and cobaltite. Native tellurium, bismuth/mercury/silver/nickel and lead tellurides, electrum, galena, selenium-bearing galena and native arsenic are present as trace phases. The dominance of chalcopyrite-pyrrhotite-(± pyrite) mineralization throughout the deposit suggests that Little Deer formed from low pH (~2-4), low oxygen fugacity (~ -40 to -45), and high temperature (>300°C) fluids, typical of a mature VMS system.

The low abundance of trace elements at Little Deer and their textural association to the main sulfide phases (which are void of enrichment in these trace elements), suggests that trace phases formed via annealing (sweating) out of the main sulfides during post-VMS deformation and metamorphism.

On a global scale, the mineralogy, mineral assemblages and mineralization styles at Little Deer are similar to the massive sulfide deposits of Cyprus; the Italian Apennine deposits; and the Norwegian Caledonides. On a regional scale, Little Deer

mineralization is similar to ophiolitic VMS accumulations at Betts Cove, Tilt Cove, Colchester, Little Bay and Whalesback.

In situ sulfur isotope signatures for sulfide minerals at Little Deer range from $\delta^{34}S$ = -5.6‰ to +15.2‰, with values for chalcopyrite ranging from 0.6‰ to 10.5‰ (average: 3.8‰); pyrrhotite from -0.3‰ to +6.0‰ (average: 3.5‰); and pyrite from -5.6‰ to +15.2‰ (average: 4.3‰). A comparison between measured $\delta^{34}S$-values and calculated $\delta^{34}S$-values for thermochemical sulfate reduction of Late Cambrian seawater sulfate, suggests that Little Deer sulfur was primarily derived via thermochemical sulfate reduction, with or without an input of leached igneous sulfur from the surrounding basaltic/ultramafic rocks. Overall, the $\delta^{34}S$-values obtained at Little Deer are within the ranges found for Late Cambrian VMS deposits globally; this suggests that thermochemical sulfate reduction was an important global mechanism for the formation of reduced sulfur in Late Cambrian VMS deposits.

[2.2] Introduction

The Central Mobile Belt of the Newfoundland Appalachians is host to more than 40 VMS deposits; collectively they represent a reserve of ~46 million tonnes of sulfide rich material (Swinden and Kean, 1988; Piercey, 2007; Piercey and Hinchey, 2012) (Fig. 2.1). This district has been an important location for mineral exploration, development and mining since the mid-19th century. World-class deposits, such as those in the Buchans VMS district, have provided significant Zn, Cu, Pb, and precious metals to both the Canadian and global markets. The majority of VMS production in the northern Appalachians has been from polymetallic deposits associated with bimodal volcanic sequences (e.g., Bathurst, Buchans, Rambler); however, historical production from mafic-hosted (Cyprus-type) deposits (hosted in ophiolitic rocks) have

also produced considerable amounts of Cu, S, and - to a lesser extent - Zn and precious metals (.g., Swinden and Kean, 1988). Furthermore, exploration, production, and research on these deposits has greatly improved our understanding of the regional to local controls on the localization and genesis of eastern Canadian VMS mineralization (Swinden and Kean, 1988; Goodfellow and McCutcheon, 2003; Piercey, 2007).

The Little Deer deposit, Springdale Peninsula, north-central Newfoundland (Figs. 2.1 - 2.3), is a mafic-type VMS (Kean *et al.*, 1995) deposit hosted in a northern Appalachian ophiolite terrain; it is a past-producer (Cu) and currently an active exploration target for Cornerstone Capital Resources and Thundermin Resources Inc. Despite its discovery in 1952, only sporadic research has been done on the Little Deer deposit (Papezik and Fleming, 1967; Fleming, 1970; West, 1972; Kean *et al.*, 1995), with very little modern research (e.g., Kean *et al.*, 1995). New exploratory drilling has presented an opportunity to study the Little Deer deposit and provide further documentation and understanding of ophiolite-hosted VMS mineralization in the northern Appalachians.

The goals of this research are to: 1) provide a coherent understanding of the mineralogy, mineral assemblages, mineral textures and mineralization styles present at Little Deer; 2) highlight metal zoning in the deposit; 3) establish the source of sulfur (i.e.. biogenic and/or marine and/or magmatic) via the study of sulfur isotopic data; and 4) evaluate the role of primary deposition versus secondary modification (deformation and metamorphism). Goals (1) through (3) will allow postulation for the physicochemical conditions of ore formation to be made while also enhancing our

understanding of Late Cambrian, ophiolite-hosted VMS deposits in the northern Appalachians and globally.

[2.3] Geological Setting

The Newfoundland Appalachians are separated into four tectonostratigraphic zones and their associated subzones based on their differing stratigraphy, structure, fauna and metallogeny (Fig. 2.1) (Williams, 1979; Williams *et al.*, 1988; van Staal., 2007; van Stall and Barr, in press; Piercey, 2007). From west to east these are: the Humber; Dunnage (subzones: Notre Dame and Exploits); Gander; and Avalon zones (Williams, 1979; Williams *et al.*, 1988); together the Dunnage and Gander Zones comprise the Central Mobile Belt of Newfoundland (Fig. 2.1). These four zones record a series of Early Paleozoic [600 – 300 Ma (Williams and Grant, 1988)] orogenic episodes (the Taconic, Penobscot, Salinic, Acadian and Neoacadian orogenies) that culminated in the formation of the Appalachian Orogen, which records the opening and subsequent closure of the Iapetus (Precambrian to Early Paleozoic) and Rheic (Early Ordovician) oceans (Williams, 1979; van Staal, 2007; van Staal and Barr, in press).

The Little Deer, mafic-dominated (Cyprus-type) VMS deposit is located within the Dunnage Zone of the Central Mobile Belt (Figs. 2.1-2.3). The Dunnage Zone contains an assemblage of accreted Late Cambrian - Middle Ordovician island arcs, extensional arcs and back-arc terrains that formed at the margins of (and within) the Iapetus Ocean (Norman and Strong, 1975; Kidd, 1977; Williams *et al.*, 1988; Swinden, 1996; van Staal, 2007). The Dunnage Zone is further subdivided into the Notre Dame (peri-Laurentian) and Exploits (peri-Gondwanan) subzones (Williams *et*

al., 1988) (Fig. 2.1); Little Deer lies within the Notre Dame subzone (Kean *et al.*, 1995).

The Notre Dame subzone is bound to the west by the Baie Verte-Bromton Line and to the east by the Red Indian Line (Fig. 2.1) and preserves three Cambrian-Middle Ordovician obducted oceanic terrains, including: 1) the Lushs Bight Oceanic Tract (LBOT, 510 - 501 Ma); 2) the Baie Verte Oceanic Tract (BVOT, ~489 - 477 Ma) and 3) the Annieopsquotch Accretionary Tract (~481 - 460 Ma), as well as the Notre Dame Arc (488 - 435 Ma) (Dunning and Krogh, 1985; Kean *et al.*, 1995; Cawood *et al.*, 1996; van Staal, 2007; van Staal *et al.*, 2007; van Staal and Barr, in press). Together, these document a protracted history of suprasubduction-zone formation, obduction, and subsequent magmatic overprinting occurring as a result of the onset of the Taconic Orogeny (van Staal, 2007; van Staal *et al.*, 2007).

Three principal VMS mineralization episodes have been identified within the Notre Dame subzone: 1) VMS mineralization within the highly chloritized, highly sheared, pillow lavas of the Late Cambrian (~510 - 501 Ma) Lushs Bight (associated with suprasubduction zone rifting) and Sleepy Cove (associated with arc rifting) groups. Examples of VMS occurrences associated with this mineralization event include: Whalesback, Little Bay and Little Deer (Swinden and Kean, 1988; Swinden 1991, 1996; Kean *et al.*, 1995); 2) VMS mineralization in the volcanic sections of Lower Ordovician (~488 Ma) ophiolite sequences - formed during suprasubduction zone rifting. Examples of VMS occurrences associated with this mineralization event include: Tilt Cove, Betts Cove, and deposits of the Rambler Camp (Tuach and Kennedy, 1978; Dunning and Krogh, 1985; Tuach, 1988; Swinden, 1991, 1996; Skulski *et al.*, 2010); and 3) VMS mineralization associated with well-established

(mature) Lower Ordovician (~473 Ma) island arc rocks. All VMS accumulations within this episode are hosted by bimodal tholeiitic to calc-alkalic sequences primarily in the Buchans-Roberts Arm belt (Dunning *et al.*, 1987). Examples of VMS occurrences associated with this mineralization event include: Buchans, Gullbridge and Pilley's Island (Swinden and Kean, 1988; Swinden 1991, 1996).

The Little Deer VMS deposit is hosted in the Lushs Bight Group (LBG) of the LBOT (510 - 501 Ma) (Figs. 2.2-2.4). The LBG consists of an obducted (500 - 490 Ma) island arc ophiolitic sequence containing variably epidotized pillow basalts, sheeted dykes, gabbro and ultramafic rocks (Kean *et al.*, 1995; van Staal, 2007). Numerous Ordovician stocks, plugs and plutons (e.g., the Colchester and Cooper Cove plutons) intrude the LBG and are interpreted to be contemporaneous with LBG volcanism (Kean *et al.*, 1995). The LBG is a succession of northeast (early deformation) and southeast (later deformation) trending anticline and syncline folds - rendering the structural aspect of this group, complex (Kean *et al.*, 1995). West (1972) suggested that the Little Deer VMS deposit lies on the southern limb of a major anticline, close to the axial hinge of this fold. Lushs Bight Group anticlinoria and synclinoria are cross cut by north-northeast, northwest and southeast trending faults - many of which have a thrust component (Kean *et al.*, 1995).

Little Deer is situated within a chlorite-schist zone (trends 065°. dips 70 - 75 ° SE) hosted within island arc tholeiitic pillow lavas of the LBG; the chlorite-schist zone is 1050m in length and 60m in width (Papezik and Fleming, 1967; Fleming, 1970; West, 1972; Kean *et al.*, 1995). The basaltic host rocks for Little Deer have undergone varying degrees of chlorite, sericite, quartz and epidote alteration. Based on their alteration facies, Papezik and Fleming (1967) and Fleming (1970) divided the

Little Deer area into the Whalesback Volcanics (highly epidotized tholeiitic pillow lavas) and the St. Patrick's Volcanics (highly chloritized tholeiitic pillow lavas). The Little Deer VMS deposit, according to this division, is located within the Whalesback Volcanics (Fig. 2.3) (Papezik and Fleming, 1967 and Fleming, 1970).

The Lushs Bight Group is host to numerous other VMS deposits (Fig. 2.4) such as the Whalesback; Colchester; McNeily; Little Bay; Lady Pond and Miles Cove deposits (Kean *et al.*, 1995; Swinden *et al.*, 1995 and van Staal, 2007). Mineralization is almost exclusively associated with chlorite-schist (shear) zones developed within tholeiitic pillow lavas (Kean and Evans, 1988; Kean *et al.*, 1995). It is interpreted that this intimate relationship between VMS mineralization and shear zones is a consequence of chlorite alteration zones being remobilized as thrust faults during subsequent tectonism (Kean *et al.*, 1995).

[2.4] Principal Sulfide Types, Styles and Textures of the Little Deer VMS Deposit

[2.4.1] Methodology

Sulfide host rocks, ore types, and textures were documented from the macro- to micro-scale utilizing drill core and graphic logs to document the mineralogy, mineral assemblages, mineral textures, mineralization styles and metal zoning in the Little Deer deposit. For subsequent micro-scale work, representative samples of Little Deer mineralization were taken at various depths along the plunge of the deposit (micro-scale work is discussed in section 2.7).

[2.4.2] Stratigraphy and Host Rocks

Basalts hosting the Little Deer VMS deposit are dominantly pillow lavas and variably deformed massive mafic flows. The pillow lavas are typically 5-20cm in width and display varying degrees of chlorite, quartz, sericite and epidote alteration

giving the host rock a variety of colors (Fig. 2.5A-F). Pillow lavas that have weak to moderate epidote (± quartz) alteration are commonly amygdaloidal; amygdules can be filled with pyrite, pyrrhotite, quartz, calcite, and (rarely) sphalerite.

The pillow lava sequence (and Little Deer mineralization) is cross-cut by two types of dykes. Basaltic mafic dykes are brown to light black/grey in color with an aphanitic texture (Fig. 2.5G); they occasionally display chilled margins. The second type of dykes are porphyritic mafic/andesitic dykes containing subhedral-euhedral quartz ± plagioclase ± amphibole phenocrysts - that are up to 1cm in size - in an aphanitic groundmass (Fig. 2.5H). Within the drill core analyzed, there is no evidence of a crosscutting relationship between the two types of dykes.

[2.4.3] Sulfide Facies

Sulfide mineralization at Little Deer is a stockwork composed of disseminated and stringer-style mineralization with occasional semi-massive to massive sulfide horizons. Mineralization is dominated by chalcopyrite, pyrrhotite, pyrite, and minor sphalerite (additional phases are observed by various microscopic techniques - section 2.7). Sulfide mineralization has distinct macro-scale textures and consists of three main facies, each with minor variations internally.

[2.4.3.1] Pyrite Dominated Sulfides.

This facies commonly occurs at the beginning and at the end of each sulfide intersection (Fig. 2.6). Pyrite in this facies occurs dominantly as stringers/ribbons consisting of individual pyrite porphyroblasts that follow the schistosity (fabric) of the host rock (Fig. 2.7A). However, pyrite porphyroblasts also occur individually; speckled throughout the host rock they give this facies a buckshot appearance (Fig. 2.7B). Pyrite porphyroblasts can become amalgamated to form larger porphyroblasts

(± pyrrhotite tails) (Fig. 2.7C); pyrite porphyroblasts also commonly overprint calcite and quartz veins (Fig. 2.7D). Within this facies, pyrite can occur alone or with disseminated chalcopyrite and/or pyrrhotite or with weak stringers of chalcopyrite and/or pyrrhotite. This facies highlights the multiple pyrite generations that exist at the Little Deer deposit.

[2.4.3.2] Chalcopyrite-Pyrrhotite Dominated Sulfides.

This facies is dominated by varying proportions of chalcopyrite and pyrrhotite that occur as stringer-type mineralization in basalt or as semi-massive to massive sulfides.

Stringer mineralization is dominated by varying abundances of chalcopyrite and pyrrhotite that form an anastomosing network throughout the basaltic host rocks coincident with chlorite ± quartz ± sericite alteration (Figs. 2.7E & F). Pyrrhotite (in the stringers) ranges from fine-grained to granular, whereas chalcopyrite often exhibits a sugary, granular texture (Figs. 2.7E-G). In places, chalcopyrite-pyrrhotite-dominated stringers mirror the schistosity of the host rock with the greatest sulfide accumulations occurring at the hinge zone and along the axial trace of crenulation cleavage folds; this produces a hinge zone thickening texture (Fig. 2.7G). Chalcopyrite-pyrrhotite dominated stringer facies often contain pyrite porphyroblasts that are proximal to the stringers; pyrite stringers, although rare, are found grading into, and out of, this facies (Fig. 2.7H).

Semi-massive to massive chalcopyrite-pyrrhotite-dominated sulfides have abrupt and sharp margins; rarely do stringers grade into semi-massive to massive sulfides. The semi-massive to massive sulfides are dominated by durchbewegung

textures, but can also have metamorphic banding with alternating chalcopyrite and pyrrhotite (Figs. 2.7I-K).

Pyrrhotite-dominant semi-massive horizons have minor chalcopyrite and are associated with sericite/quartz altered basalt fragments (Fig. 2.7J). Chalcopyrite dominant semi-massive horizons have patches and/or bands of pyrrhotite and are associated with chlorite ± quartz altered rock fragments (Figs. 2.7I & K). Both facies have minor pyrite as individual porphyroblasts and/or amalgamated porphyroblasts and/or coarse grained pyrite patches/masses (Fig. 2.7L); coarse grained pyrite patches replace chalcopyrite and pyrrhotite (Fig. 2.7L). Semi-massive to massive pyrite is rare, but occurs associated with chalcopyrite-pyrrhotite dominated semi-massive to massive horizons (Fig. 2.7M).

Despite chalcopyrite-pyrrhotite stringers and semi-massive to massive horizons exhibiting strong evidence of the effects of metamorphism and deformation (Figs. 2.7I-N), it is interpreted that this facies represents primary VMS mineralization that has been texturally modified during post-VMS greenschist metamorphism (Bachinski, 1977; Kean *et al.* 1995) and deformation. Possible evidence for unscathed primary mineralization at Little Deer is highlighted by fine-grained, thick, chalcopyrite-dominated stringers (lacking durchbewegung texture) that anastomose around tear-shaped (possible pillow lava) rock fragments (Fig. 2.7O).

[2.4.3.3] Pyrite-Sphalerite-Pyrrhotite Sulfides.

This facies is rare and is dominated by pyrite that occurs as individual grains or as groups of fine to coarse grained porphyroblasts (Fig. 2.7P). Sphalerite mineralization is typically found as fine-grained disseminations between pyrite crystals and throughout the host rock (Fig. 2.7P); however, sphalerite also forms weak

veinlets/wisps (Fig. 2.7Q). Pyrrhotite occurs in weak-moderate stringers. This facies is associated with Fe-rich jasperoidal horizons/patches and intense epidote and quartz altered host rocks (Fig. 2.7P & Q). Franklin (2008) suggested that this association could represent the exhalation of metal-rich fluids onto the ancient seafloor.

[2.5] Bulk Rock Analyses Data

[2.5.1] Analytical Methods

Twenty two samples from 15 diamond drill cores were submitted to ALS Minerals, North Vancouver, British Columbia, for multi-element analysis. Samples submitted were representative of various styles of mineralization at Little Deer and therefore provide the means to document the metal and other chemical compositional data for the sulfides at Little Deer. All samples were weighed, dried, and crushed in mild steel to where 85% of material passed 75 microns (ALS method code: PREP-31b). Samples were dissolved using a four acid near total digestion and were analyzed using inductively coupled plasma mass spectrometry (ICP-MS). This method allowed for analysis of the following 48 elements: Ag, Al, As, Ba, Be, Bi, Ca, Cd, Ce, Co, Cr, Cs, Cu, Fe, Ga, Ge, Hf, In, K, La, Li, Mg, Mn, Mo, Na, Nb, Ni, P, Pb, Rb, Re, S, Sb, Sc, Se, Sn, Sr, Ta, Te, Th, Ti, Tl, U, V, W, Y, Zn, Zr (ALS method code: ME-MS61). Samples where Cu, Zn, S, and Ag exceeded 10,000 ppm were analyzed further by inductively coupled plasma emission spectroscopy (ICP-ES) to obtain accurate wt% values.

Three internal standards, High Lake High Cu (HLHC); High Lake Low Cu (HLLC), and High Lake High Zn (HLHZ), obtained by Dr. Stephen Piercey from MMG Ltd. were submitted to ALS minerals to monitor precision and accuracy for key metals of interest (Cu, Pb, Zn, Ag and Au). QA/QC results are provided in Table 2.1;

all data for Cu, Pb, Zn, Ag and Au fall within three standard deviations of accepted values, suggesting adequate accuracy.

[2.5.2] Results

Table 2.2 displays the bulk rock results for the 22 samples analyzed; six different ore types that represent variants of the three facies established at Little Deer were analyzed: chalcopyrite-dominated stringers; pyrite-dominated stringers; pyrrhotite-dominated stringers; pyrrhotite-dominated semi-massive horizons; chalcopyrite-dominated semi massive horizons and pyrite-sphalerite-pyrrhotite horizons.

Figure 2.8(A) highlights that the majority of sulfides at Little Deer are Cu-rich with only pyrite-sphalerite-pyrrhotite samples and some pyrite-dominated stringer samples having Zn-rich affinities. The data overlap the field for Cyprus-type VMS deposits (Zaccarini and Garuti, 2008), as is expected given the ophiolitic tectonic setting of Little Deer. Analyses located outside this field (i.e. Zn-rich samples) portray a bias as these samples were chosen for their presence and abundance of sphalerite.

Figure 2.8(B) indicates that Little Deer is poor in Au and Ag, regardless of facies, with the majority of samples plotting outside the Cyprus-type VMS field. Samples that have the greatest enrichment in Ag and Au are from pyrite-sphalerite-pyrrhotite facies and to a lesser extent the pyrrhotite-dominated samples; this indicates a possible link between these ore types and increased Au-Ag concentrations.

[2.6] 3D Geometry of Metal Zoning at Little Deer.

[2.6.1] Methodology

The 3D geometry of metal zoning in Little Deer has been undertaken using the company assay database and Target for ArcGIS version 10.0. The assay database for

Little Deer comprises 274 drill holes with 4712 assay samples from a depth range of 1.52m – 1135.50m. The 3D distribution focuses on Cu and Zn as these are of greatest commercial interest at Little Deer. The parameters used to construct the model for each element are highlighted in Table 2.3.

[2.6.2] Results

Contoured plots for Cu and Zn are show in Figure 2.9. Figure 2.9(A) and (C) indicate that higher Cu concentrates are located primarily at greater depths (Fig. 2.9A) and throughout the core of the Little Deer deposit (Fig. 2.9C); higher Cu-concentrations are attributed to the chalcopyrite-pyrrhotite facies of sulfides. In contrast, Zn-rich zones (Fig. 2.9B-C) are located primarily at shallower depths and at the extremities of the deposit (Fig. 2.9B); they are associated with low Cu values (Fig. 2.9C) and are spatially distinct from Cu-rich areas (Figs. 2.9A-B). Higher Zn-concentrations are associated with the Fe-rich jasperoidal, pyrite-sphalerite-pyrrhotite facies of mineralization.

[2.7] Micro-scale Mineralogy: Styles and Textures

[2.7.1] Analytical Methods

Forty three representative samples from 22 diamond drill cores were chosen for transmitted and reflected light microscopy and SEM to understand the sulfide mineralogy, mineral assemblages, associations and textures present in the Little Deer sulfides. In addition to the main phases present in drill core, microscopy and SEM analysis allowed for the identification of other trace phases, and their associations within/to the main sulfide phases, to be established. Transmitted and reflected light microscopy was undertaken at Memorial University using a Nikon LV100POL. Scanning electron microscopy analyses were undertaken using the FEI Quanta 400

environmental SEM equipped with energy dispersive spectrometer (EDX) and silicon drift detectors. Operating conditions included an operating voltage of 25kV with a beam current of 13μA. Imaging and semi-qualitative element maps were obtained using the Bruker 4010 EDX system and associated software. All SEM work was undertaken at the Core Research Equipment and Instrument Training Network (CREAIT-NETWORK), Bruneau Innovation Centre, Memorial University of Newfoundland (Memorial University of Newfoundland).

[2.7.2] Results

Microscopic and SEM data corroborate and further develop the macro-scale characteristics of Little Deer, in that the deposit is dominated by chalcopyrite, pyrrhotite and pyrite with minor sphalerite and cobaltite (Table 2.4). Bismuth telluride; mercury telluride; silver telluride; nickel telluride; lead telluride; native tellurium; electrum; galena; selenium-bearing galena and native arsenic and are also present in varying amounts as accessory (trace) phases (Table 2.4).

Chalcopyrite occurs in disseminated, stringer, semi-massive and massive styles of mineralization where crystals principally form massive sheets - regardless of the mineralization style (Fig. 2.10A-C & E). Chalcopyrite associated with stringer style mineralization often replaces a previous euhedral phase (Figs. 2.10B & C). Chalcopyrite is rarely found without pyrrhotite and vice versa (Figs. 2.10A, C-E).

Pyrrhotite occurs in disseminated, stringer, semi-massive and massive styles of mineralization and principally consists of coarse, anhedral-subhedral annealed, interlocking pyrrhotite crystals, regardless of facies style (Figs. 2.10A & D). Pyrrhotite porphyroblasts are associated with chalcopyrite-pyrrhotite semi massive to massive horizons (Fig. 2.10E).

Pyrite is associated with all the main sulfide minerals and facies within Little Deer and occurs in three crystal forms. Euhedral pyrite occurs primarily within the basaltic host rocks (Figs. 2.11A-C) and often becomes rounded with annealed textures forming triple junctions (Fig. 2.11B). Euhedral pyrite is primarily inclusion free; however, it can contain inclusions of sphalerite, galena, chalcopyrite, and pyrrhotite (Figs. 2.11A & C). Euhedral pyrite occurs dominantly in the pyrite-sphalerite-pyrrhotite sulfide facies. The second style of pyrite includes rounded porphyroblasts associated with all sulfide facies at Little Deer. This crystal form occurs in two modes: 1) individual rounded pyrite porphyroblasts (Fig. 2.11D); and 2) amalgamated pyrite porphyroblasts where numerous individual pyrite porphyroblasts coalesce to form one large individual porphyroblast (Figs. 2.11E-F). Pyrite of this style can contain inclusions of chalcopyrite (Fig. 2.11E), pyrrhotite, and rarely, sphalerite. Pyrite porphyroblasts can overprint the host rock (Fig. 2.11F), and some porphyroblasts have brittle deformation where fractures are filled by chalcopyrite and/or pyrrhotite (Fig. 2.11G). Other pyrite porphyroblasts have ductile deformation features and form pinch and swell structures (Fig. 2.11H). The third style of pyrite is cobaltoan pyrite. This form of pyrite is rare and crystals primarily occur within chalcopyrite-dominated mineralization (Figs. 2.12A-B). It has been identified primarily via SEM through energy dispersive spectrometry (EDX) scans of pyrite grains.

Cobaltite occurs in two crystal forms with both forms occurring primarily in pyrrhotite-dominated semi-massive to massive sulfide horizons. Euhedral cobaltite crystals are exclusively found within the host rock (Figs. 2.10D & 2.12C), whereas anhedral (rounded) to subhedral crystals are located within (primarily pyrrhotite) sulfide mineralization (Fig. 2.12D).

Sphalerite, although minor, occurs as anhedral crystals randomly speckled throughout all facies of mineralization; however, sphalerite is dominant in the pyrite-sphalerite-pyrrhotite facies where it exhibits chalcopyrite disease (Figs. 2.12E & F).

Native tellurium, bismuth/mercury/silver/nickel and lead tellurides; electrum; galena; selenium-bearing galena and native arsenic are present as trace phases at Little Deer. The trace phases occur in two principal locations: 1) within cracks and at sulfide grain boundaries (Figs. 2.13A & B); and 2) enclosed within the main sulfide phases (Figs. 2.13C & D). There is no association between a style of mineralization (i.e. disseminated, stinger or semi-massive) and a specific trace phase species/assemblage. Furthermore, there is no correlation between a specific sulfide phase or sulfide facies and a particular trace phase species/assemblage. Trace phases occur alone as individual blebs of a specific species (Figs. 2.13A-D), or mixed together with different trace phases (Figs. 2.13E-H).

[2.8] Mineral Chemistry

[2.8.1] Analytical Methods

Chalcopyrite, pyrrhotite, pyrite, sphalerite, and cobaltite (representative of the facies, mineral assemblages and mineral textures established at Little Deer) were analyzed from nine samples (from eight diamond drill cores) for their mineral chemistry using electron microprobe analyses (EPMA) at the University of Toronto, Canada. Analyses were undertaken using a Cameca SX50/51 (DCI 1300 DLL) equipped with 3 tunable wavelength dispersive spectrometers. Operating conditions were 40 degree takeoff angle with a beam energy of 25kV, a beam current of 20μA with a 1 micron beam diameter. Elements were acquired using analyzing crystals LiF for Fe Kα, Cu Kα, Zn Kα, As Kα, Te Lα, Hg Lα, Co Kα, Ni Kα, Se Kα, and PET for

Sn Lα, Pb Mα, Bi Mα, S Kα, Mo Lα, Au Mα, Ag Lα, Sb Lα. Counting time was 20 seconds for Fe Kα, S Kα, Cu Kα, Zn Kα, Pb Mα, Au Mα, Ag Lα, Sb Lα, Sn Lα, Te Lα, Bi Mα, Hg Lα, Mo Lα, Se Kα, and 40 seconds for Co Kα, Ni Kα, As Kα. Off-peak counting time was 20 seconds for Fe Kα, S Kα, Cu Kα, Zn Kα, Pb Mα, Au Mα, Ag Lα, Sb Lα, Sn Lα, Te Lα, Bi Mα, Hg Lα, Mo Lα, Se Kα, and 40 seconds for Co Kα, Ni Kα, As Kα. Off-peak correction method was 'linear' for Cu Kα, Co Kα, Se Kα; 'Average' for Au Mα, Sb Lα, Te Lα, Bi Mα, Fe Kα, Ni Kα, Zn Kα; 'High Only' for Mo Lα, Sn Lα, S Kα, As Kα and 'Low Only' for Ag Lα, Hg Lα, Pb Mα. Unknown and standard intensities were corrected for deadtime and standard intensities were corrected for drift over time. Interference corrections were applied to: S for interference by Co; As for interference by Pb; Sn for interference by Co; Bi for interference by Au, and to Mo for interference by Pb. The data were processed using Analytical and Automation Software, the Enterprise version of 'Probe for Windows' written by J. Donovan and marketed by Advanced Microbeam (University of Toronto).

[2.8.2] Results

Only elemental values that exceed the minimum detection limit (MDL) are presented and discussed within the results section. Elements that exceed a value 0.1wt% are classified as major elements, whereas elements that fall below 0.1wt% (but are above their elemental MDL) are classified herein as trace elements. If an element has values classified at wt% and ppm levels, all results are presented as ppm for simplicity. Mineral formulae have been calculated based on the atoms per formula unit (apfu) and the number of sulfur atoms per formula unit for a given phase (see Appendix A.2, Table A.2, Appendix A.3 and Table A.3 for calculation methods).

[2.8.2.1] Chalcopyrite.

Table 2.5 displays the major element results of 48 chalcopyrite analyzed from four different ore types (representing variants of the three facies established at Little Deer): chalcopyrite-dominated stringers; pyrite-dominated stringers; pyrrhotite-dominated semi-massive sulfides and chalcopyrite-dominated semi massive sulfides. Chalcopyrite is primarily stoichiometric with mineral formulas dominantly falling within the range of $Cu_{0.97\text{-}1.06}Fe_{0.96\text{-}1.05}S_{2.00}$ (Table 2.5). Chalcopyrite from chalcopyrite-dominated stringers, pyrrhotite-dominated semi-massive sulfides, and chalcopyrite-dominated semi massive sulfides have slightly higher Cu and Fe contents than chalcopyrite from pyrite-dominated stringers, with mineral formulae in the range of $Cu_{0.98\text{-}1.06}Fe_{0.97\text{-}1.05}S_{2.00}$ (Table 2.5). However, most Cu and Fe contents in chalcopyrite fall within the range outlined above (Table 2.5). There are no substitutions of other elements within chalcopyrite analyzed at Little Deer (Table 2.5).

[2.8.2.2] Pyrrhotite.

Table 2.6 displays the major and trace element results for 47 pyrrhotite crystals analyzed from five different ore types: chalcopyrite-dominated stringers; pyrite-dominated stringers; pyrrhotite-dominated semi-massive sulfides, chalcopyrite-dominated semi massive sulfides and pyrite-sphalerite-pyrrhotite horizons.

Overall, pyrrhotite has a restricted composition, regardless of ore type, with mineral formulae ranging from $Fe_{0.92\text{-}0.95}S_{1.00}$ (Table 2.6). Pyrrhotite is primarily non-stoichiometric with impurities of Ni and Co that likely substitute for Fe in the pyrrhotite structure (Figs. 2.14 A-C; Table 2.6). While the relationships between Ni, Co, and Fe are non-systematic (Fig. 2.14A-C), there is a general trend towards higher Ni and Co in pyrrhotite-dominated semi-massive sulfides (Fig. 2.14A-C; Table 2.6);

higher Co contents are found in samples at shallower depths down plunge in the deposit (Table 2.6).

[2.8.2.3] Pyrite.

Table 2.7 displays the major and trace element results for 39 pyrite crystals analyzed from five different ore types: chalcopyrite-dominated stringers; pyrite-dominated stringers; pyrrhotite-dominated semi-massive sulfides, chalcopyrite-dominated semi-massive sulfides and pyrite-sphalerite-pyrrhotite horizons.

Pyrite has mineral formulae ranging from $Fe_{0.92\text{-}1.00}S_{2.00}$ with most formulae being between $Fe_{0.97\text{-}0.99}S_{2.00}$ (Table 2.7). Pyrite has trace abundances of Zn, Cu, Co, and Ni, with no systematic relationships except for Co (Fig. 2.14D), where the greatest enrichment in Co is associated with chalcopyrite-rich samples, regardless of facies (Fig. 2.14D; Table 2.7); these pyrite grains are considered cobaltoan pyrite. In general, there is a decrease in Fe with increasing Co in pyrite, when Co is present (Fig. 2.14D).

[2.8.2.4] Sphalerite.

Table 2.8 displays the major and trace element results for 41 sphalerite crystals analyzed from four different ore types: pyrite-dominated stringers; pyrrhotite-dominated semi-massive horizons; chalcopyrite-dominated semi-massive horizons and pyrite-sphalerite-pyrrhotite horizons.

Sphalerite is dominantly Zn-rich with formulae ranging from $Zn_{0.78\text{-}0.89}Fe_{0.08\text{-}0.16}S_{2.00}$ (Table 2.8). There is little variation between ore types with the exception of sphalerite from the pyrite-sphalerite-pyrrhotite facies, which shows a tight cluster with little variance (Fig. 2.14E; Table 2.8). Sphalerite is non-stoichiometric and has minor Co, Cu and Ni in its structure; many samples have >200ppm Co and >1%Cu, which is

attributed to chalcopyrite disease (Figs. 2.14F-G; Table 2.8). Sphalerite in chalcopyrite-dominated semi-massive sulfides have the highest Co contents, whereas sphalerite in the pyrite-dominated assemblages are least enriched in Co (Fig. 2.14F; Table 2.8).

[2.8.2.5] Cobaltite.

Table 2.9 displays the major and trace element results for 25 cobaltite crystals analyzed from two different ore types: chalcopyrite-dominated semi-massive horizons and pyrrhotite-dominated semi-massive horizons.

Cobaltite crystals have mineral formulae that primarily fall in the range of $(Co_{0.68-0.82},Fe_{0.07-0.28})As_{0.75-0.91}S_{1.00}$, with minor exceptions (i.e. #285-286) (Table 2.9). Most samples are non-stoichiometric with appreciable Cu and Ni contents (Table 2.9). There are inverse relationships between the Fe and Co (Fig. 2.14H), and Fe and Ni (Fig. 2.14I) contents of cobaltite, and a sympathetic relationship between Co and Ni contents (Fig. 2.14J). Cobaltite from pyrrhotite-rich semi-massive sulfides has the highest enrichment in Ni (Fig. 2.14J; Table 2.9).

[2.9] Sulfur Isotopes

[2.9.1] Analytical Methods

Sulfur isotope compositions for chalcopyrite, pyrrhotite, and pyrite (in their various associations and assemblages) were obtained for 8 samples from 6 diamond drill holes via secondary ion mass spectroscopy (SIMS) at the MAF-IIC Microanalysis Facility of Memorial University of Newfoundland. Information on sample preparation; instrumentation; analytical parameters; calibration of instrumental fractionation and accuracy and reproducibility regarding the SIMS analyses, is available in Appendix A, Section A.4; this information is from Layne (unpublished).

The sulfur isotope signatures were obtained in situ and utilized to test the source of sulfur in the deposit. The results obtained are presented as per mil (‰) deviations from the Vienna Canyon Diablo Troilite. Detailed

[2.9.2] Results

Measured δ^{34}S-values for the 8 samples analyzed from Little Deer are presented in Table 2.10 and Figure 2.15. Table 2.11 and Figure 2.16 present the δ^{34}S-ranges for the five ore types analyzed; each ore type represents variants of the three facies established at Little Deer (chalcopyrite-dominated semi-massive sulfides; pyrrhotite-dominated semi-massive sulfides chalcopyrite-dominated stringers; pyrite-dominated stringers and disseminated pyrite). Little Deer δ^{34}S-values are also compared to sulfur isotope values found in Late Cambrian VMS deposits occurring in Newfoundland and worldwide (Fig. 2.17).

The δ^{34}S-values from Little Deer range from -5.6‰ to +15.2‰, including: chalcopyrite (+0.6‰ to 10.5‰ [average: 3.8‰]); pyrrhotite (-0.3‰ to +6.0‰ [average: 3.5‰]) and pyrite (-5.6‰ to +15.2‰ [average: 4.3‰]) (Fig. 2.15; Table 2.10). While there is greater variability in the δ^{34}S-values of sulfides associated with pyrrhotite-dominated semi-massive horizons, δ^{34}S-values are dominantly uniform, regardless of sulfide phase or sulfide facies (Fig. 2.16; Table 2.11).

[2.10] Discussion

[2.10.1] Little Deer Mineralization: Evolution of Mineralization

The dominant style of mineralization at Little Deer consists of a Cu-rich stockwork comprising of disseminated and stringer-style mineralization with occasional semi-massive to massive sulfide horizons. A subordinate mineralization

style, the pyrite-sphalerite-pyrrhotite facies, lies stratigraphically above, but spatially separated from, the Cu-rich stockwork (Figure 2.9A-C).

Mineralization at Little Deer is relatively simple and is dominated by chalcopyrite, pyrrhotite and pyrite, with minor sphalerite and cobaltite. Native tellurium; bismuth/mercury/silver/nickel and lead tellurides; electrum; galena; selenium-bearing galena and native arsenic are present as trace phases. The composition, mineralogy, and textures associated with mineralization at Little Deer is interpreted to represent the effects of both primary VMS formation and subsequent deformation and greenschist metamorphism (Bachinski, 1977; Kean *et al.*, 1995). Outlined in Figure 2.18 is the interpreted paragenesis for Little Deer; the paragenetic diagram includes both primary VMS-related mineralization (discussed in this section), and secondary deformation and metamorphism features (discussed in section 2.10.2).

The Little Deer deposit has both low temperature (*i.e.*, Zn-rich) and high temperature (*i.e.*, Cu-rich) assemblages that may represent either zone refining or potential boiling relationships within a Late Cambrian VMS environment (Delaney and Cosens, 1982; Eldridge *et al.*, 1983; Ohmoto, 1996; Hannington *et al.*, 1999; Slack *et al.*, 2003; Robb, 2005). Low temperature assemblages at Little Deer include the pyrite-sphalerite-pyrrhotite facies, which is associated with (Fe)-rich jasper horizons and intense epidote ± quartz alteration in basalts (Figs. 2.7P & Q). Franklin (2008) argued that this assemblage may represent the exhalation of metal-rich fluids onto the ancient seafloor. Pyrrhotite within the pyrite-sphalerite-pyrrhotite facies, although minor, is often found as inclusions within pyrite of this facies (Figs. 2.11A & C) suggesting formation of pyrite via the conversion of pre-existing pyrrhotite (Schoonen and Barnes, 1991; Ohmoto, 1996):

$$Fe^{2+} + H_2S_{(aq)} \rightarrow FeS_{(s)} + 2H^+$$

[Eq. 1]

$$FeS_{(s)} + H_2S_{(aq)} \rightarrow FeS_{2(s)} + Fe^{2+} + H_{2(aq)}$$

[Eq. 2]

The conversion of Fe to pyrrhotite and subsequently to pyrite signals a transition to higher temperature (>150 °C), more reduced hydrothermal fluids (increased H_2S and H_2) that likely represent the heating up, and evolution of, the hydrothermal system. The occurrence of sphalerite with pyrrhotite, and pyrite, suggests that sphalerite also precipitated during the initial lower temperature, high Fe, high H_2S stages of VMS mineralization (Fig. 2.18). However, hematitic horizons associated with the pyrite-sphalerite-pyrrhotite facies, although indicative of low temperature (~150 °C), high Fe hydrothermal fluids, also suggest oxygenated, low H_2S conditions, which favored the precipitation of (Fe)-rich horizons over the precipitation of pyrite (Ohmoto, 1996; Badrzadeh *et al.*, 2011):

$$2Fe^{2+} + 3H_2O_{(l)} \rightarrow Fe_2O_{3(s)} + 4H^+ + H_2$$

[Eq. 3]

The occurrence of sulfide phases requiring high Fe and high H_2S conditions (primarily pyrrhotite), with hematite, a phase formed under high Fe and low H_2S conditions, is reconciled by the acknowledgement that most hematite preserved in VMS deposits was precipitated during the later, lower temperature waning stages of VMS evolution (Ohmoto, 1996) (Fig 2.18). It is considered therefore, that the pyrite-sphalerite-pyrrhotite facies (not including the Fe-rich horizons) records an earlier mineralizing event (Fig. 2.18).

Chalcopyrite disease in sphalerite within the pyrite-sphalerite-pyrrhotite facies documents the evolution of Little Deer from a primitive, lower temperature (~150 - 250°C) to a mature, higher temperature (~250 - 350°C) stage of VMS evolution (Fig. 2.18); chalcopyrite disease represents the dissolution of sphalerite by chalcopyrite during the maturation of the deposit (Figs. 2.12E & F) (Eldridge *et al.*, 1983; Ohmoto, 1996; Ohmoto and Goldhaber, 1997):

$$2ZnS_{(s)} + FeS_{2(s)} + 2Cu^{+} + Fe^{2+} \rightarrow 2CuFeS_{2(s)} + 2Zn^{2+}$$

[Eq. 4]

The abundance of chalcopyrite disease at Little Deer, together with an expected substitution of Cu for Zn within the sphalerite crystal lattice, most likely accounts for the mineral chemistry of sphalerite, in some cases, containing >1% Cu (Fig. 2.14G & Table 2.8). The transition to a hotter, mature VMS system is further documented by chalcopyrite replacing a previous euhedral phase (Figs. 2.10B & C), most likely earlier formed euhedral pyrite (Fig. 2.18):

$$FeS_2 + CuCl_2^{-} = CuFeS_2 + 2Cl^{-}$$

[Eq. 5]

Additionally, the abundance of pyrrhotite with chalcopyrite in the chalcopyrite-pyrrhotite dominated facies at Little Deer is interpreted to represent high temperature maturation of the VMS system. While many phases at Little Deer have elevated Co contents, i.e., pyrrhotite, pyrite and sphalerite (Figs. 2.14B-D & F; Tables 2.6–2.8), the majority of cobaltoan pyrite and Co-rich phases are associated with the chalcopyrite-dominated semi-massive sulfides, consistent with a high temperature origin (Figs. 2.12A-B). Tivey *et al.*, (1995) and Huston *et al.*, (1995) have shown that Co contents in pyrite increase with increasing temperature, also consistent with the

cobaltoan pyrite at Little Deer having formed at high temperatures (Fig. 2.18). Similarly, sphalerite in chalcopyrite-dominated semi-massive sulfides has the highest Co values, whereas sphalerite associated with the lower temperature, pyrite-sphalerite-pyrrhotite dominated assemblages are least enriched in Co (Fig 2.14F); this highlights that Co-rich mineral compositions are strongly associated with the high temperature mineralization stage at Little Deer.

The association of chalcopyrite-pyrrhotite-(± pyrite) signifies high sulfidation; high temperature (~350°C); low pH (~2-4); and low oxygen fugacity (~ -40 - -45) conditions during the mature, Cu-rich stage of VMS evolution (Barnes, 1979; Barton and Skinner, 1979; Hannington *et al.*, 1999).

The evolution of Little Deer from low temperature sulfide (Zn-Fe-rich) assemblages to higher temperature (Cu-rich) sulfide assemblages is partially supported by the spatial associations of Cu and Zn in the 3D metal zoning models (Figs. 2.9A - C). The Zn-rich horizons/areas, attributed to the hematitic, pyrite-sphalerite-pyrrhotite facies, are located at shallower depths and at the extremities of the deposit (Figs. 2.9B & C), whereas the Cu-rich areas, attributed to the chalcopyrite-pyrrhotite-dominated facies, occur dominantly at depth and throughout the core of the Little Deer deposit (Figs. 2.9A & C). This distribution may represent the dissolution and reprecipitation of early lower temperature Zn-Fe-rich sulfides by later, hotter, Cu-rich fluids with the transportation of the former to more distal locations in the stockwork (i.e., zone refinement) as the VMS system evolved.

It is notable, however, that although Little Deer mineralization is typical of an ophiolite-hosted (Cyprus-type) VMS system, Little Deer consists of stockwork mineralization only and lacks the ideal structure of a Cyprus-style VMS deposit (i.e. a

massive sulfide mound underlain by a stockwork; Fig. 2.19). While zone refining can explain the above relationships, it is also possible that boiling may have been an important mechanism for the mineralization at Little Deer. In particular, the stringer dominated nature of mineralization, and the chalcopyrite-pyrrhotite-(± pyrite) dominated mineral assemblage at Little Deer, may have been controlled by the pressure dependency of adiabatically rising hydrothermal fluids (Delaney and Cosens, 1982; Hannington *et al.*, 1999; Robb, 2005). The dominance of stringer mineralization, lack of a massive sulfide mound and a spatial separation of Zn-rich sulfides from Cu-rich sulfides (Figs. 2.9A - C), may have resulted via boiling as the hydrothermal fluids intersected the depth-to-boiling point curve at ~1500m (Delaney and Cosens, 1982; Hannington *et al.*, 1999; Robb, 2005). The resultant drop in temperature and pressure would have led to the brecciation of the footwall rocks, and combined with the solubility differences between Cu and Zn, could have allowed for the precipitation of a Cu-rich stockwork with Zn(± Pb) precipitation occurring at the sea floor (e.g., Delaney and Cosens, 1982; Hannington *et al.*, 1999; Robb, 2005).

While boiling may account for the absence of a massive sulfide mound at Little Deer, equally possible is that the sulfide mound has been removed due to deformation. Given the abundant evidence for extensive deformation at Little Deer (Section 2.10.2.), and regionally (Kean *et al.*, 1995) (Figs 2.1 & 2.2), it is also possible that the massive sulfide mound may have been tectonically displaced (e.g., Sundblad, 1980).

[2.10.2] Ore Mineral Textural Evolution: The Effects of Deformation and Metamorphism on Mineralization.

While the metal assemblages, and some textures, at Little Deer likely represent primary VMS metal assemblages, with minor exceptions, the sulfides have textures indicative of modification by post-VMS deformation and greenschist metamorphism (Bachinski, 1977; Kean *et al.* 1995). These effects have not only destroyed and replaced primary textural features, but have also complicated the establishment of an exact paragenesis for sulfide mineralization (Fig. 2.18).

The response of the sulfides at Little Deer to deformation and metamorphism is a function of the competency contrasts between each sulfide phase and the host rock; the more ductile sulfides, chalcopyrite and pyrrhotite, responded more readily to the effects of deformation and metamorphism than the more refractory sulfides, sphalerite and pyrite (Kelly and Clark, 1975; Craig, 1983; Marshall and Gilligan, 1993; Craig and Vaughan, 1994; Craig, 2001).

The effects of deformation are recorded in all three facies at Little Deer where mineralization mimics structural fabrics and textures of the host basalts, including: asymmetrical folding (Fig. 2.7A) and crenulation cleavage formation with thickening of sulfides in the hinge zones of folds (Cook *et al.*, 1990; Marshall and Gilligan, 1993) (Fig. 2.7G); pressure shadow formation (Fig. 2.7C); durchbewegung textures (Fig. 2.7 I-M); rolled pyrite (Fig. 2.11D) (Craig and Vaughan, 1994); brittle deformed pyrite infilled by ductile deformed chalcopyrite (± pyrrhotite) (Fig. 2.11G); and pinch and swell structures (Fig. 2.11H) also record the effect of deformation on the ores.

The semi-massive to massive sulfide horizons at Little Deer are considered to represent larger scale versions of micro-scale structures, i.e., they represent the

accumulation of sulfides into the hinge zones of folds (Fig. 2.7G). This may explain why semi-massive to massive sulfide horizons at Little Deer have abrupt and sharp margins and rarely grade from stringers into semi-massive/massive sulfide in drill core, as would be expected in an idealized Cyprus-style VMS system (Fig. 2.19). Moreover, it may explain the observations of Pressacco (2010) and Putrich *et al.*, (2011) that semi-massive to massive horizons at Little Deer have an *en echelon* occurrence.

Greenschist metamorphism (Bachinski, 1977; Kean *et al.* 1995); combined with deformation, has also texturally modified, and influenced the occurrence and abundance of, the Little Deer sulfides, in particular pyrite, pyrrhotite and cobaltite, as well as affecting the occurrence of the trace phases native tellurium; bismuth/mercury/silver/nickel and lead tellurides. Metamorphism has resulted in the metamorphic banding of some semi-massive to massive sulfide ores (Fig. 2.7I) and the coarsening and annealing of crystals (Figs. 2.10D, 2.11A-B & E) producing well-developed triple junctions (Fig. 2.11B).

While three styles of pyrite crystals are present at Little Deer [euhedral, porphyroblastic (individual and amalgamated) and cobaltoan pyrite], metamorphism has had significant affect on only two forms: euhedral and porphyroblastic. Despite pyrite occurring as a primary phase during the early stages of low temperature VMS formation (Fig. 2.18), it is unlikely that its current euhedral textural form represents the initial texture of primary pyrite. The tendency for pyrite to recrystallize as euhedral forms when subjected to metamorphism (Craig, 1973; Craig and Vaughan, 1994) and the dominant euhedral pyrite association with the pyrite-sphalerite-

pyrrhotite facies, suggests that euhedral pyrite at Little Deer is simply recrystallized primary pyrite.

Porphyroblastic pyrite occurs in two forms: amalgamated (Fig. 2.11E) and individual (Fig. 2.11D), both of which are located primarily within the chalcopyrite-pyrrhotite-dominated stringer and semi-massive/massive sulfide facies. The metamorphic textures observed in both forms of porphyroblasts (Fig. 2.11D & E), combined with the effects of deformation, indicate the following possible evolutionary sequence: coarsening/recrystallization of primary pyrite (± the incorporation of other sulfides) (Fig. 2.11E) → amalgamation of numerous individual pyrite porphyroblasts to form a single larger pyrite porphyroblast (Fig. 2.11E) → formation of rolled pyrite (Fig. 2.11D). Rolled pyrite represents pyrite that has undergone the most intense deformation; the smooth rounded texture of rolled pyrite is most likely the result of being rolled in a ductile matrix (Craig and Vokes, 1992; Craig and Vaughan, 1994). In some cases individual pyrite porphyroblasts are located within the host rock and often display chaotic textures due to host rock overprinting (Figs. 2.11F & G); pyrrhotite edges and/or tails can be present in these porphyroblasts (Figs. 2.7C & 2.11F) and suggest that some porphyroblasts at Little Deer may have evolved via the retrograde re-equilibration of pyrrhotite.

Pyrrhotite porphyroblasts (Fig. 2.10E) are suggested to have formed in a similar manner to that of rolled pyrite through the amalgamation and subsequent rolling of pre-exiting pyrrhotite crystals within a ductile matrix during metamorphism and deformation (Craig and Vokes, 1992; Craig and Vaughan, 1994). This suggests that pyrrhotite at Little Deer, although texturally modified by metamorphism is dominantly primary (Plimer and Finlow-Bates, 1978; Craig and Vokes, 1992).

Cobaltite is suggested to be exclusively metamorphic in origin and is primarily associated with pyrrhotite (Fig. 2.12C & D) and, to a lesser extent, sphalerite; these phases notably have trace contents of Co in their structures (Figs. 2.14C & F; Tables 2.6 & 2.8). Post-VMS native arsenic veins are also documented both at Little Deer and regionally (Papezik, 1967). It is therefore postulated that cobaltite formed via reactions between Co and S, present in the above sulfides, during the introduction of As-rich fluids during regional metamorphism and deformation:

$$(FeCo)S_{(Co\text{-bearing pyrrhotite})} + As_{(aq)} = CoAsS_{(cobaltite)} + Fe_{(aq)} \quad [Eq.6]$$

$$(ZnFeCo)S_{(Co\text{-bearing sphalerite})} + As_{(aq)} = CoAsS_{(cobaltite)} + (Zn,Fe)S_{(sphalerite)} \quad [Eq.7]$$

Although cobaltite occurs in two crystal forms (euhedral and rounded) (Fig. 2.12C & D), both are likely to be of the same generation only having responded differently to the effects of metamorphism and deformation. This difference is attributed to the matrix viscosity within which they were formed: those hosted in rigid host rock produced euhedral cobaltite (Figs. 2.10D & 2.12C), whereas those hosted in ductile sulfide mineralization formed rounded cobaltite (Fig. 2.12D). The dominant occurrence of cobaltite in pyrrhotite-dominated mineralization is attributed to the readiness of pyrrhotite to deform and recrystallize, and subsequently yield Co from its crystal structure, when subjected to stress (Kelly and Clark, 1975; Marshall and Gilligan, 1993; Craig and Vaughan, 1994; Craig, 2001).

It is suggested that the trace phases, including native tellurium, bismuth, mercury, silver, nickel and lead tellurides, have a metamorphic origin. While it is possible they have magmatic affinities (see arguments in Section 2.10.3 against

magmatic fluids), their textural associations within cracks and at sulfide grain boundaries, small size, association with deformed grains and general rarity, are best explained via formation during metamorphism and deformation. Additionally, the mineral chemistry of the main sulfides present at Little Deer is relatively simple (Tables 2.5-2.9): pyrrhotite, pyrite and sphalerite contain minor Ni, Co and Cu; cobaltite contains minor Ni, Cu, Te (rare) and Se (rare); and chalcopyrite is free of impurities. The relatively low concentrations of the trace elements that comprise the above trace minerals, and their textural association to sulfide phases without enrichments in these elements, suggest that these trace phases formed via annealing "sweating" out during post-VMS deformation and metamorphism (Craig and Vokes, 1992; Huston *et al.*, 1995).

On a global scale, the mineralogy at Little Deer, its paragenesis (Fig. 2.18), and textural evolution is similar to the massive sulfide deposits of the Italian Apennines (Zaccarini and Garuti, 2008); the Norwegian Caledonides (Barrie *et al.*, 2010); and the VMS deposits of Cyprus (Franklin *et al.*, 1981). On a regional scale, Little Deer mineralization is similar to VMS accumulations at Betts Cove, Tilt Cove, Colchester, Little Bay and Whalesback (Bachinski, 1977; Franklin *et al.*, 1981; Kean *et al.*, 1995).

[2.10.3] Source(s) of Sulfur in the Little Deer VMS Deposit

The mechanisms by which sulfur isotopes fractionate are well understood (Ohmoto and Rye, 1979; Rollinson, 1993; Ohmoto and Goldhaber, 1997). In VMS deposits, the derivation of sulfur is attributed to: 1) biogenic sulfur obtained from bacterial sulfate reduction (BSR) of seawater sulfate; 2) a magmatic input and/or a leaching of reduced sulfur from underlying host rocks; and 3) reduced sulfur obtained

via the thermochemocal sulfate reduction (TSR) of seawater sulfate (Ohmoto and Rye, 1979; Ohmoto and Goldhaber, 1997).

While BSR is important in some VMS systems, particularly those that formed at lower temperatures, and/or during periods of global anoxia (e.g., Goodfellow and Peter, 1996), it is unlikely that this mechanism was important at Little Deer. Under normal, open-ocean conditions with infinite seawater sulfate supply, like those during the formation of Little Deer (e.g., hematite-rich cherts above the mineralization), BSR derived H_2S, and associated sulfide minerals, would contain distinctly negative $\delta^{34}S$-values. While there are low $\delta^{34}S$-values recorded at Little Deer (Fig. 2.15; Table 2.10), the majority of $\delta^{34}S$-values are distinctly positive (Fig. 2.15; Table 2.10) and therefore inconsistent with a significant BSR input. Furthermore, the Cu-rich assemblages found at Little Deer are consistent with high temperature fluids (~350°C), rendering it highly unlikely for bacteria to play a significant role (if any) in the reduction of SO_4^{2-}, as optimum temperature ranges for BSR are <50°C (Rollinson, 1993; Ohmoto and Rye, 1979; Ohmoto and Goldhaber, 1997). Finally, although not definitive, textural evidence for the presence of bacterial derived sulfides (e.g., framboidal pyrite) are not established at Little Deer. Collectively, the role of BSR in the genesis of reduced sulfur for the sulfides at Little Deer, is considered negligible.

Magmatic contributions, although documented for some VMS deposits, remain uncertain for the majority of deposit (Sawkins, 1986; Stanton, 1990; Sillitoe *et al.*, 1996; Yang and Scott, 1996; Herzig *et al.*, 1998; Gemmell *et al.*, 2004; Hannington *et al.*, 1999). Sulfides derived from a magmatic fluid are considered to have $\delta^{34}S$-values ~0‰ (Ohmoto and Rye, 1979; Ohmoto and Goldhaber, 1997; Huston, 1999); however, sulfides derived from the leaching of igneous sulfur from basaltic and

ultramafic rocks also have δ^{34}S-values ~0‰ (Ohmoto and Rye, 1979; Ohmoto and Goldhaber, 1997; Huston, 1999). Therefore, deciphering if δ^{34}S-values ~0‰ at Little Deer (Fig. 2.15, Table 2.10) are the result of a direct input of magmatic fluids and/or from a leaching of igneous sulfur, is difficult. However, a magmatic sulfur contribution to Little Deer mineralization is considered unlikely due to the abundance of chalcopyrite. Where magmatic volatiles are involved in metal transportation in the submarine environment (i.e., high sulfidation VMS systems), deposits are notably devoid of Cu phases, largely due to the fact that boiling fluids (due to depth to boiling curve constraints) cannot carry Cu (Hedenquist and Lowenstern, 1994; Hannington *et al.*, 1999; Gemmell *et al.*, 2004). Furthermore, magmatic-associated VMS deposits are enriched in epithermal/magmatic suite elements (e.g., As, Sb, Bi, Mo etc) and complex sulfosalt assemblages (e.g., Hannington *et al.*, 1999; Roth *et al.*, 1999; Gemmell *et al.*, 2004; Dubé *et al.*, 2007). Neither feature above is observed in the Little Deer deposit, therefore suggesting that the δ^{34}S-values ~0‰ at Little Deer could have originated from the leaching of igneous sulfur from the surrounding basaltic, and underlying ultramafic, rocks (Fig. 2.4).

While δ^{34}S-values ~0‰ at Little Deer can be explained via the leaching of igneous sulfur, the heavier δ^{34}S-values cannot (Fig. 2.15; Table 2.10), therefore an additional mechanism is required to explain the high δ^{34}S-values. Thermochemical sulfate reduction (TSR) is the main mechanism at higher temperatures (>120°C) (Goldstein and Aizenshtat, 1994) for the reduction of seawater sulfate to sulfide; TSR results in δ^{34}S-values that are less variable than BSR due to smaller depletions in ^{34}S relative to seawater sulfate (Hoefs, 2009). The high temperature Cu-rich mineral assemblages at Little Deer, combined with the heavy and homogenous δ^{34}S-values

recorded for the majority of the sulfides (Fig. 2.15; Table 2.10), indicates that TSR was most likely the main mechanism for the production of reduced sulfur at Little Deer (e.g., Shanks and Seyfried, 1987; Goldstein and Aizenstat, 1994; Huston *et al.*, 2001). Given Little Deer's ophiolitic setting, the formation of reduced sulfur via TSR (>250°C) could easily have proceeded via the reaction of seawater sulfate with iron in the surrounding mafic rocks (e.g., Shanks and Seyfried, 1987; Huston *et al.*, 2001):

$$HSO_4^- + 8FeO_{(rock)} + H^+ = H_2S + 4Fe_2O_3$$

[Eq. 8]

To further evaluate the role of TSR as the source of reduced sulfur in the Little Deer sulfides, TSR has been modeled for various Late Cambrian seawater sulfate compositions (28, 29 and 30‰, respectively) and compared to the measured $\delta^{34}S$-values for the Little Deer sulfides (Figs. 2.15 & 2.20; Tables 2.10 & 2.12). Calculations were undertaken following the methods of Ohmoto and Rye (1979), Ohmoto and Goldhaber (1997) and Huston (1999). Predicted $\delta^{34}S$-values for chalcopyrite, pyrrhotite and pyrite were calculated using Equation [9]:

$$1000\ln \alpha_{i\text{-}H2S} = A\ (10^6/T^2) + B = \delta^{34}S_i - \delta^{34}S_{H2S}$$

[Eq. 9]

Constants A and B in Equation [9] were taken from Ohmoto and Rye (1979); $\alpha_{i\text{-}H2S}$ is the fractionation factor between the sulfide phase (i = chalcopyrite, pyrrhotite, or pyrite) and the H_2S generated from TSR; T is temperature in Kelvin; $\delta^{34}S_i$ is the predicted sulfur isotope value for the sulfide in question, and $\delta^{34}SH_2S$ is the sulfur isotopic value of H_2S derived from TSR of seawater sulfate; $\delta^{34}SH_2S$ was calculated using Equation [10]:

$$\delta^{34}S_{H2S} = \delta^{34}SO_{4\,(parent)} + 1000^{(0.975\,-1)}$$

[Eq. 10],

which relates the sulfur isotope compositions of H_2S derived from seawater sulfate as a function of the Rayleigh distillation equation (Eq. 11):

$$\delta SO_{4\,(t)} = (\delta SO_{4\,(t\,=\,0)} + 1000) \times f^{\,(0.975)} - 1000$$

[Eq. 11]

This equation calculates the $\delta^{34}S$-value of SO_4 at a certain time ($\delta SO_{4(t)}$) relative to the parent composition of seawater sulfate ($\delta^{34}SO_{4(t=0)} = \delta^{34}SO_{4\,(parent)}$). This is a function related to the amount of sulfate reduced to H_2S as measured by f, where f represents the atomic fraction of the parent SO_4 ($\delta^{34}SO_{4(t=0)} = \delta^{34}SO_{4\,(parent)}$) reduced to H_2S ($\delta^{34}S_{H2S}$) relative to the original amount of SO_4 present. For example, when f = 1, no sulfate has been reduced to sulfide; when f = 0.8, 20% of sulfate has been reduced to sulfide, and when f = 0, all sulfate has been reduced to sulfide. Equations [9-11] are dependent upon an assumption being made for the $\delta^{34}S$-value of seawater sulfate (SO_4). While $\delta^{34}S$‰ of seawater sulfate has varied through time, $\delta^{34}S$-values for Late Cambrian seawater sulfate range from ~28 - 30‰ (Claypool *et al.*, 1980).

The results of TSR modeling are presented in Figure 2.20 and Table 2.12; only $\delta^{34}S$-values calculated for 350°C, the likeliest temperature for Cu-dominant sulfide precipitation, are presented (e.g., Lydon, 1988; Ohmoto, 1996; Franklin *et al.*, 2005). The chalcopyrite-pyrrhotite-pyrite rich assemblage at Little Deer suggests low fO_2 fluid conditions, and therefore f values for equation [11] are likely to be 0.8 or greater (Fig. 2.20; Table 2.12). Under the above conditions, the calculated $\delta^{34}S$-values for chalcopyrite, pyrrhotite and pyrite range from -0.2 to +13.4‰ for chalcopyrite, +0.3 to 13.9‰ for pyrrhotite, and +1.0 to 15‰ for pyrite. These predicted values (Fig. 2.20 &

Table 2.12) overlap with the ranges recorded for the Little Deer sulfides and could even account for the magmatic-like $\delta^{34}S$-values (~0‰) observed (Figs. 2.15 and 2.20; Table 2.10). These results imply that TSR was an important process in the formation of reduced sulfur during the evolution of the Little Deer deposit and highlights that the leaching of sulfur from surrounding igneous lithologies is not a requirement in order to achieve $\delta^{34}S$-values ~0‰. However, deciphering between TSR sulfur and leached igneous sulfur is not possible at present.

It is notable that despite different substrates and deposit types, the majority of Late Cambrian VMS deposits have similar ranges in $\delta^{34}S$ (Fig. 2.17); this suggest commonalities in their origin and highlights that TSR of Late Cambrian seawater sulfate was an important global mechanism for the production of reduced sulfur during VMS formation.

[2.11] Conclusions

The main conclusions of this study are:

1) The Little Deer VMS deposit is an Appalachian mafic-(Cyprus)-style VMS deposit consisting of a Cu-dominated VMS stockwork with occasional semi-massive to massive sulfide horizons. The deposit formed from high temperature (>300°C) VMS-related fluids via zone refining and (or) boiling. The metal assemblages and bulk mineralogy of the sulfides are interpreted to represent primary VMS mineralization; however, sulfides have been significantly texturally modified during greenschist metamorphism and deformation leading to abundant textural remobilization and recrystallization, including the formation of secondary minerals (e.g., cobaltite and telluride phases).

2) Based on measured and calculated $\delta^{34}S$-values for chalcopyrite, pyrrhotite and pyrite, it is suggested that reduced sulfur in sulfides from Little Deer was primarily derived through TSR of Late Cambrian seawater sulfate, with or without an input of leached igneous sulfur from surrounding basaltic/ultramafic rocks. The $\delta^{34}S$-values obtained at Little Deer are within the range observed for Late Cambrian VMS deposits globally, suggesting that TSR was an important global mechanism for the production of reduced sulfur during Late Cambrian VMS formation.

3) On a global scale, the mineralogy, paragenesis, and textural evolution of the sulfides at Little Deer is similar to the massive sulfide deposits of the Italian Apennines; the Norwegian Caledonides and the VMS deposits of Cyprus. On a regional scale, Little Deer mineralization is similar to VMS accumulations at Betts Cove, Tilt Cove, Colchester Little Bay and Whalesback.

[2.12] References

Bachinski, D.J. 1977. Alteration associated with metamorphosed ophiolitic cupriferous iron sulfide deposits: Whalesback Mine, Notre Dame Bay, Newfoundland. Mineralium Deposita, v.12, p. 48-63.

Badrzadeh Z, Barrett TJ, Peter JM, Gimeno D, Sabzehei M, Aghazadeh M., 2011. Geology, Mineralogy and Sulfur Isotope Geochemistry of the Sargaz Cu–Zn Volcanogenic Massive Sulfide Deposit, Sanandaj–Sirjan zone, Iran. Miner. Deposita, v. 46, p. 905-923.

Barnes, H.L., 1979. Solubilities of ore minerals H.L. Barnes (Ed.), Geochemistry of Hydrothermal Ore Deposits (Second Edition), John Wiley and Sons, New York, Ch. 8. p. 404–460.

Barrie, C.D., Boyle, A.P., Cook, N.J. and Prior, D.J. 2010. Pyrite deformation textures in the massive sulfide ore deposits of the Norwegian Caledonides. Tectonophysics, v. 483, p. 269-286.

Barton, P.B., and Skinner, B.J., 1979. Sulfide mineral stabilities H.L. Barnes (Ed.), Geochemistry of Hydrothermal Ore Deposits (Second Edition), John Wiley and Sons, New York, p. 278–403.

Cawood, P.A., van Gool, J.A.M., and Dunning, G.R., 1996. Geological development of eastern Humber and western Dunnage zones; Corner Brook–Glover Island region, Newfoundland. Canadian Journal of Earth Sciences, v. 33, p. 182–198.

Claypool, G.E., Holser, W.T., Kaplan, I.R., Sakai, H., Zack, I., 1980. The age curves of sulfur and oxygen isotopes in marine sulfate and their mutual interpretation. Chem. Geol, v. 28, p. 199–260.

Cook, N.J., Halls, C., Kaspersen, P.O., 1990. The geology of the Sulitjelma ore field, northern Norway; some new interpretations. Economic Geology, v.85, p. 1720–1737.

Craig, J.R., 1983. Metamorphic features in Appalachian massive sulfides. Mineralogical Magazine, v.47, p. 515-525.

Craig, J.R., 2001. Ore-mineral textures and the tales they tell. Canadian Mineralogist, v.39 (4), p. 937–956.

Craig, J.R., and Vokes, F.M., 1992. Ore mineralogy of the Appalachian–Caledonian stratabound sulfide deposits. Ore Geology Reviews, v.7 (2) p. 77–123.

Craig, J.R., and Vaughan, D.J. 1994. Ore Microscopy and Ore Petrography (Second Edition). Wiley Interscience, New York, N.Y, 434 pages.

Delaney, J.R., Cosens, B.A., 1982. Boiling and metal deposition in submarine hydrothermal systems. Marine Technol Soc J, v.16 (3) p. 62-65.

Dubé, B., Mercier-Langevin, P., Hannington, M.D., Lafrance, B., Gosselin, P., and Gosselin, G., 2007. The LaRonde Penna world-class Au-rich volcanogenic massive sulfide deposit, Abitibi, Québec: Mineralogy and geochemistry of alteration and implications for genesis and exploration. Economic Geology, v. 102, p. 633–666.

Dunning, G.R. and Krogh, T.E. 1985. Geochronology of ophiolites of the Newfoundland Appalachians. Canadian Journal of Earth Sciences, v.22, p. 1659-1670.

Dunning, G.R., Kean, B.F., Thurlow, J.G., and Swinden, H.S., 1987. Geochronology of the Buchans, Roberts Arm, and Victoria Lake Groups and Mansfield Cove Complex, Newfoundland. Canadian Journal of Earth Sciences, v.24, p. 1175–1184.

Eldridge, C.S., Barton, P.B., Ohmoto, H., 1983. Mineral textures and their bearing on formation of the Kuroko orebodies. Econ Geol Monograph 5, p. 241–281.

Faure, G., and Mensing, T.M., 2005. Isotopes: Principles and Applications. Hoboken, John Wiley and Sons, p.824.

Fleming, J.M. 1970. Petrology of the volcanic rocks of the Whalesback area, Springdale Peninsula, Newfoundland. Unpub. M.Sc. thesis, Memorial University, 107 pages.

Franklin, J.M., Lydon, J.W., and Sangster, D.F., 1981. Volcanic-associated massive sulphide deposits. Economic Geology, 75th Anniversary Volume, p. 485–627.

Franklin, J.M., Gibson, H.L., Galley, A.G. and Jonasson, I.R. 2005. Volcanogenic massive sulfide deposits. In Economic Geology 100th Anniversary Volume. Edited by J.W. Hedenquist, J.F.H. Thompson, R.J. Goldfarb and J.P. Richards. Littleton, CO, Society of Economic Geologists, p. 523-560.

Franklin, J. M., 2008. Review of the Little Deer project: Notes re: Property Visit, October 14-15, 2008, Internal Report for Thundermin Resources and Cornerstone Capital Resources, p.5.

Galley, A.G., Hannington, M. and Jonasson, I. 2007. Volcanogenic massive sulphide deposits. In Mineral Deposits of Canada: A Synthesis of Major Deposit-types, District Metallogeny, the Evolution of Geological Provinces, and Exploration Methods. Edited by W.D. Goodfellow. Mineral Deposits Division, Geological Association of Canada, Special Publication 5, pages 141-161.

Gemmell, J.B., Sharpe, R., Jonasson, I.R., and Herzig, P.M., 2004. Sulfur isotope evidence for magmatic contributions to submarine and subaerial gold mineralization: Conical Seamount and the Ladolam gold deposit, Papua New Guinea. Economic Geology, v. 99, p. 1711–1725.

Goldstein, T.P., and Aizenshtat, Z., 1994. Thermochemical sulfate reduction-a review. J. Thermal Analysis, v.42, p. 241–290.

Goodfellow, W.D. and Peter, J.M., 1996. Sulphur isotope composition of the Brunswick No. 12 massive sulphide deposit, Bathurst Mining Camp, New Brunswick: Implications for ambient environment, sulphur source, and ore genesis. Canadian Journal of Earth Sciences, v. 33, p. 231-251.

Goodfellow, W.D., McCutcheon, S.R., 2003. Geologic and genetic attributes of volcanic sediment-hosted massive sulfide deposits of the Bathurst Mining Camp, northern New Brunswick—A synthesis. In: Goodfellow, W.D., McCutcheon, S.R., Peter, J.M. (Eds.), Massive Sulphide Deposits of the Bathurst Mining Camp, New Brunswick, and Northern Maine. Economic Geology Monograph, v. 11, p. 245–310.

Hannington, M.D., Poulsen, K.H., Thompson, J.F.H., and Sillitoe, R.H., 1999. Volcanogenic gold in the massive sulfide environment. Reviews in Economic Geology, v.8, p. 324-356.

Harrison A.G. and Thode H.G., 1957. The kinetic isotope effect in the chemical reduction of sulphate. Tram. Faraday Soc., v.53, p.1648-1651.

Hedenquist, J.W., Lowenstern, J.B., 1994. The role of magmas in the formation of hydrothermal ore deposits. Nature, 370, p. 519–527.

Herzig, P.M., Petersen, S., Hannington, M., 1998. Geochemistry and sulfur-isotopic composition of the TAG hydrothermal mound, Mid-Atlantic Ridge, 26°N. In: Herzig PM, Humphris SE, Miller J (eds) Proc ODP 158, Scientific Results, College Station, TX, p. 47–70.

Hinchey, J.G. 2011. The Tulks Volcanic Belt, Victoria Lake supergroup, central Newfoundland - geology, tectonic setting, and volcanogenic massive sulfide mineralization. Newfoundland and Labrador Department of Natural Resources, Geological Survey, Report 2011-02, pages 167.

Hoefs, J., 2009. Stable Isotope Geochemistry, Berlin Heidelberg, Springer-Verlag, p. 71.

Huston, D.L., Power, M., Gemmell, J.B., Large, R.R., 1995. Design, calibration and geological application of the first operational Australian laser ablation sulphur isotope microprobe. Aust J Earth Sci, v.42, p.549–555.

Huston, D.L., 1999. Stable isotopes and their significance for understanding the genesis of volcanic-hosted massive sulfide deposits. A Review, Rev. Econ. Geol. v.8, p. 157–179.

Huston, D.L., Brauhart, C.W., Drieberg, S.L., Davidson, G.J., Groves, D.I., 2001. Metal leaching and inorganic sulfate reduction in volcanic-hosted massive sulfide mineral systems: evidence from the paleo-Archean Panorama district, Western Australia. Geology, v. 29 p. 687–690.

Hutchinson, R.W., and Searle, D.L., 1971. Stratabound pyrite deposits in Cyprus and relation to other sulfide ores. Mining Geology Society of Japan. Special Publication, v.3, p. 198-2005.

Kean, B. F., and Evans, D.T.W., 1988. Mineral deposits of the Lushs Bight Group, in Swinden, H.S., and Kean, B. F., eds., The Volcanogenic Sulphide Districts of Central Newfoundland, A guidebook and reference manual for volcanogenic sulphide deposits in the early Paleozoic oceanic volcanic terranes of central Newfoundland: St. John's, NL, Canada, Mineral Deposits Division, Geological Association of Canada, p. 80-90.

Kean, B.F., Evans, D.T.W. and Jenner, G.A. 1995. Geology and mineralization of the Lushs Bight Group. Newfoundland and Labrador Department of Natural Resources, Geological Survey, Report 95-02, 204 pages.

Kelly, W.C., Clark, B.R., 1975. Sulphide deformation studies: III. Experimental deformation of chalcopyrite to 2000 bars and 500°C Econ. Geol.. v.70, p. 431–453.

Kidd, W. S. F., 1977. The Baie Verte Lineament, Newfoundland: Ophiolite complex floor and mafic volcanic fill of a small Ordovician marginal basin. In Island arcs, deep sea trenches and back-arc basins. Edited by M. Talwani, and W. C. Pitman. American Geophysical Union, Maurice Ewing Series 1, p. 407-418.

Large, R.R., 1977. Chemical evolution and zonation of massive sulphide deposits in volcanic terrains: Economic Geology, v. 72, p. 549-572.

Large, R.R., 1992. Australian Volcanic-Hosted Massive Sulfide Deposits: Features, Styles, and Genetic Models. Economic Geology, v. 87, p. 471-510.

Lydon, J.W., 1988. Ore deposit models #14: Volcanogenic massive sulphide deposits Part 2: genetic models. In: Roberts R.G., Sheahan, P.A., (eds) Ore deposit models. Geosci Can, v.15 (1), p. 43-65.

Marcoux, E., Moëlo, Y., Leistel, J.M., 1996. Bismuth and cobalt minerals as indicators of stringer zones to massive sulfide deposits, Iberian Pyrite Belt. Mineralium Deposita, v.31, p. 1-26.

Marshall, B., Gilligan, L.B., 1993. Remobilization, syn-tectonic processes and massive sulphide deposits. Ore Geol Rev, v.8, p.39–64.

Memorial University of Newfoundland. The Scanning Electron Microscope (SEM). [Online]. Available at: http://www.mun.ca/research/ocp/creait/maf/SEM.php. [Accessed on: 26.03.2012].

Memorial University of Newfoundland. The Secondary Ion Mass Spectrometry (SIMS) Laboratory. [Online]. Available at:

http://www.mun.ca/research/ocp/creait/maf/SIMS.php [Accessed on: 26.03.2012].

Norman, R.E., and Strong, D.F., 1975. The geology and geochemistry of ophiolitic rocks exposed at Mings Bight, Newfoundland. Canadian Journal of Earth Sciences, v.12, p. 777-797.

Ohmoto, H., 1996. Formation of volcanogenic massive sulphide deposits: the Kuroko perspective. Ore Geol. Rev. v.10, p. 135–177.

Ohmoto, H., Rye, R.O. 1979. Isotopes of sulfur and carbon. In: Geochemistry of hydrothermal ore deposits (Second Edition). Holt Rinehart and Winston, New York, p.509-567.

Ohmoto, H., Goldhaber, M.B., 1997. Sulfur and carbon isotopes. In: Barnes HL (ed.) Geochemistry of hydrothermal ore deposits, 3rd edn. New York, Wiley, p. 435–486.

Ohmoto, H., Mizukami, M., Drummond, S.E., Eldridge, C.S., Pisutha-Arnond, V., and Lenagh, T.C., 1983. Chemical processes of Kuroko formation: Economic Geology Monograph 5, p. 570–604.

Papezik, V.S., 1967. Native Arsenic in Newfoundland. The Canadian Mineralogist, p.101-108.

Papezik, V.S. and Fleming, J.M. 1967. Basic volcanic rocks of the Whalesback area, Newfoundland. Geological Association of Canada, Special Paper, v.4, p.181-192.

Piercey, S.J., 2007. Volcanic Massive Sulfide (VMS) of the Newfoundland Appalachians: An Overview of their Setting, Classification, Grade-Tonnage

Data and Unresolved Questions, Newfoundland and Labrador Department of Natural Resources Geological Survey, Report 07-1, p.169-178.

Piercey, S. J., and Hinchey, J. G., 2012. Volcanogenic massive sulphide (VMS) deposits of the Central Mobile Belt, Newfoundland. Geological Association of Canada–Mineralogical Association of Canada Joint Annual Meeting, Field Trip Guidebook B4. , Open File NFLD/3173, Newfoundland and Labrador Department of Natural Resources, Geological Survey, p. 56.

Plimer, I.R., and Finlow-Bates, T., 1978. Relationship between primary iron sulphide species, sulphur source, depth of formation and age of submarine exhalative deposits Mineral. Deposita, v.13, p. 399–410.

Pressacco, R., 2010. Memorandum: Mineral Resource Update for the Little Deer Project undertaken by Scott Wilson Roscoe Postle Associates Inc. for Thundermin Resources Inc. and Cornerstone Capital Resources Inc., National Instrument 43-101 Memorandum: Toronto, ON, Canada, p. 1-26.

Putrich, E., Ewert, W., Rodgers, K., Pearson, J.L., Orava, D. and Hayden, A. 2011. Technical report and preliminary economic assessment of the Little Deer Copper Deposit, Newfoundland, Canada for Cornerstone Capital Resources and Thundermin Resources, Toronto, ON, Canada. National Instrument 43-101 Technical Report, 86 pages.

Robb, L., 2005. Introduction to ore-forming processes. Blackwell, Oxford, p. 174-186.

Rollinson, H. R., 1993. Using Geochemical Data: Evaluation, Presentation, Interpretation. United Kingdom, Longman Group UK Ltd, p.304.

Roth, T., Thompson, J.F.H., Barrett, T.J. 1999. The precious metal-rich Eskay Creek deposit, Northwestern British Columbia. In Volcanic-Associated Massive

Sulfide Deposits. In: Barrie, C.T. Hannington, M.D. (Eds.), Volcanic-Associated Massive Sulfide Systems: Processes and Examples in Modern and Ancient Settings. Reviews in Economic Geology, v.8, p. 357–373.

Sawkins, F.J., 1986. Some thoughts on the genesis of Kuroko-type deposits, in Geology in the real world-the Kingsley Dunham volume: Institute of Mining and Metallurgy, p. 387–394.

Sawkins, F.J., 1994. Integrated tectonic-genetic model for volcanic-hosted massive sulfide deposits. Geology, v. 18, p. 1061–1064.

Schoonen, M.A.A., and Barnes, H.L., 1991. Reactions forming pyrite: I. Nucleation of FeS_2 below 100°C. Geochim. Cosmochim. Acta, v.55, p. 1495–1504.

Shanks, W.C., III, and Seyfried, W.E., Jr., 1987. Stable isotope studies of vent fluids and chimney minerals, southern Juan de Fuca Ridge: Sodium metasomatism and seawater sulfate reduction. Journal of Geophysical Research, v. 92, p. 11 387–399.

Sillitoe, R.H., Hannington, M.D., Thompson, J.F.H., 1996. High sulfidation deposits in the volcanogenic massive sulfide environment, Economic Geology, p. 91 - 204.

Skulski, T., Castonguay, S., McNicoll, V., van Staal, C., Kidd, W., Rogers, N., Morris, W., Ugalde, H., Slavinski, H., Spicer, W., Moussallam, Y. and Kerr, I. 2010. Tectonostratigraphy of the Baie Verte Oceanic Tract and its ophiolite cover sequence on the Baie Verte Peninsula. In Current Research. Newfoundland and Labrador Department of Natural Resources, Geological Survey, Report 10-1, pages 315-225.

Slack, J.F., Foose, M.P., Flohr, M.J.K., 2003. Exhalative and subsea-floor replacement processes in the formation of the Bald Mountain massive sulfide deposit, Northern Maine. Econ Geol Monograph, v.11, p.513–547.

Stanton, R.L., 1990. Magmatic evolution and the ore type-lava affiliations of volcanic exhalative ores. Australasia Institution of Mining and Metallurgy, Monograph, v.14, p. 101-107.

Sundblad, K., 1980. A tentative "volcanogenic" formation model for the sediment-hosted Ankarvattnet Zn-Cu-Pb massive sulphide deposit, Central Swedish Caledonides. Norg. Geol. Unders. Bulletin 57, p. 211–227.

Swinden, H.S. 1991. Paleotectonic settings of volcanogenic massive sulphide deposits in the Dunnage Zone, Newfoundland Appalachians. Canadian Institute of Mining and Metallurgy Bulletin, v.84, p. 59-89.

Swinden, H.S. 1996. The application of volcanic geochemistry in the metallogeny of volcanic-hosted sulphide deposits in central Newfoundland. In Trace Element Geochemistry of Volcanic Rocks: Applications for Massive Sulfide Exploration. Edited by D.A. Wyman. Geological Association of Canada, Short Course Notes, v.12, p. 329-358.

Swinden, H. S., and Kean, B. F., 1988. Eds. Volcanogenic sulphide districts of central Newfoundland: St. John's, Newfoundland, Geological Association of Canada, Mineral Deposits Division, ed. 1, p.1-238.

Swinden, H.S., and Dunsworth, S.M., 1995. Metallogeny, in Williams, H., ed., The Appalachian/Caledonian Orogen: Canada and Greenland. Geological Survey of Canada, Geology of Canada, No. 6, p. 681-814.

Tivey, M.K., Humphris, S.E., Thompson, G., Hannington, M.D., Rona, P.A., 1995. Deducing patterns of fluid flow and mixing within the TAG active hydrothermal mound using mineralogical and geochemical data. J Geophys Res, v.100, p.12527–12555.

Tuach, J. 1988. Geology and sulphide mineralization in the Pacquet Harbour Group. In The Volcanogenic Sulfide Districts of Central Newfoundland. Edited by H.S. Swinden and B.F. Kean. Geological Association of Canada, p. 49-53.

Tuach, J. and Kennedy, M.J. 1978. The geologic setting of the Ming and other sulfide deposits, Consolidated Rambler Mines, Northeast Newfoundland. Economic Geology, v.73, p. 192-206.

University of Toronto. Microprobe Lab. [Online] Available at: http://www.geology.utoronto.ca/facilities/electron-probe-x-ray-microanalyzer-empa [Accessed 26.03.2012]

van Staal, C. 2007. Pre-Carboniferous tectonic evolution and metallogeny of the Canadian Appalachians. In Mineral Deposits of Canada: A Synthesis of Major Deposit-types, District Metallogeny, the Evolution of Geological Provinces, and Exploration Methods. Edited by W.D. Goodfellow. Mineral Deposits Division, Geological Association of Canada, Special Publication 5, p. 793-818.

van Staal, C.R., Whalen, J.B., McNicoll, V.J., Pehrsson, S., Lissenberg, C.J., Zagorevski, A., van Breemen, O., and Jenner, G.A., 2007. The Notre Dame arc and the Taconic orogeny in Newfoundland, in Hatcher, R.D., Jr., Carlson, M.P., McBride, J.M., and Martínez Catalán, J.R., eds., 4-D Framework of Continental Crust: Geological Society of America Memoir 200, p. 511–552.

van Staal, C. and Barr, S.M. In press: Lithospheric architecture and tectonic evolution of the Canadian Appalachians and associated Atlantic margin. Chapter 2 in Tectonic Styles in Canada: the Lithoprobe Perspective. Edited by J.A. Percival, F.A. Cook and R.M. Clowes. Geological Association of Canada, Special Paper 49.

West, J.M. 1972. Structure and ore-genesis; Little Deer Deposit, Whaleback Mine, Springdale, Newfoundland. Unpub. M.Sc. thesis, Queen's University, p.1-71.

Williams, H. 1979. Appalachian Orogen in Canada. Canadian Journal of Earth Sciences, v.16, p. 792-807.

Williams, H., and Grant, A.C., 1998, Tectonic Assemblages, Atlantic Region, Canada: Geological Survey of Canada, Tectonic Assemblages, Atlantic Region, Canada, Open File 3657, scale: 1:3,000,000.

Williams, H., Colman-Sadd, S.P. and Swinden, H.S. 1988. Tectonostratigraphic subdivisions of central Newfoundland. In Current Research, Part B. Geological Survey of Canada, Paper 88-1B, p. 91-98.

Yang, K. and Scott, S.D., 1996. Possible contribution of a metal-rich magmatic fluid to a sea-floor hydrothermal system. Nature, v.383, p. 420–423.

Zaccarini, F. and Garuti, G., 2008. Mineralogy and chemical composition of VMS deposits of northern Apennine ophiolites, Italy: evidence for the influence of country rock type on ore composition. Miner Petrol, v.84, p. 61–83.

Chapter 2 Figure

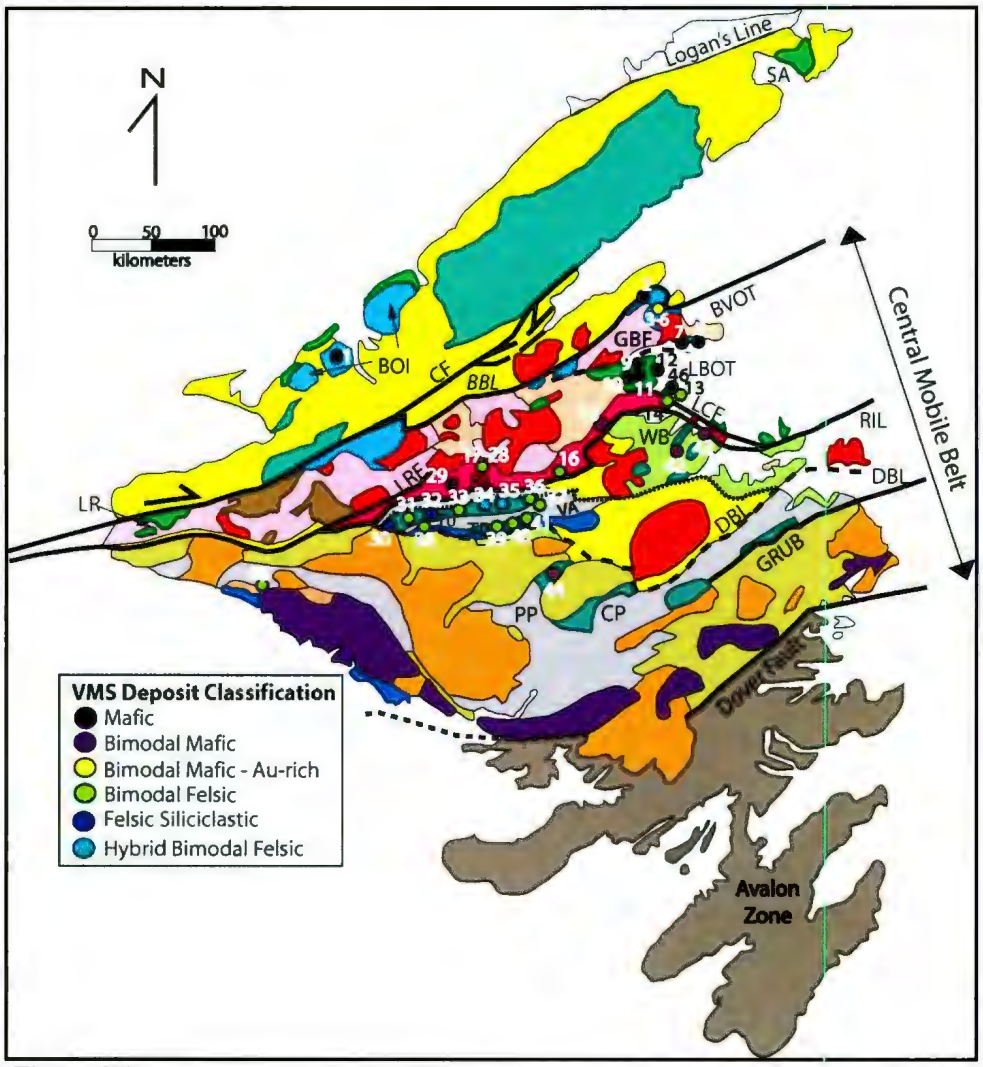

Figure 2.1 The tectonostratigraphic zones (and subzones), accretionary tracts and VMS deposits of the Newfoundland Appalachians. The Little Deer VMS deposit (# 10) is situated in the Notre Dame Subzone of the Dunnage Zone. Legend for map on page 83. Abbreviations: BBL - Baie Verte Brompton Line; BOI - Bay of Islands; BVOT - Baie Verte Oceanic Tract; CF - Cabot Fault; CP - Coy Pond Complex; DBL - Dog Bay Line; GBF - Green Bay Fault; GRUB - Gander River Ultramafic Belt; LBOT - Lushs Bight Oceanic Tract; LCF - Lobster Cove Fault; LR - Long Range; LRF - Lloyds River Fault; PP - Pipestone Pond Complex; RIL - Red Indian Line; SA - St. Anthony; TP - Tally Pond Belt; TU - Tulks Volcanic Belt; VA - Victoria Arc and WB - Wild Bight Group. Map Modified from van Staal (2007) and van Staal and Barr (in press). Volcanogenic massive sulfide (VMS) deposit classification from Piercey (2007), Hinchey (2011), and Piercey and Hinchey 2012).

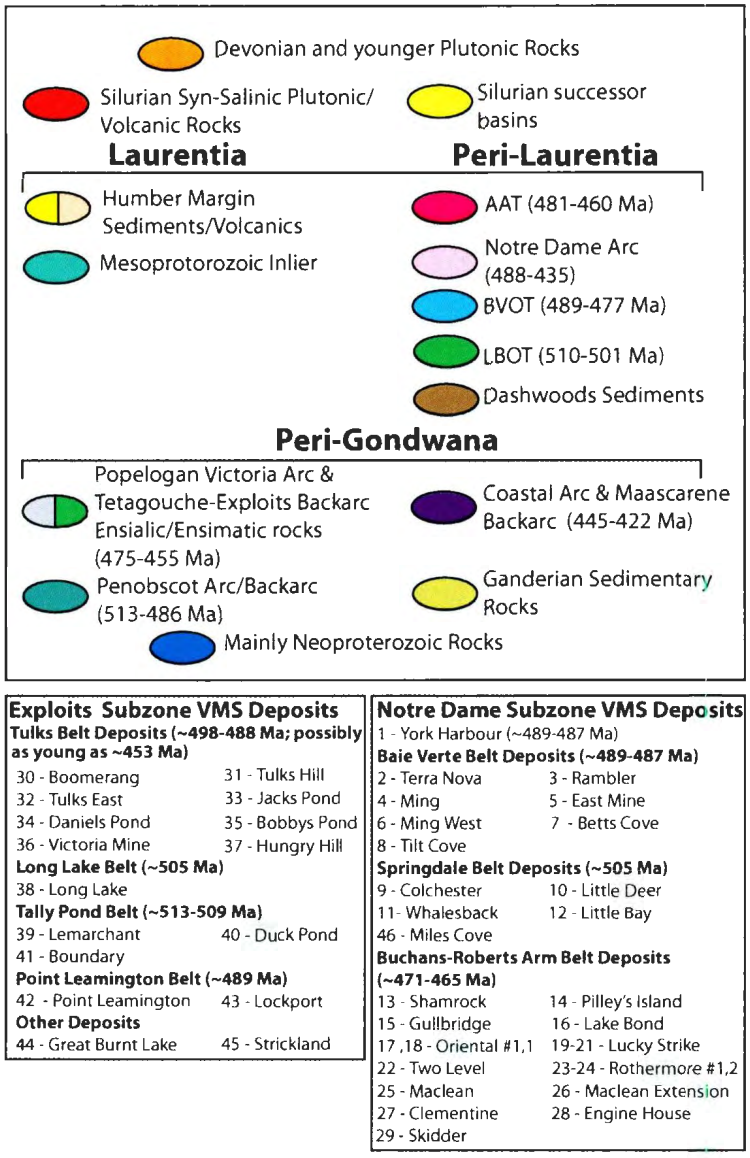

Exploits Subzone VMS Deposits

Tulks Belt Deposits (~498-488 Ma; possibly as young as ~453 Ma)

30 - Boomerang	31 - Tulks Hill
32 - Tulks East	33 - Jacks Pond
34 - Daniels Pond	35 - Bobbys Pond
36 - Victoria Mine	37 - Hungry Hill

Long Lake Belt (~505 Ma)

38 - Long Lake

Tally Pond Belt (~513-509 Ma)

39 - Lemarchant	40 - Duck Pond
41 - Boundary	

Point Leamington Belt (~489 Ma)

42 - Point Leamington	43 - Lockport

Other Deposits

44 - Great Burnt Lake	45 - Strickland

Notre Dame Subzone VMS Deposits

1 - York Harbour (~489-487 Ma)

Baie Verte Belt Deposits (~489-487 Ma)

2 - Terra Nova	3 - Rambler
4 - Ming	5 - East Mine
6 - Ming West	7 - Betts Cove
8 - Tilt Cove	

Springdale Belt Deposits (~505 Ma)

9 - Colchester	10 - Little Deer
11- Whalesback	12 - Little Bay
46 - Miles Cove	

Buchans-Roberts Arm Belt Deposits (~471-465 Ma)

13 - Shamrock	14 - Pilley's Island
15 - Gullbridge	16 - Lake Bond
17 ,18 - Oriental #1,1	19-21 - Lucky Strike
22 - Two Level	23-24 - Rothermore #1,2
25 - Maclean	26 - Maclean Extension
27 - Clementine	28 - Engine House
29 - Skidder	

Figure 2.1 cont: Legend for the tectonostratigraphic zones (and subzones), accretionary tracts and VMS deposits of the Newfoundland Appalachians. Volcanogenic massive sulfide (VMS) deposit classification from Piercey (2007), Hinchey (2011), and Piercey and Hinchey 2012).

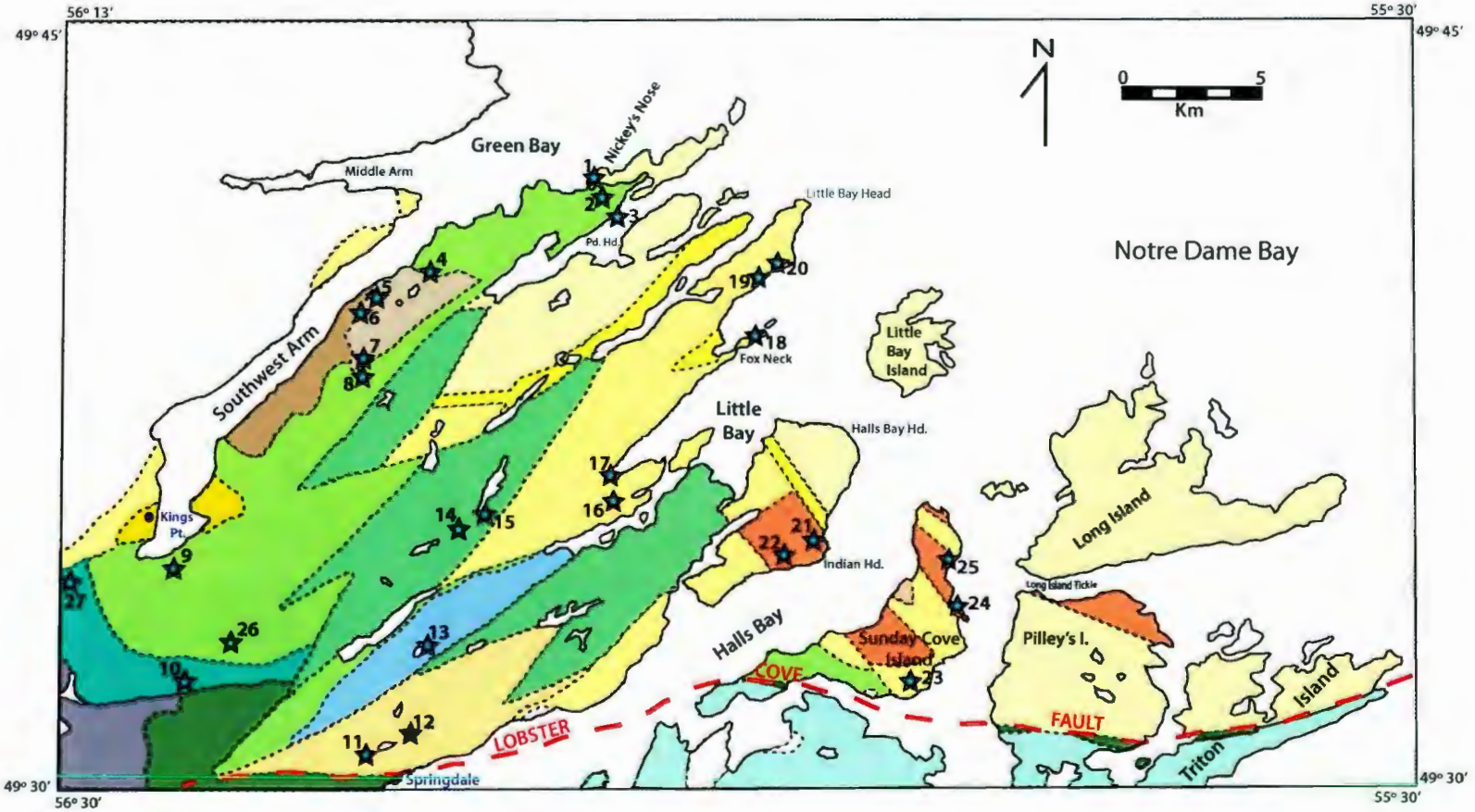

Figure 2.2 Geological map of the Springdale Peninsula together with VMS occurrences within the region (legend for map on page 85). From Kean *et al.* (1995).

Figure 2.2 cont.

Legend for the geological map of the Springdale Peninsula with VMS identification. From Kean *et al.* (1995).

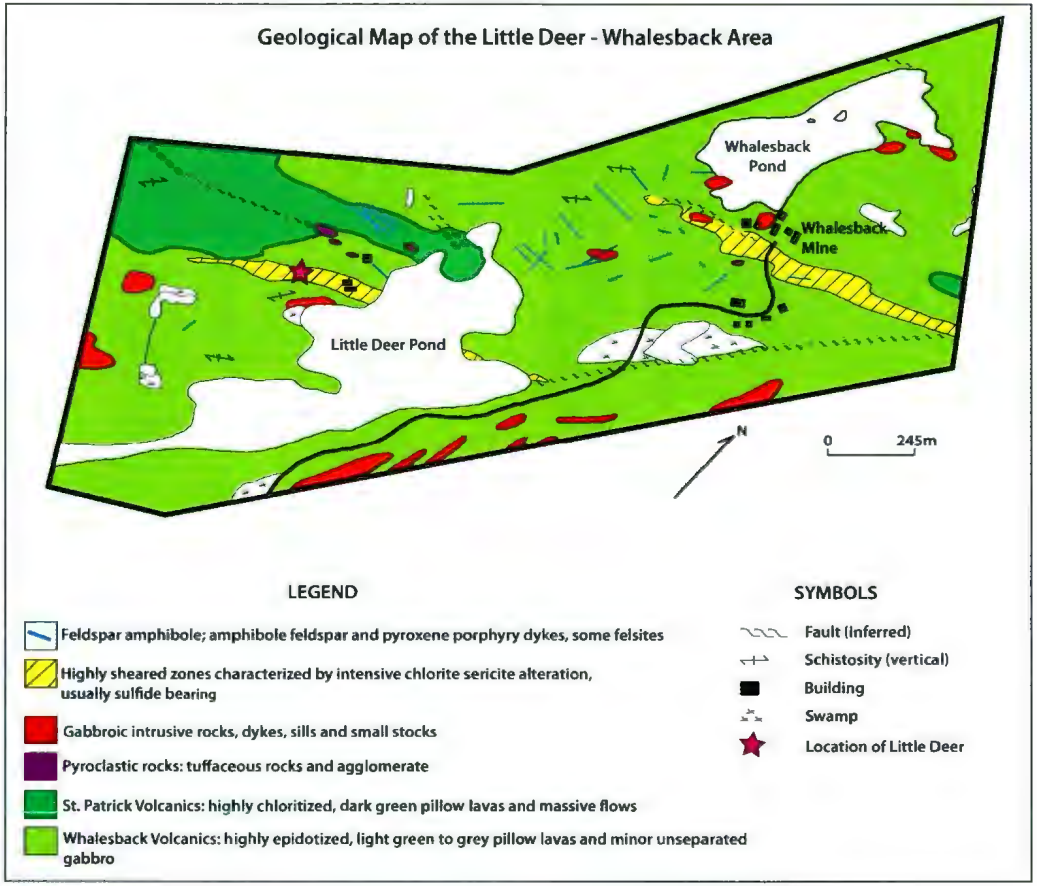

Figure 2.3 See page 87 for figure caption

Figure 2.3 cont
Local geology of the Whalesback – Little Deer area. Based on their alteration facies, Papezik and Fleming (1967) and Fleming (1970) divided the Little Deer area into the 'Whalesback Volcanics' (highly epidotized tholeiitic pillow lavas) and the St. Patrick's Volcanics (highly chloritized tholeiitic pillow lavas). The Little Deer VMS deposit, according to this division, is located in a schist zone within the Whalesback Volcanics. From Papezik and Fleming (1967); Fleming (1970) and Kean *et al.* (1995) (coordinates for map not available on original map).

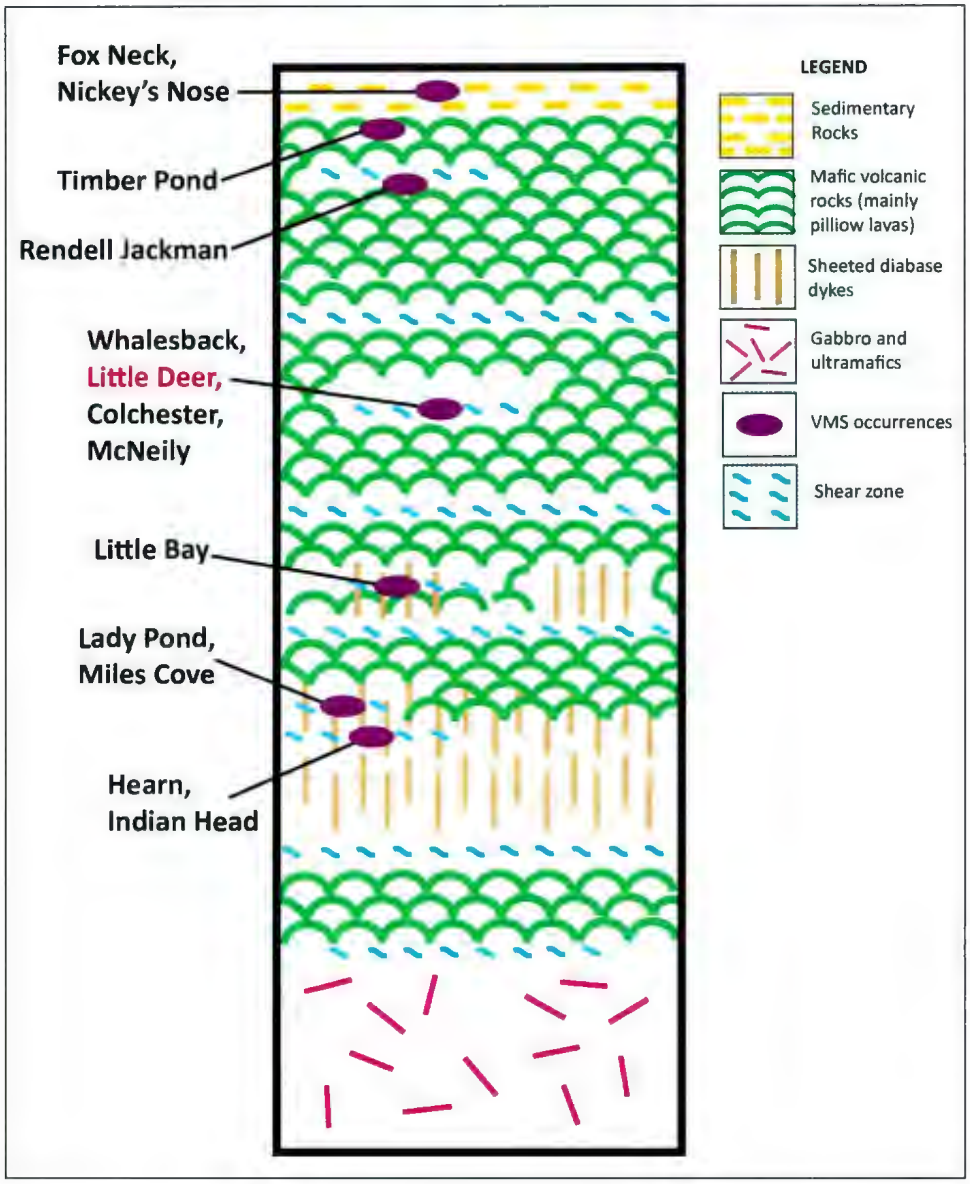

Figure 2.4 Stratigraphic setting for VMS occurrences within the Lushs Bight Group. Mineralization is almost exclusively associated with chlorite-schist zones developed within the pillow lava section of the ophiolite sequence. From Kean *et al.* (1995).

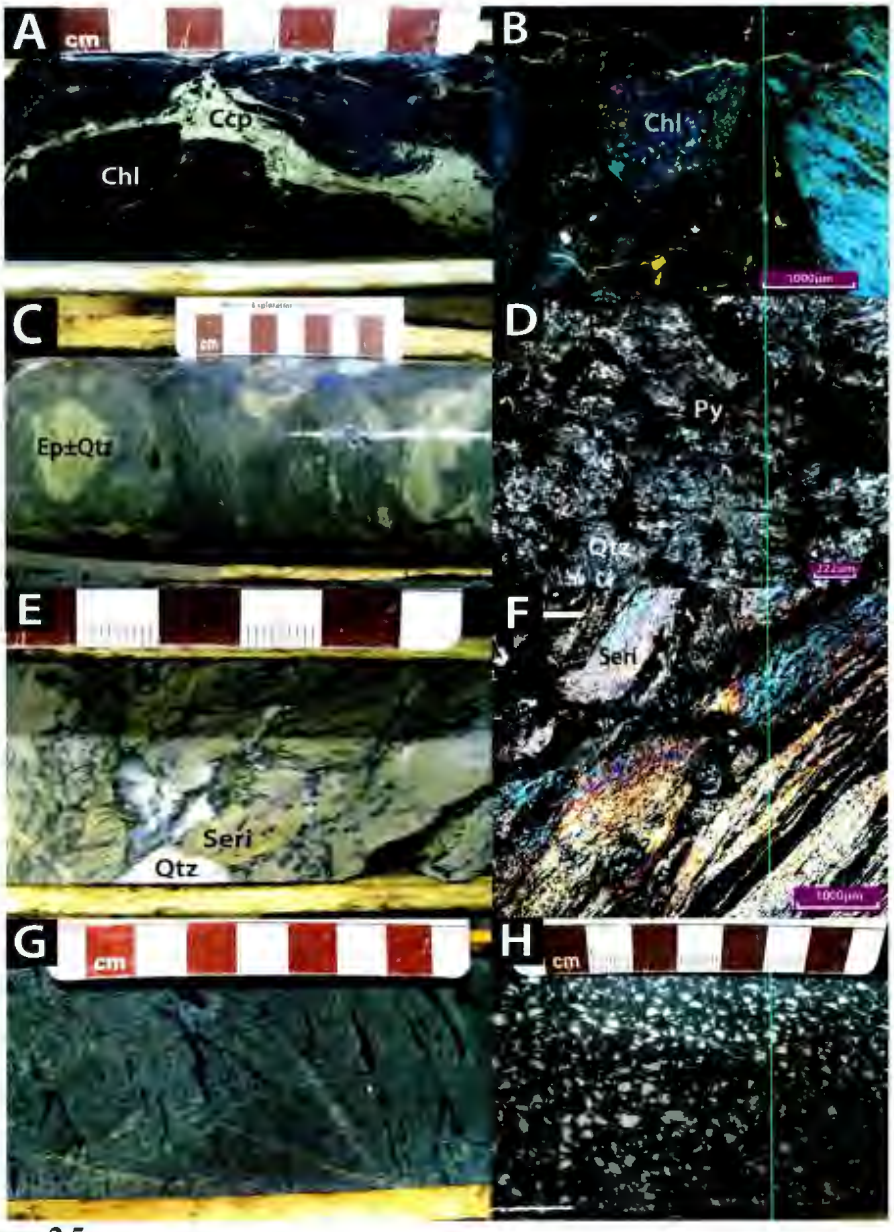

Figure 2.5

Lithologies at Little Deer. (A) Intensely chlorite altered basalt with a dark green to black appearance. (B) Chlorite alteration (cross polarized light) has a peacock blue color; chlorite has been identified as ripidolite. (C) Epidote (± quartz) altered host rock with apple green color. (D) Quartz alteration viewed under cross polarized light. (E) Intensely sericite (± quartz) altered host rock with white/bleached color. (F) Sericite alteration (cross polarized light). (G) Mafic dyke that is light grey in color with an aphanitic texture. (H) Porphyritic dyke - phenocryst assemblage consisting of subhedral-euhedral plagioclase crystals occurring within an aphanitic groundmass.

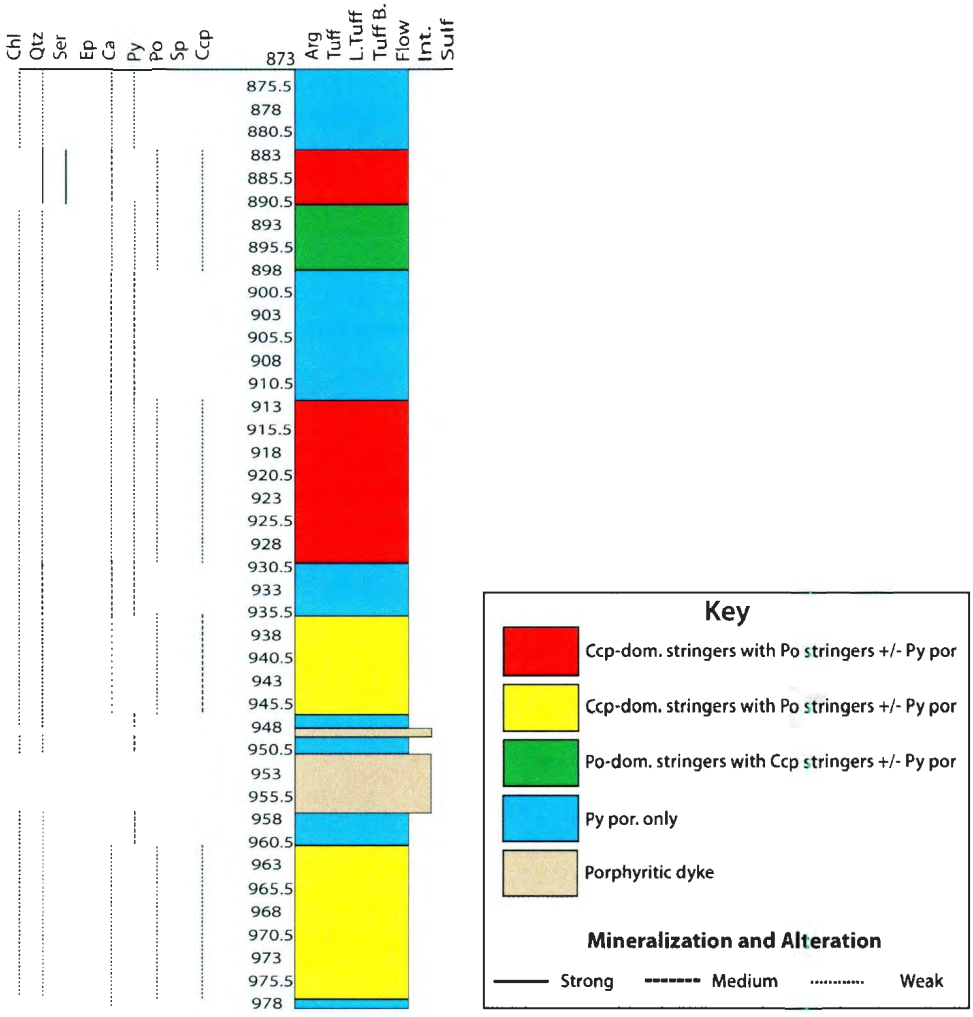

Figure 2.6

Representative graphic log, LD-08-16A, from Little Deer. Pyrite dominated facies commonly occurs at the beginning and at the end of each sulfide intersection (i.e. each section of drill core logged). Pyrrhotite-dominated stringers are commonly associated with chalcopyrite-stringers ± pyrite porphyroblasts; likewise, chalcopyrite-dominated stringers are commonly associated with pyrrhotite-stringers ± pyrite porphyroblasts. All graphic logs from Little Deer are available in Appendix A, Section A.1. Abbreviations: Arg. = Argillite; L. Tuff = Lapilli Tuff; Tuff B. = Tuff Breccia; Flow = Flow; Int. = Intrusion and Sulf. = Massive Sulfide

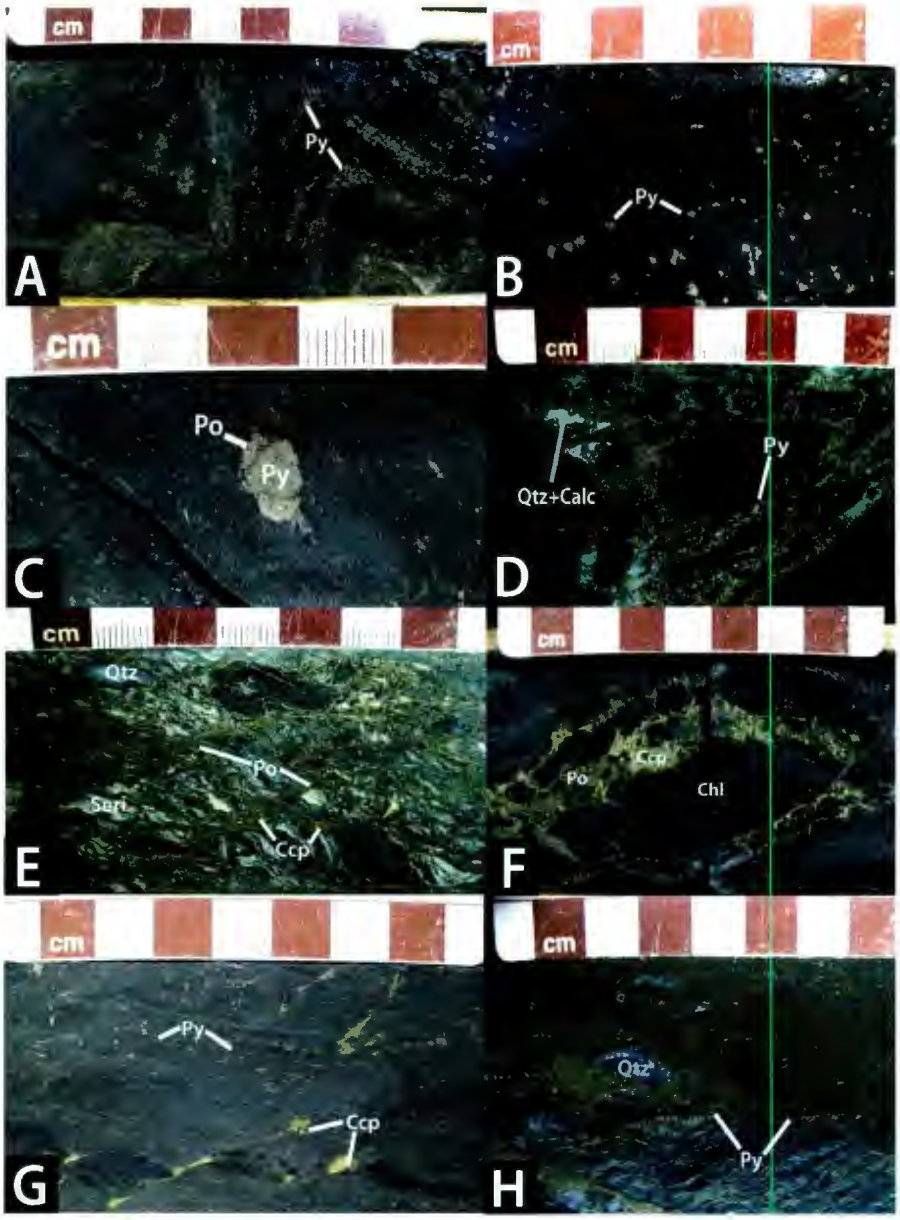

Figure 2.7

Mineralization at Little Deer. **(A)-(D) Pyrite-dominated facies:** (A) Pyrite porphyroblasts following the fabric of the host rock. (B) Buck shot sulfides with pyrite porphyroblasts. (C) Amalgamated pyrite forming a larger pyrite porphyroblast with pyrrhotite tail. (D) Pyrite overprinting calcite and quartz veins. **(E)-(O) Chalcopyrite-pyrrhotite-dominated facies:** (E) Pyrrhotite stringers anastomosing through the host rock and associated with intense sericite/quartz alteration. (F) Chalcopyrite stringers anastomosing through the host rock and associated with chlorite alteration. (G) Chalcopyrite textural thickening in crenulation cleavage hinge zones (H) Pyrite stringers that are not comprised of pyrite porphyroblasts.

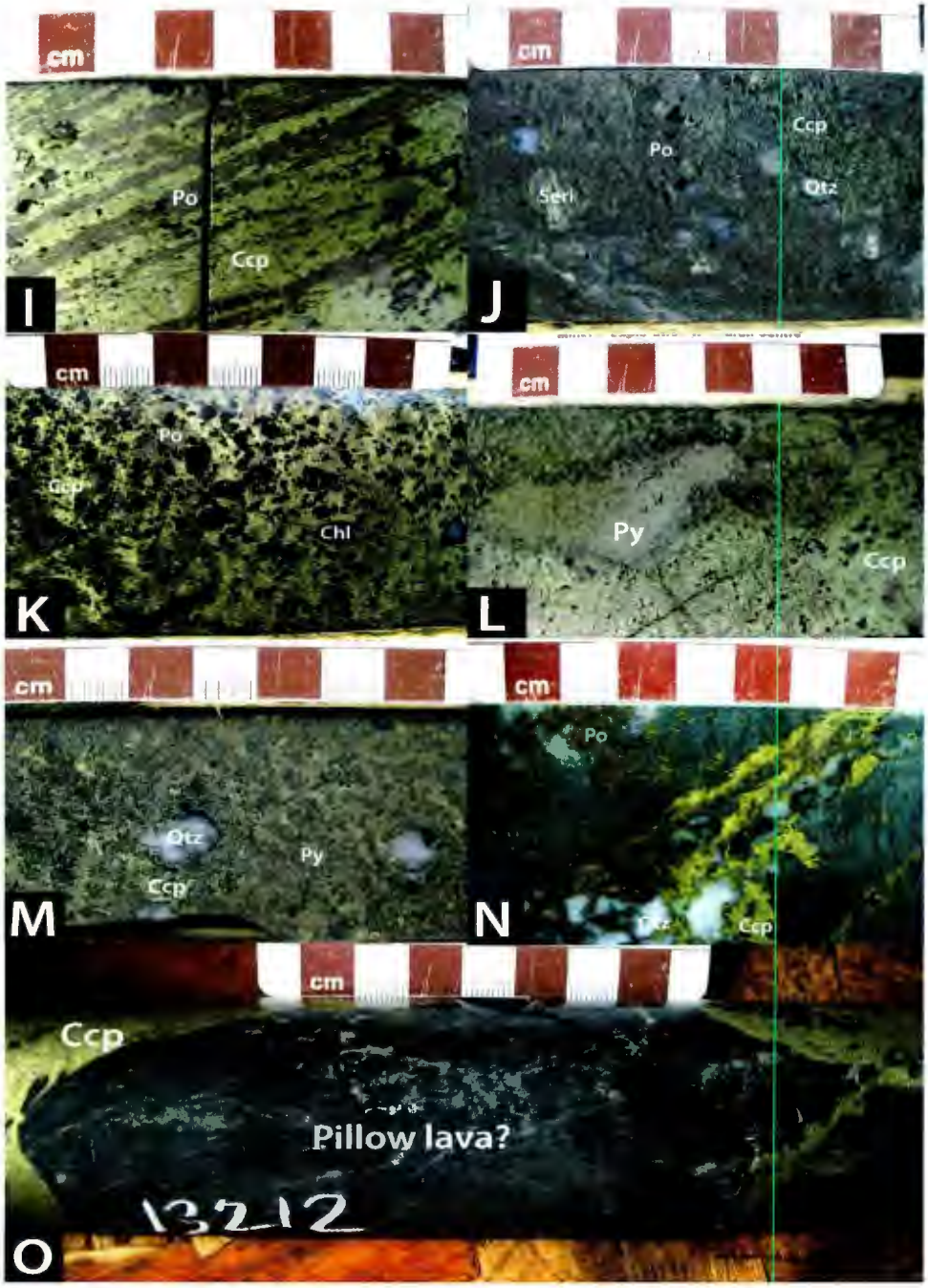

Figure 2.7 cont.

(I) Chalcopyrite and pyrrhotite metamorphic banding within a semi-massive sulfide horizon. (J) Pyrrhotite dominated semi-massive/massive horizons with sericite/quartz altered rock fragments. (K) Chalcopyrite dominated horizons with chlorite altered ± quartz altered rock fragments. (L) Coarse grained patches/masses of pyrite replacing chalcopyrite. (M) Pyrite and chalcopyrite semi-massive horizon. (N) Remobilized chalcopyrite and pyrrhotite. (O) Possible primary mineralization: chalcopyrite dominated stringers lacking durchbewegung textures that anastamose around a tear-shaped (possibly pillow lava) rock fragment.

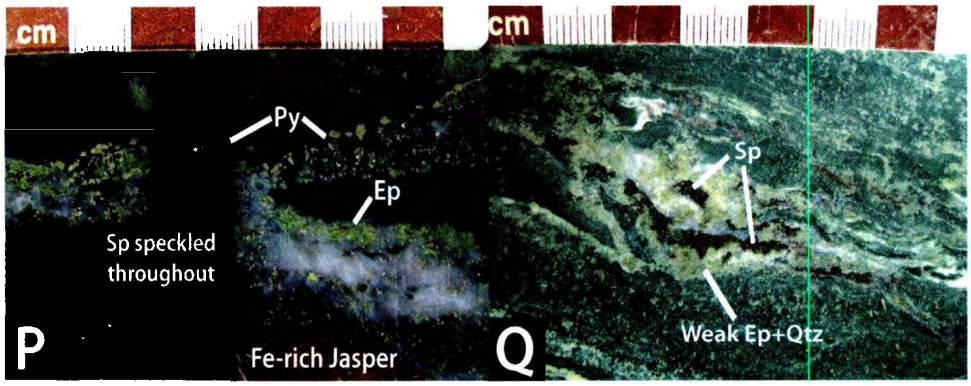

Figure 2.7 cont.

(P)-(Q) Pyrite-sphalerite-pyrrhotite dominated facies: (P) Pyrite porphyroblast horizons are associated with sphalerite, Fe-rich jasper, and epidote ± quartz alteration. (Q) Sphalerite veinlets associated with epidote and quartz alteration.

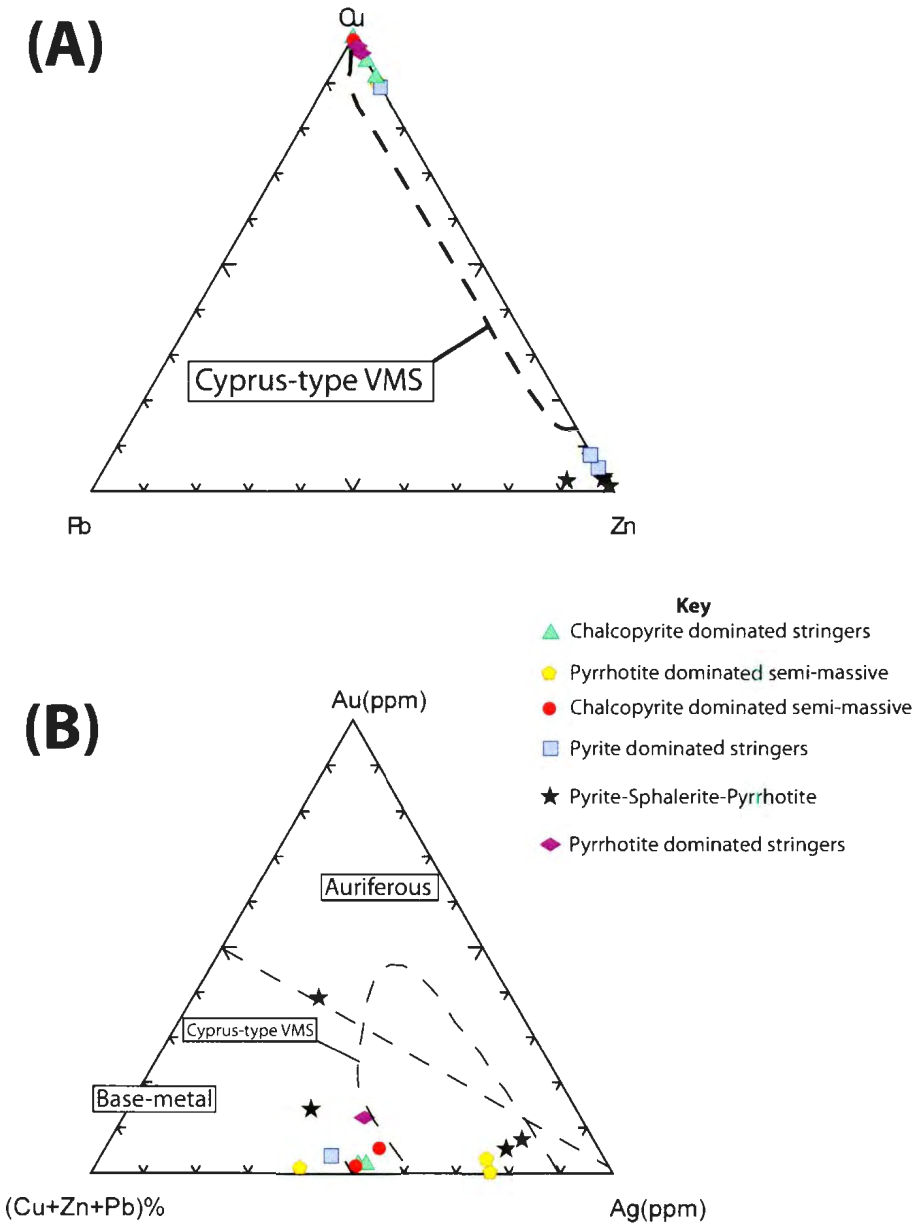

Figure 2.8

Ternary Zn-Cu-Pb (A) and Ag-Au-(Cu-Zn-Pb) (B) for Little Deer sulfide samples. Fields for Cyprus-type VMS deposits from Zaccarini and Garuti (2008).

(A)

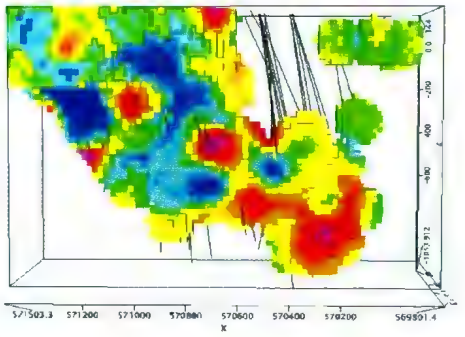


Cu (%)
0.17
0.51
0.85
1.19
1.53
1.87
2.21
2.55
2.89
3.23
3.57
3.91
4.25
4.59
4.93
5.27
5.61
5.95
6.46
6.80

(B)

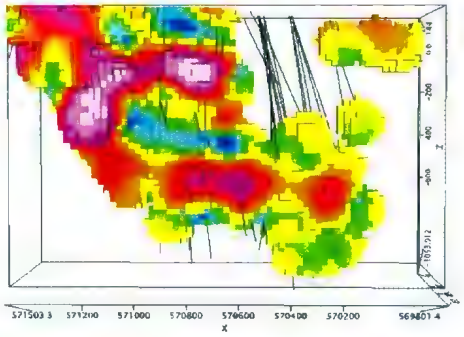


Zn (%)
0.07
0.21
0.35
0.49
0.63
0.77
0.91
1.05
1.19
1.33
1.47
1.61
1.75
1.89
2.03
2.17
2.31
2.45
2.59
2.73

(C)

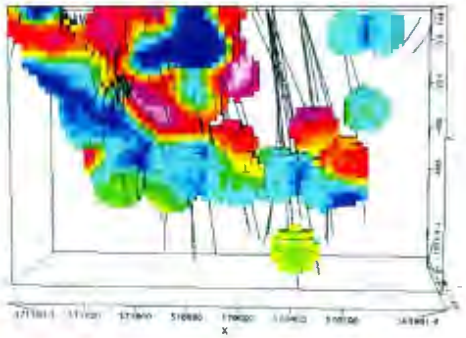


Zn (%)
Cu (%)

Figure 2.9
Contoured plots of metal concentrations for (A) Cu and (B) Zn in the Little Deer VMS deposit. C) Contour plot of Cu/(Cu+Zn) ratio in the Little Deer VMS deposit. High Cu and Cu/(Cu+Zn) zones generally correspond to the chalcopyrite-pyrrhotite dominated sulfide facies; Zn-rich zones and lower Cu/(Cu+Zn) generally correspond to the pyrite-sphalerite-pyrrhotite facies, often associated with jasper. Longitudinal section looking SSE. Parameters for models: X and Y are UTM coordinates: X channel = DH_East; Y channel = DH_North; Z is metres above sea level: Z elevation = DH_RL. The UTM datum = North American Datum, 1972 (NAD27) with a local datum transform = [NAD27] (9m) Canada – New Brunswick, NL; Projection method (UTM zone): UTM 21S.

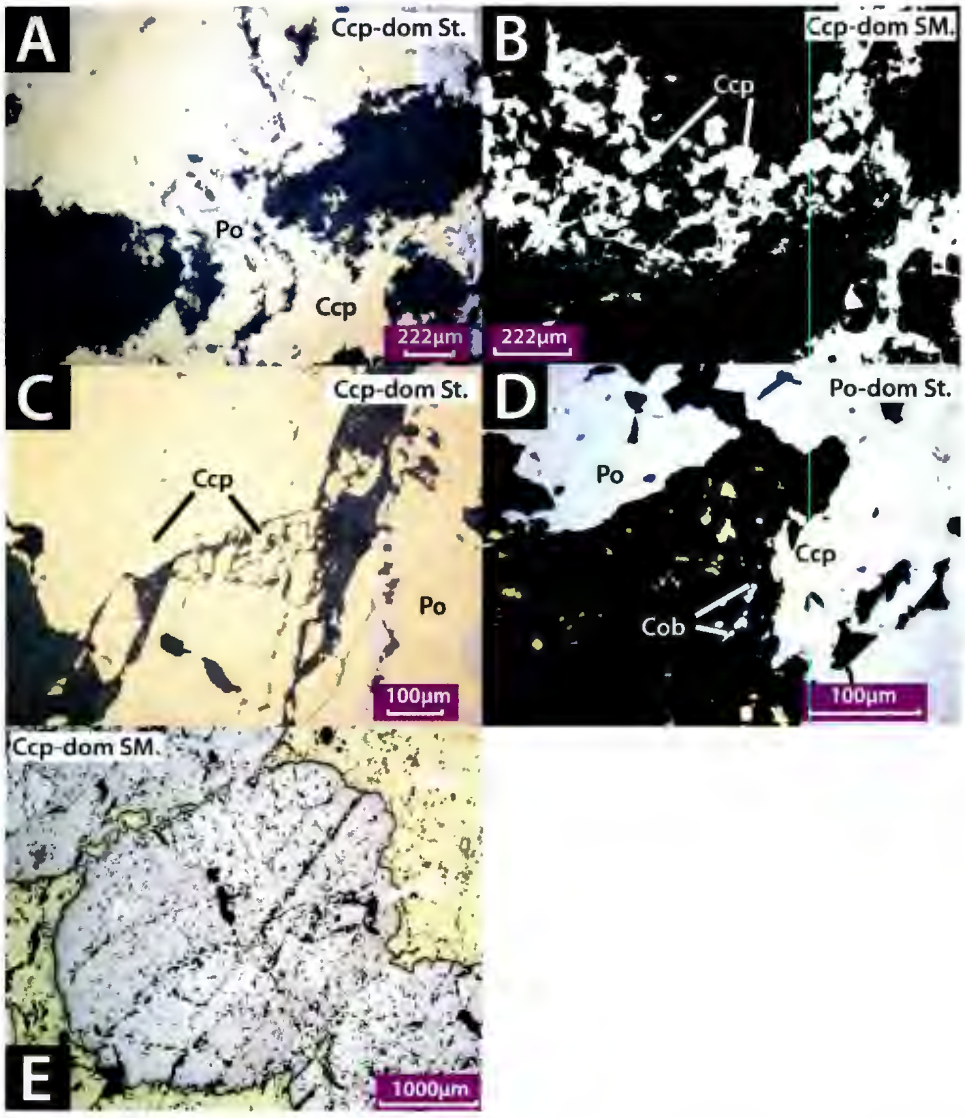

Figure 2.10

Chalcopyrite and pyrrhotite textures at Little Deer. (A) Sheet-like chalcopyrite. (B) and (C) Evidence for chalcopyrite replacing a previous euhedral crystal phase. (D) Euhedral cobaltite in host rock fragments with annealed pyrrhotite. (E) Pyrrhotite porphyroblasts.

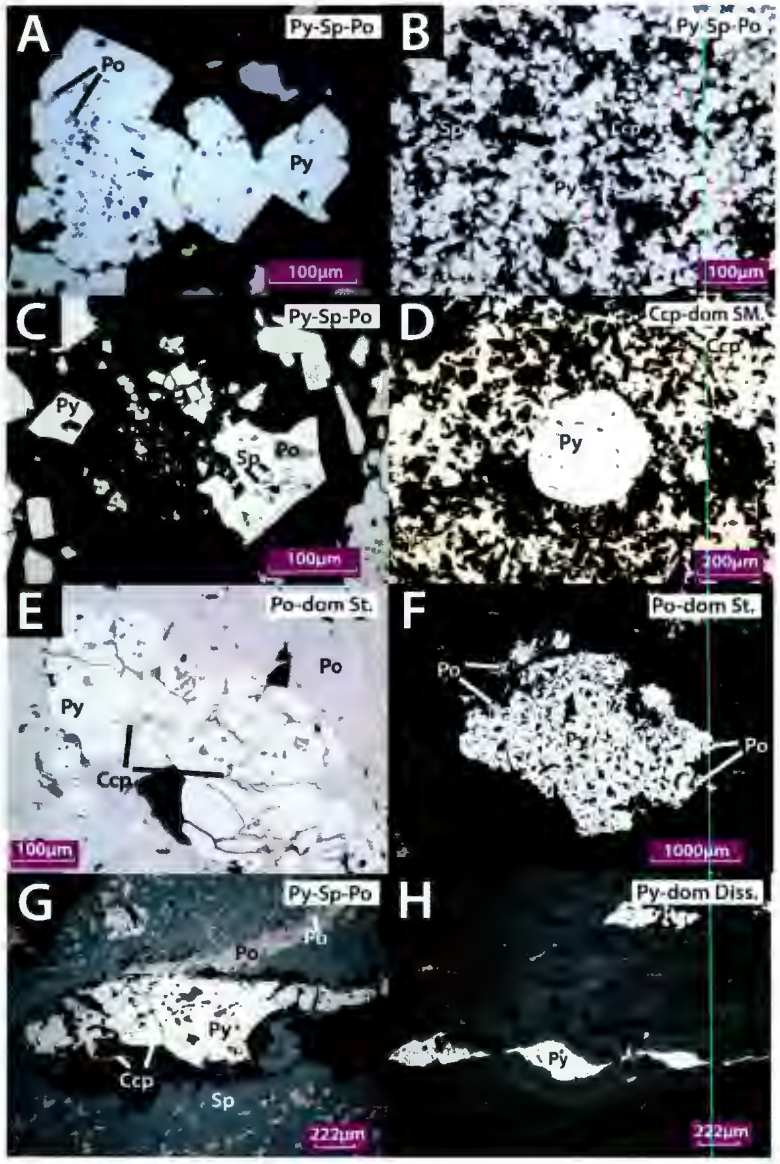

Figure 2.11

Pyrite textures at Little Deer. (A) Euhedral pyrite crystals (becoming rounded) with pyrrhotite inclusions (B) Annealed pyrite forming triple junctions (highlighted in red). (C) Pyrite containing sphalerite and pyrrhotite inclusions. (D) Individual pyrite porphyroblast with chalcopyrite inclusions. (E) Amalgamated pyrite porphyroblasts. (F) Pyrite porphyroblast overprinting the host rock. (G) Pyrite exhibiting brittle deformation, cracks filled by chalcopyrite. (H) Pinch and swell pyrite.

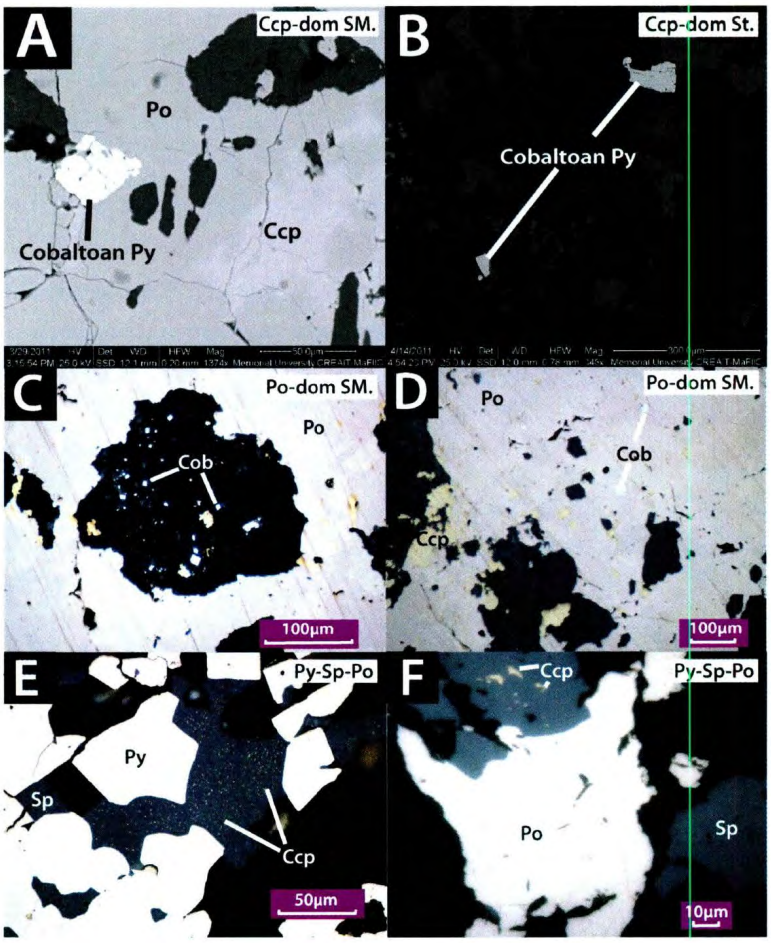

Figure 2.12

Cobaltite, sphalerite, and associated phases from the Little Deer VMS deposit. (A) and (B) Rare cobaltoan pyrite. (C) Euhedral cobaltite in host rock fragment surrounded by annealed pyrrhotite. (D) Anhedral (rounded) to subhedral cobaltite crystals located within pyrrhotite. (E) and (F) Sphalerite with chalcopyrite disease.

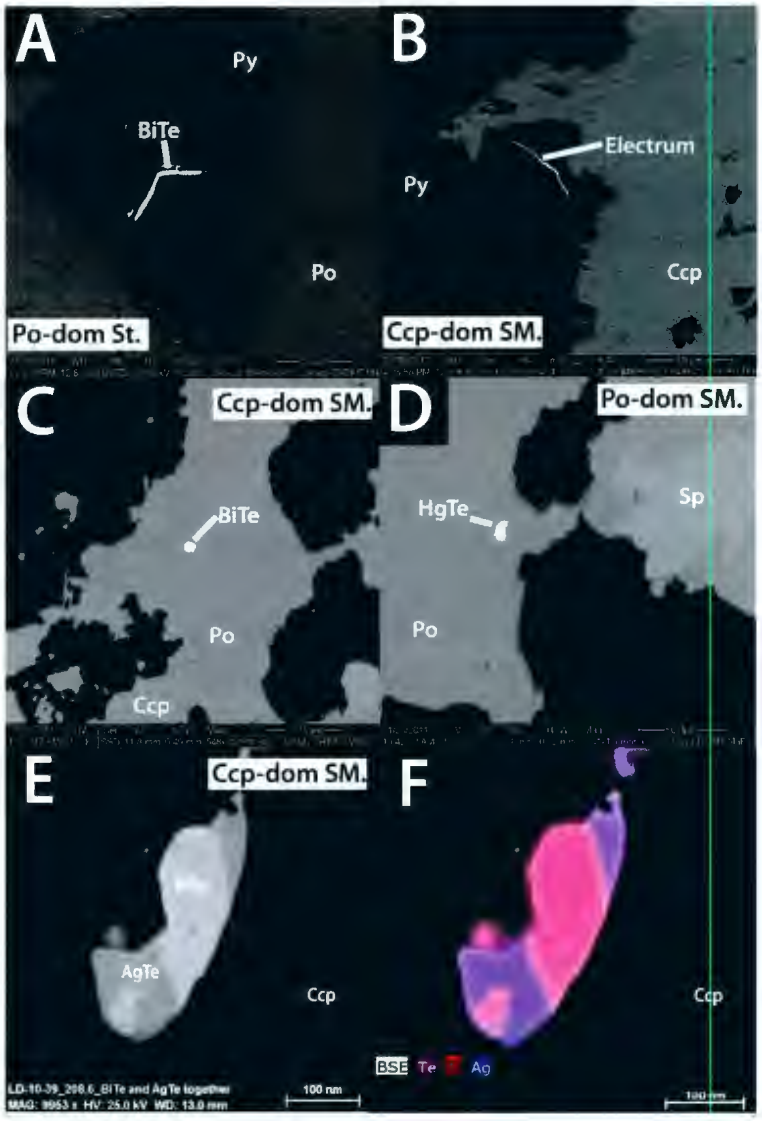

Figure 2.13

Trace phases within the Little Deer VMS deposit. (A) and (B) Trace phases (BiTe and electrum) in cracks and at sulfide grain boundaries. (C) and (D) Trace phases (BiTe and HgTe) enclosed within the main sulfide ore phases. (E) BiTe and AgTe occurring together. (F) Semi-qualitative EDS elemental map for (E). (G) BiTe and PbTe occurring together. (H) Semi-qualitative EDS elemental map for (G).

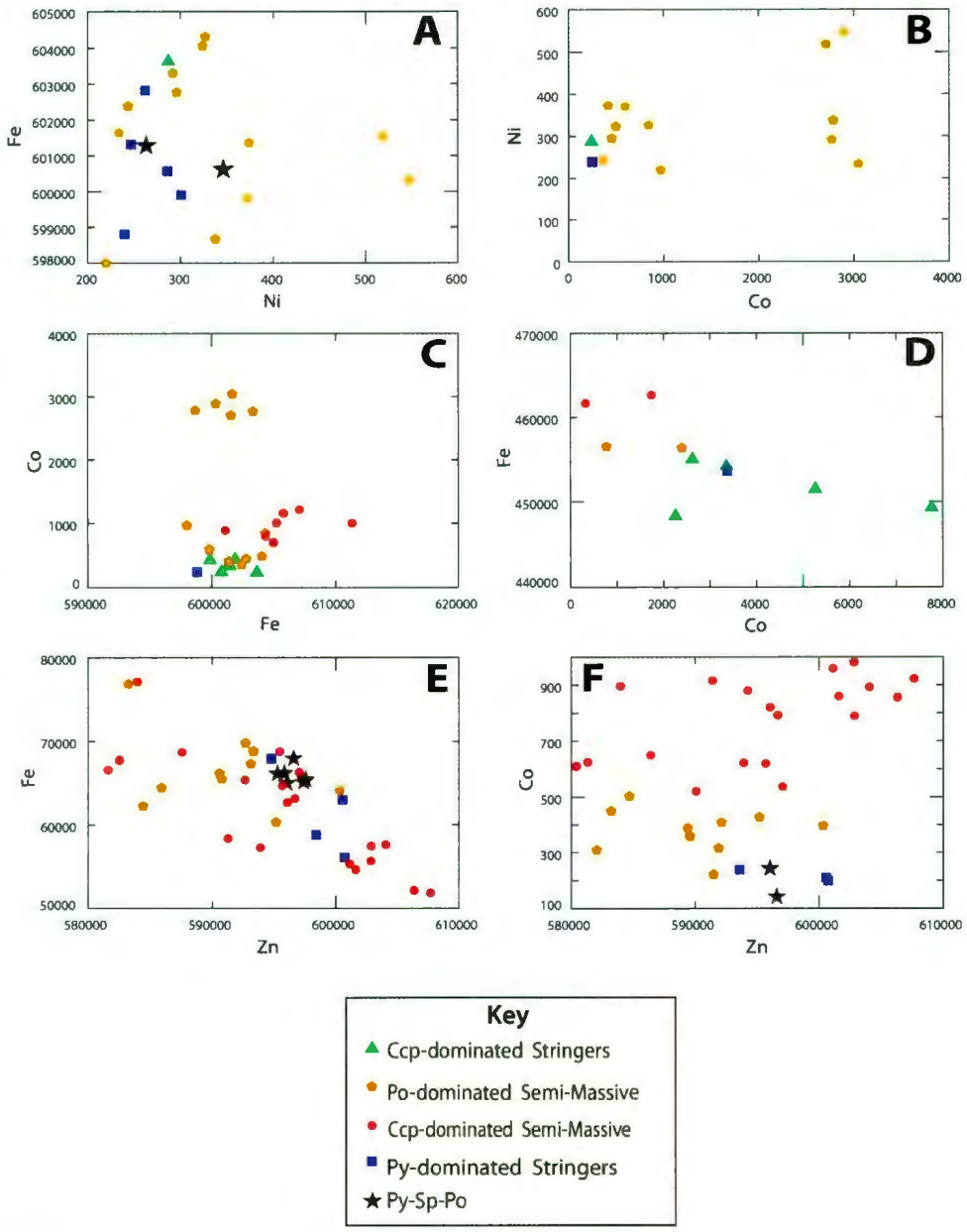

Figure 2.14

Binary plots of specific elements (concentrations in ppm) from various minerals related to the different facies at Little Deer. Only analyses above the minimum detection limit are plotted. (A-C): Pyrrhotite analyses. (D): Pyrite analyses. (E-F): Sphalerite analyses.

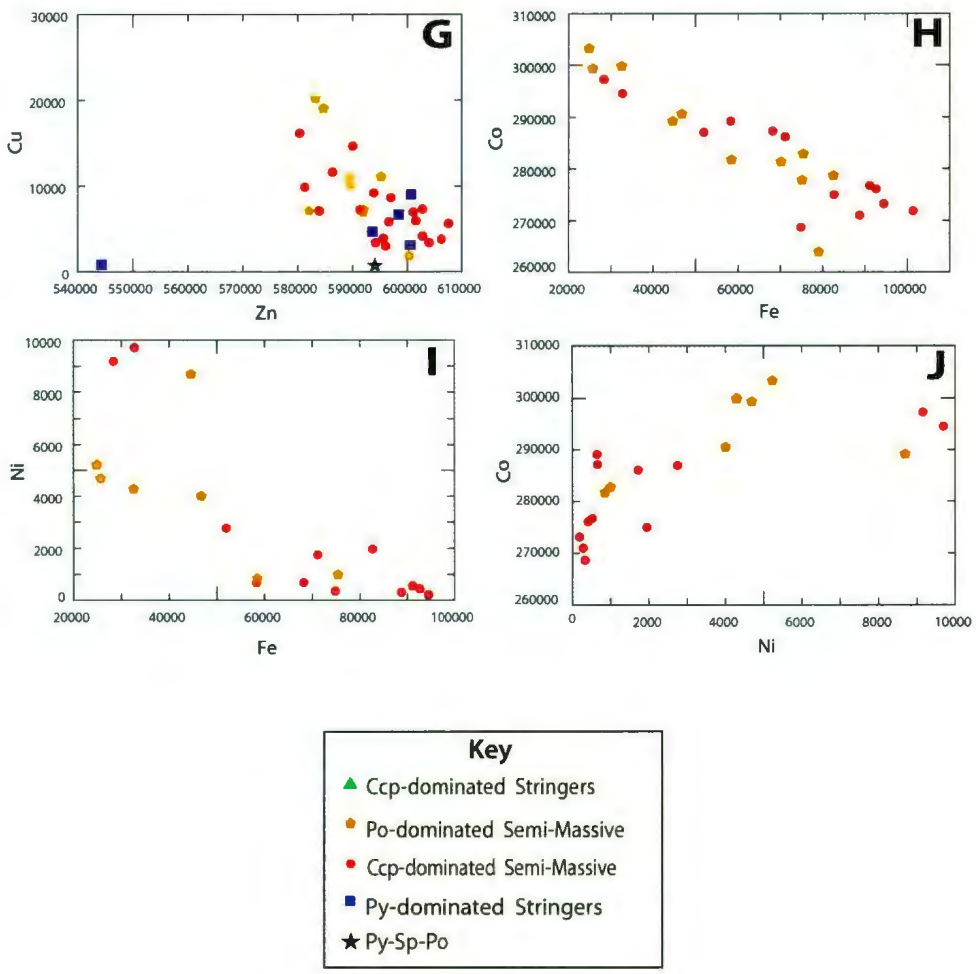

Figure 2.14 cont.
Binary plots of specific elements (concentrations in ppm) from various minerals related to the different facies at Little Deer. Only analyses above the minimum detection limit are plotted. (G): Sphalerite analyses. (H-J): Cobaltite analyses.

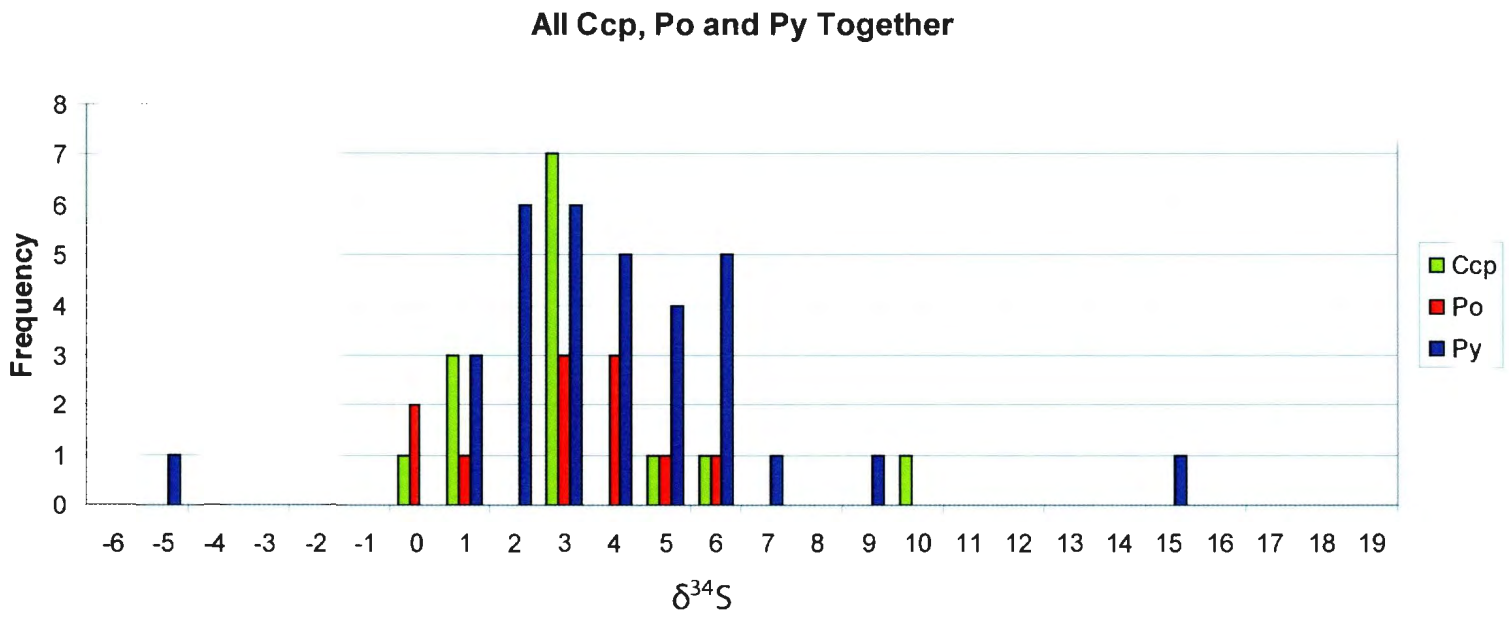

Figure 2.15
Histogram of $\delta^{34}S$-values for chalcopyrite, pyrrhotite and pyrite from the Little Deer VMS deposit – no differentiation (in this figure) has been made regarding the five ore types analysed.

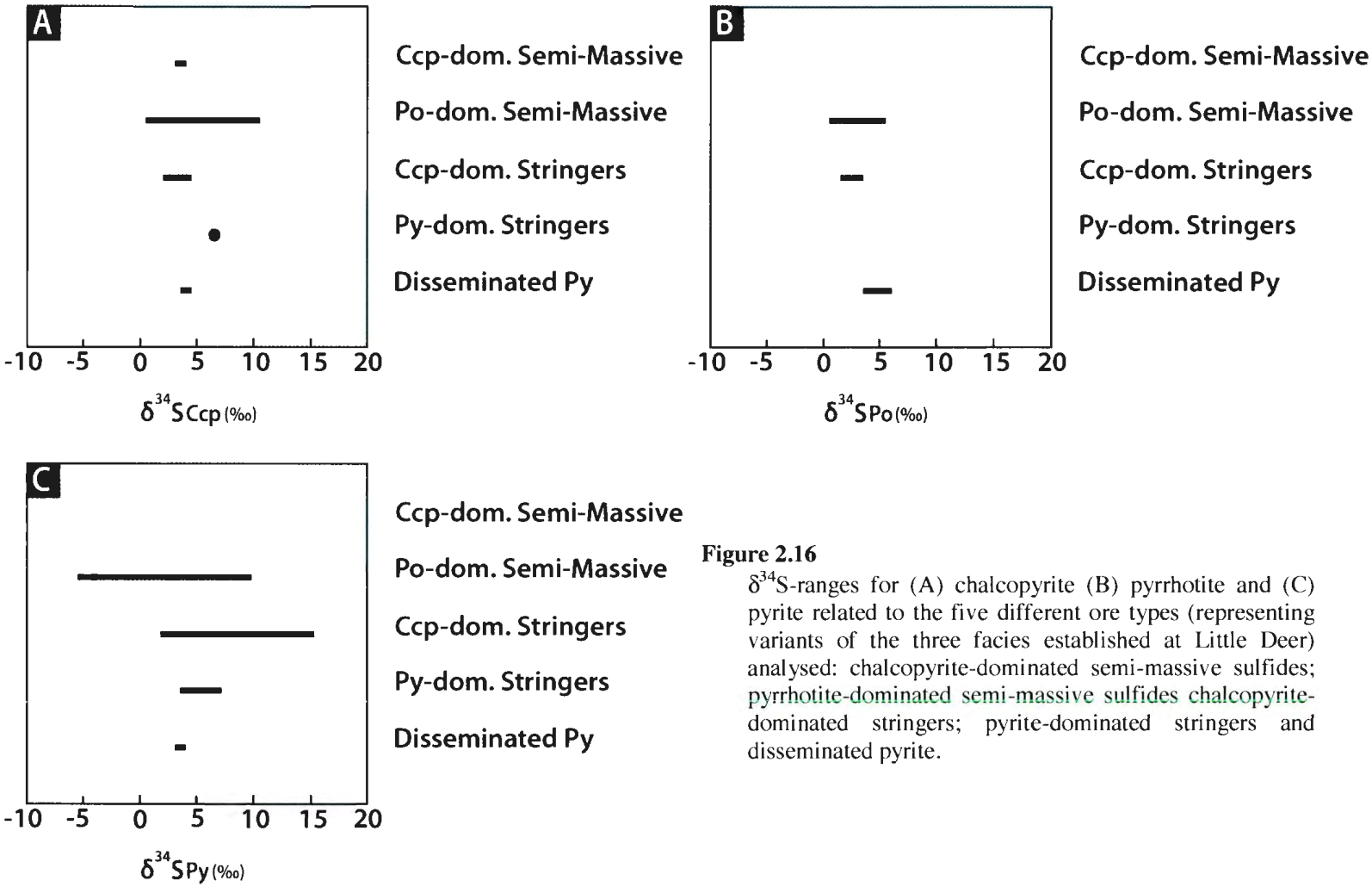

Figure 2.16

δ^{34}S-ranges for (A) chalcopyrite (B) pyrrhotite and (C) pyrite related to the five different ore types (representing variants of the three facies established at Little Deer) analysed: chalcopyrite-dominated semi-massive sulfides; pyrrhotite-dominated semi-massive sulfides chalcopyrite-dominated stringers; pyrite-dominated stringers and disseminated pyrite.

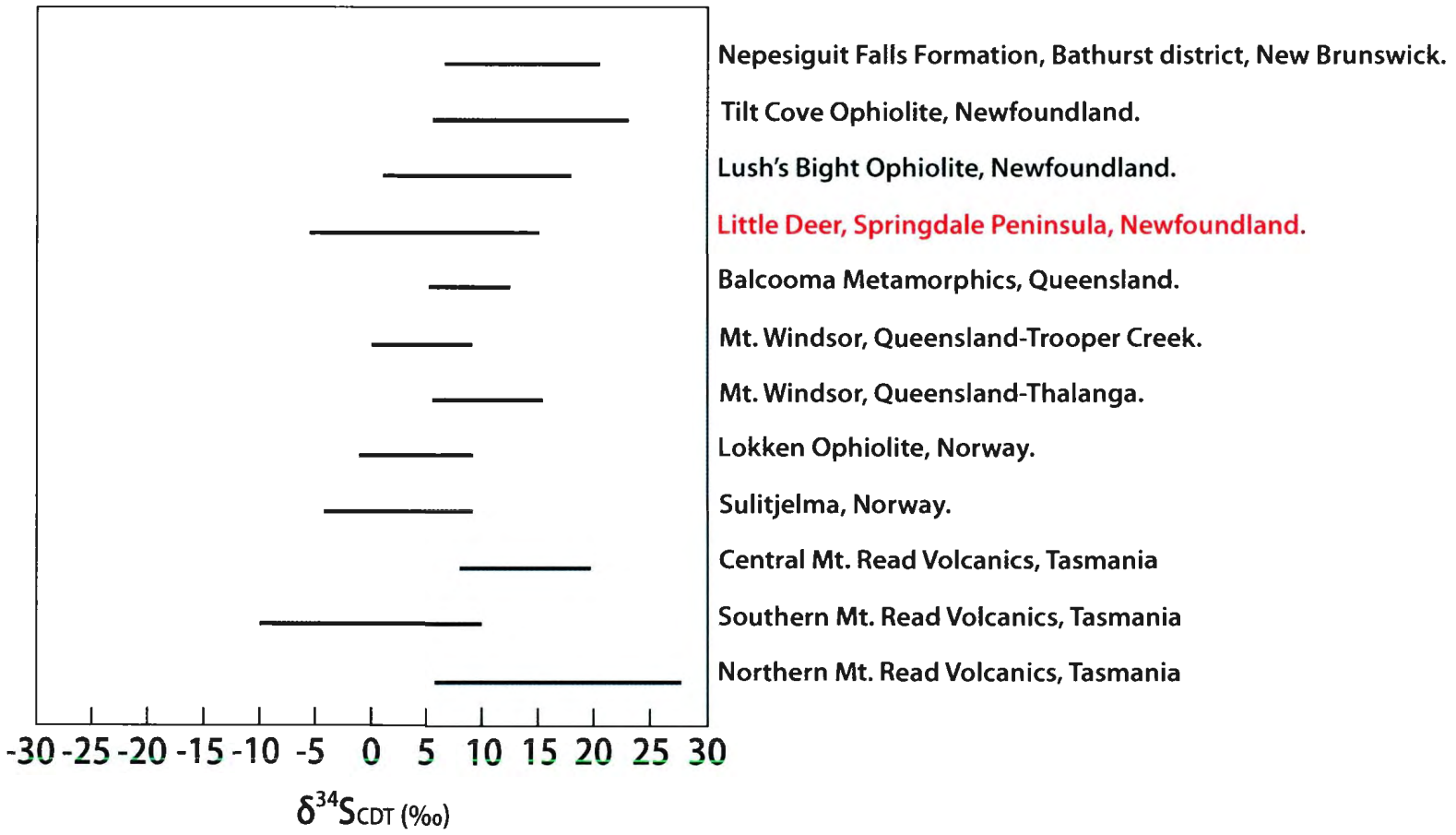

Figure 2.17
$\delta^{34}S$ ranges for Late Cambrian VMS occurrences in Newfoundland and worldwide. From Huston (1999) and Badrzadeh *et al.* (2011)

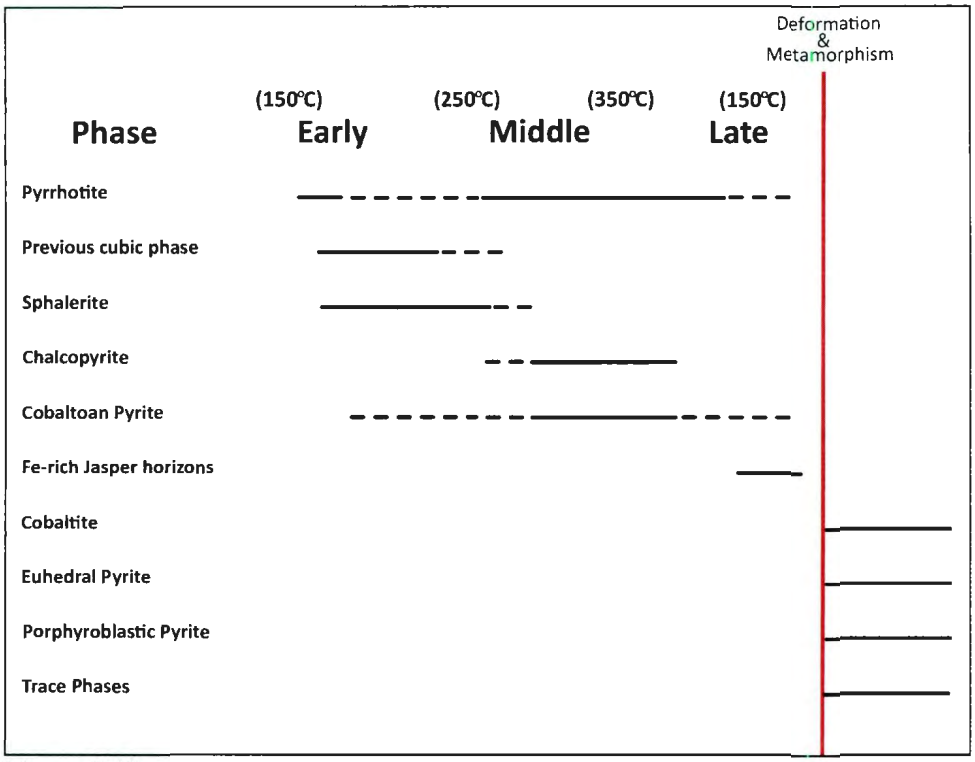

Figure 2.18

Paragenesis for sulfide mineralization at Little Deer.

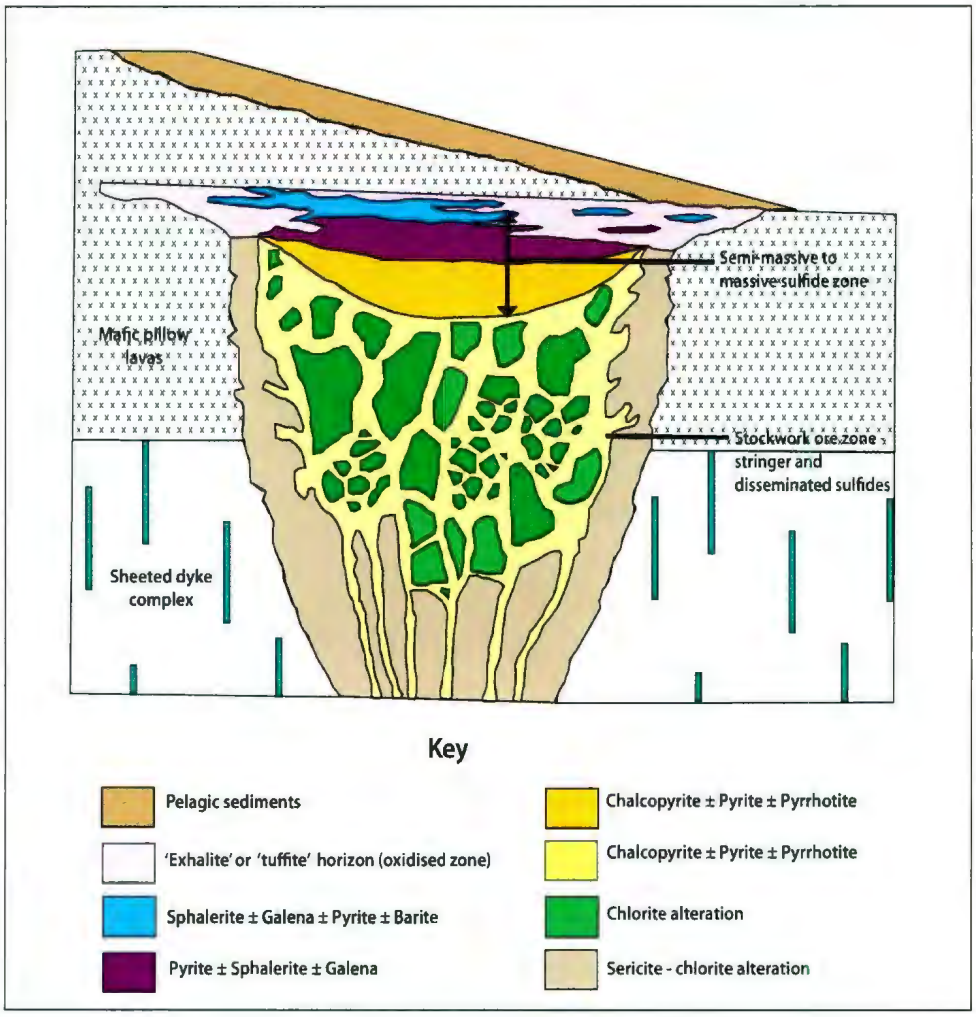

Figure 2.19
An idealised VMS model for mafic-(Cyprus)-type deposits. Although Little Deer is classified as a mafic-(Cyprus)-type deposit, the deposit consists of a stockwork only as the massive sulfide lens is absent at Little Deer. From Hutchinson and Searle (1971) and Robb (2005).

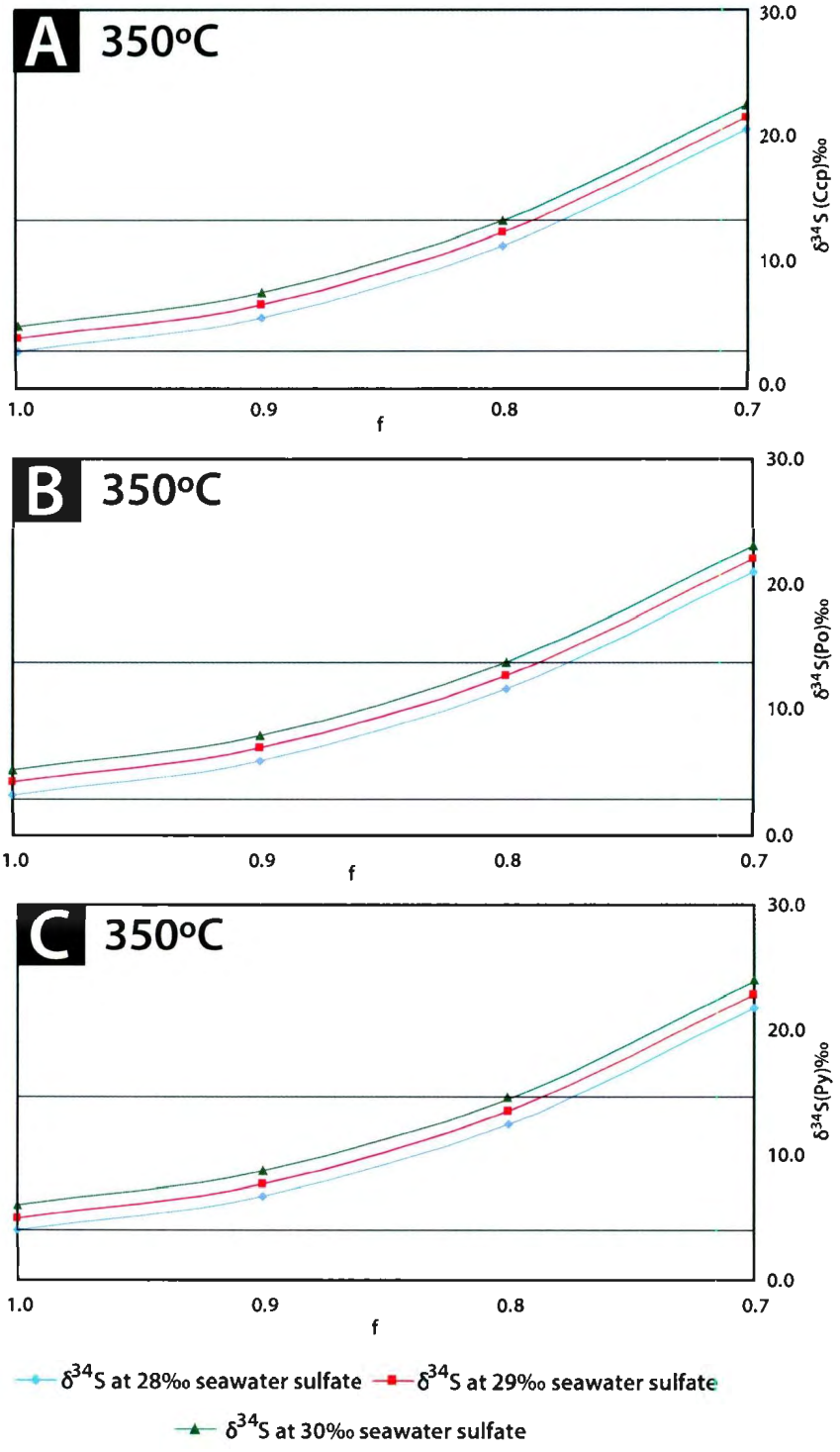

Figure 2.20 See page 109 for figure caption.

Figure 2.20 cont.
Calculated $\delta^{34}S$-values for (A) chalcopyrite; (B) pyrrhotite and (C) pyrite at a temperature of 350°C; modeled on Late Cambrian seawater sulfate compositions of 28, 29 and 30‰ respectively. In each graph the pink block highlights the $\delta^{34}S$-ranges expected for the measured sulfides if derived via thermochemical sulfate reduction of Late Cambrian seawater sulfate.

Chapter 2 Tables

Table 2.1
Results for internal reference material determinations and accepted values. 3s and (-)3s are the variations within each sample. HLHZ - High Lake High Zn, HLLC = High Lake Low Cu, HLHC = High Lake High Cu. Reference materials given to Dr. Stephen Piercey from MMG Ltd.

Standard Results and Ranges					
	Cu	**Pb**	**Zn**	**Ag**	**Au**
HLHZ	***0.80***	***0.80***	***7.78***	***104***	***1.42***
Accepted	0.76	0.82	7.66	101.2	1.31
3s	0.82	0.79	7.84	105.4	1.48
(-)3s	0.70	0.84	7.48	97	1.15
HLLC	***1.46***	***0.29***	***2.92***	***67.5***	***0.84***
Accepted	1.49	0.29	3.01	65.1	0.83
3s	1.44	0.29	2.88	68.7	0.85
(-)3s	1.54	0.29	3.15	61.5	0.81
HLHC	***4.95***	***0.16***	***2.29***	***114***	***1.97***
Accepted	5.07	0.17	2.35	110	1.97
3s	4.89	0.16	2.26	116	1.96
(-)3s	5.25	0.18	2.44	104	1.98

Table 2.2 Bulk rock assay data for sulfide mineralization from the Little Deer VMS deposit.

Sample Name	BR-98-07A_539.7	BR-07-08_631.45	BR-08-14_705.25	BR-09-22_819.68
Drill Hole	LD-98-07A	LD-07-08	LD-08-14	LD-09-22
Depth	539.7	631.45	705.25	819.68
Facies	Py-Sp-Po	Py-Sp-Po	Py-Sp-Po	Py-Sp-Po
Al (wt%)	0.5	7.2	8.3	7.3
Ca	0.2	3.1	6.8	1.7
Cu	0.1	0.0	0.0	0.1
Fe	7.6	10.1	8.3	13.2
K	0.1	0.0	0.2	0.2
Mg	0.1	2.5	3.0	4.2
Na	0.2	1.3	1.7	1.0
Ti	0.0	0.4	0.5	0.4
Zn	4.9	2.3	1.0	3.4
S	9.3	3.3	1.9	4.2
Ag (ppm)	31	2	4	0
As	192	28	5	9
Ba	20	10	30	20
Be	0	0	0	0
Bi	6	1	1	1
Cd	210	98	34	133
Ce	1	4	4	2
Co	4	48	36	61
Cr	19	72	126	88
Cs	0	0	0	0
Ga	4	16	16	17
Ge	0	0	0	0
Hf	0	1	1	1
In	0	0	0	2
La	0	1	1	1
Li	1	4	8	8
Mn	1420	6850	6590	4200
Mo	4	1	2	1
Nb	0	1	1	1
Ni	3	37	54	56
P	10	220	260	160
Pb	4070	18	51	6
Rb	2	1	4	2
Re	0	0	0	0
Sb	1	1	1	0
Sc	2	42	50	38
Se	5	3	3	3
Sn	1	2	0	0
Sr	10	107	104	47
Ta	0	0	0	0
Te	0	0	0	0
Th	0	0	0	0
Tl	0	0	0	0
U	0	0	0	0
V	16	254	275	233
W	0	0	0	0
Y	2	20	19	13
Zr	2	32	32	24
Au	3	2	0	0

Table 2.2 cont: Bulk rock assay data for sulfide mineralization from the Little Deer VMS deposit.

Sample Name	BR-10-39_297.4	BR-07-01A_ 740.6	BR-07-01A_765.2	BR-08-16B_777.55
Drill Hole	LD-10-39	LD-07-01A	LD-07-01A	LD-08-16B
Depth	297.4	740.6	756.2	777.55
Facies	Py-Sp-Po	Py-dom. St.	Py-dom. St.	Py-dom. St.
Al (wt%)	2.4	6.8	7.2	7.0
Ca	0.0	3.5	6.7	0.4
Cu	0.2	0.1	0.1	0.1
Fe	27.4	12.1	15.9	15.0
K	0.4	0.2	0.1	0.2
Mg	0.2	3.0	1.6	3.3
Na	0.0	1.4	0.1	1.6
Ti	0.1	0.4	0.4	0.3
Zn	5.6	1.8	1.2	0.0
S	30.7	3.8	11.2	4.4
Ag (ppm)	4	6	1	0
As	205	9	55	2
Ba	30	10	20	10
Be	0	0	0	0
Bi	3	1	2	0
Cd	269	70	55	0
Ce	2	3	4	2
Co	69	54	50	55
Cr	18	43	90	99
Cs	0	0	0	0
Ga	17	16	17	17
Ge	0	0	0	0
Hf	0	1	1	1
In	4	1	0	0
La	1	1	1	1
Li	3	7	5	9
Mn	738	6350	3040	964
Mo	2	1	1	0
Nb	1	1	1	1
Ni	11	32	42	46
P	30	230	100	180
Pb	23	16	26	1
Rb	8	1	1	1
Re	0	0	0	0
Sb	3	1	4	0
Sc	10	37	36	42
Se	5	4	4	10
Sn	3	0	2	0
Sr	2	36	127	18
Ta	0	0	0	0
Te	1	1	1	0
Th	0	0	0	0
Tl	0	0	0	0
U	0	0	0	0
V	87	246	225	236
W	0	0	0	0
Y	6	13	14	12
Zr	10	13	16	13
Au	2	0	0	0

Table 2.2 cont: Bulk rock assay data for sulfide mineralization from the Little Deer VMS deposit.

Sample Name	BR-07-01A_697.9	BR-08-10A_801.5	BR-09-24_753.9	BR 10-31_730.60
Drill Hole	LD-07-01A	LD-08-10A	LD-09-24	LD-10-31
Depth	697.9	801.5	753.9	730.6
Facies	Po-dom. SM	Po-dom. SM	Po-dom. SM	Po-dom. SM
Al (wt%)	2.7	4.8	5.2	6.4
Ca	0.8	1.1	2.2	0.0
Cu	6.1	0.6	8.7	0.5
Fe	37.8	29.5	25.0	25.1
K	1.0	1.2	1.2	2.8
Mg	0.5	1.0	1.6	0.8
Na	0.1	0.7	0.2	0.1
Ti	0.2	0.2	0.2	0.2
Zn	0.2	0.1	0.2	0.0
S	25.7	20.0	17.8	15.4
Ag (ppm)	20	2	6	1
As	47	14	4	7
Ba	110	180	130	130
Be	0	0	0	0
Bi	10	2	2	2
Cd	11	3	12	0
Ce	1	2	1	0
Co	720	389	647	255
Cr	49	65	63	72
Cs	0	0	0	1
Ga	6	10	13	14
Ge	1	0	1	0
Hf	0	0	0	0
In	4	0	1	0
La	0	1	0	0
Li	3	5	9	4
Mn	265	970	750	235
Mo	25	1	86	4
Nb	1	1	1	0
Ni	68	70	52	58
P	20	30	40	70
Pb	33	9	7	3
Rb	19	25	19	39
Re	0	0	1	0
Sb	1	1	3	0
Sc	12	24	24	35
Se	88	25	128	23
Sn	1	0	0	0
Sr	6	52	89	4
Ta	0	0	0	0
Te	17	1	6	2
Th	0	0	0	0
Tl	0	0	1	0
U	0	0	0	0
V	78	149	162	219
W	0	2	0	0
Y	5	9	7	4
Zr	10	11	8	6
Au	0	0	0	0

Table 2.2 cont: Bulk rock assay data for sulfide mineralization from the Little Deer VMS deposit.

Sample Name	BR-07-07_409.8	BR-09-30_700.25	BR-09-30_716.35	BR-10-37_1111.9
Drill Hole	LD-07-07	LD-09-30	LD-09-30	LD-10-37
Depth	409.8	700.25	716.35	1111.9
Facies	Ccp-dom. St.	Ccp-dom. St.	Ccp-dom. St.	Ccp-dom. St.
Al (wt%)	5.6	5.1	5.0	4.7
Ca	0.3	1.1	2.6	0.5
Cu	6.7	5.8	2.1	13.9
Fe	34.9	22.2	22.7	20.7
K	0.2	0.0	0.1	0.1
Mg	3.1	3.0	2.0	2.5
Na	0.0	0.0	0.2	0.5
Ti	0.4	0.2	0.3	0.2
Zn	0.1	0.1	0.1	0.0
S	17.9	13.9	16.5	14.8
Ag (ppm)	6	4	2	5
As	79	110	168	2
Ba	30	5	10	10
Be	0	0	0	0
Bi	3	1	1	2
Cd	8	4	6	2
Ce	1	1	1	3
Co	645	486	863	72
Cr	85	48	47	72
Cs	0	0	1	0
Ga	13	14	13	11
Ge	1	1	1	0
Hf	1	0	1	1
In	1	1	1	0
La	0	0	0	1
Li	9	6	8	14
Mn	1020	2020	1100	571
Mo	7	2	70	4
Nb	1	1	1	0
Ni	60	28	51	56
P	20	110	80	100
Pb	12	5	9	3
Rb	4	1	2	3
Re	0	0	0	0
Sb	0	6	1	5
Sc	30	27	33	27
Se	115	69	147	21
Sn	1	0	1	1
Sr	2	21	78	16
Ta	0	0	0	0
Te	10	4	6	1
Th	0	0	0	2
Tl	0	0	1	1
U	0	0	0	0
V	222	164	212	161
W	1	0	0	0
Y	16	11	24	7
Zr	22	12	13	17
Au	0	0	0	0

Table 2.2 cont: Bulk rock assay data for sulfide mineralization from the Little Deer VMS deposit.

Sample Name	BR-10-39_274.2	BR-10-31_688.60	BR-10-38_679.1	BR-10-39_208.6
Drill Hole	LD-10-39	LD-10-31	LD-10-38	LD-10-39
Depth	274.2	688.6	679.1	208.6
Facies	Ccp-dom. St.	Ccp-dom. SM	Ccp-dom. SM	Ccp-dom. SM
Al (wt%)	2.5	3.4	3.5	1.5
Ca	0.2	0.3	2.5	0.0
Cu	8.2	12.1	9.9	15.1
Fe	33.2	24.4	22.4	35.2
K	0.3	0.1	0.0	0.4
Mg	0.6	1.5	0.8	0.1
Na	0.0	0.3	0.4	0.0
Ti	0.2	0.2	0.2	0.1
Zn	0.8	0.2	0.2	0.1
S	32.2	18.0	18.5	33.1
Ag (ppm)	10	15	28	16
As	28	65	316	210
Ba	80	20	5	90
Be	0	0	0	0
Bi	5	1	1	11
Cd	34	10	12	6
Ce	2	2	1	0
Co	727	475	600	919
Cr	21	12	39	14
Cs	0	0	0	0
Ga	8	8	10	6
Ge	1	1	1	1
Hf	0	1	0	0
In	2	1	1	3
La	1	1	0	0
Li	2	8	2	1
Mn	380	1560	483	136
Mo	11	27	33	11
Nb	1	1	1	1
Ni	26	22	32	29
P	10	120	40	5
Pb	22	13	15	32
Rb	4	3	0	6
Re	0	0	0	0
Sb	1	0	10	1
Sc	10	16	14	6
Se	102	167	98	161
Sn	1	1	0	1
Sr	2	8	95	3
Ta	0	0	0	0
Te	7	8	3	19
Th	0	0	0	0
Tl	9	0	0	1
U	0	0	0	0
V	93	130	111	75
W	0	0	0	1
Y	22	10	12	7
Zr	11	13	8	6
Au	0	2	0	0

Table 2.2 cont: Bulk rock assay data for sulfide mineralization from the Little Deer VMS deposit.

Sample Name	BR-10-35_661.50	BR 10-39_215.0
Drill Hole	LD-10-35	LD-10-39
Depth	661.5	215
Facies	Po-dom. St.	Po-dom. St.
Al (wt%)	3.5	5.7
Ca	2.6	0.0
Cu	1.9	2.6
Fe	45.2	28.6
K	0.1	2.6
Mg	1.1	0.1
Na	0.2	0.1
Ti	0.2	0.3
Zn	0.1	0.0
S	26.9	21.5
Ag (ppm)	6	3
As	12	18
Ba	20	390
Be	0	0
Bi	2	2
Cd	4	3
Ce	1	1
Co	1140	558
Cr	39	69
Cs	0	1
Ga	9	13
Ge	1	1
Hf	0	1
In	1	1
La	0	0
Li	4	1
Mn	676	18
Mo	14	12
Nb	1	1
Ni	79	33
P	5	20
Pb	15	9
Rb	2	56
Re	0	0
Sb	2	0
Sc	19	32
Se	134	82
Sn	0	1
Sr	97	11
Ta	0	0
Te	3	5
Th	0	0
Tl	0	0
U	0	0
V	136	341
W	0	1
Y	10	16
Zr	5	24
Au	0	1

Table 2.3
3D Gridding parameters used for each element to construct the 3D metal distribution models of Little Deer.

3D Gridding – Advanced Parameters			
	Cu	**Zn**	**(Cu/(Cu+Zn))**
Cell size for Z	25	25	25
Blank distance (voxel cells)	4	4	4
Log option	Linear	Linear	Linear
Log minimum	1	1	1
Maximum radius (voxel cells)	16	16	16
Minimum points	16	16	16
Maximum points	32	32	32
Strike	0	0	0
Dip	90	90	90
Plunge	0	0	0
Strike weight	1	1	1
Dip plane weight	1	1	1
3D Gridding – Variogram Parameters			
Model	Spherical	Spherical	Spherical
Range	200	200	200
Sill	1.75	0.55	0.135
Nugget	0	0	0

Table 2.4

Sulfide and trace phases in mineralization at Little Deer.

Dominant Phases	Mineral Ab.	Formula	Minor Phases	Mineral Ab.	Formula	Trace Phases	Mineral Formula
Chalcopyrite	Ccp	$CuFeS_2$	Sphalerite	Sp	ZnS	Bismuth Telluride	BiTe
Pyrrhotite	Po	$Fe_{(1-x)}S$	Cobaltite	Cob	CoAsS	Mercury Telluride	HgTe
Pyrite	Py	FeS_2				Silver Telluride	AgTe
						Lead Telluride	PbTe
						Nickel Telluride	NiTe
						Native Tellurium	Te
						Electrum	(Au,Ag)
						Galena	PbS
						Selenium-bearing galena	SePbS
						Cobaltoan Pyrite	$(Fe,Co)S_2$
						Native Arsenic	As

Table 2.5
Electron microprobe analyses for chalcopyrite. Atomic proportions based on 4 atoms per formula unit and recalculated based on 2 sulfur per formula unit.

Sample Name	LD-10-41_231.75	LD-10-41_231.75	LD-10-41_231.75	LD-10-41_231.75	LD-10-41_231.75	LD-10-41_231.75	LD-10-32A_1020.71
Drill Hole	LD-10-41	LD-10-41	LD-10-41	LD-10-41	LD-10-41	LD-10-41	LD-10-32A
Depth	231.75	231.75	231.75	231.75	231.75	231.75	1020.71
Facies	Ccp-dom. St.	Ccp-dom. St.	Ccp-dom. St.	Ccp-dom. St.	Ccp-dom. St.	Ccp-dom. St.	Ccp-dom. St.
Probe analysis	151	153	155	157	159	161	193
Fe (wt%)	30.0	29.9	29.9	29.9	30.2	30.0	30.0
S	35.2	35.3	35.3	35.3	35.1	35.1	35.0
Cu	34.4	34.5	34.4	34.5	34.4	34.5	34.7
Total	**99.6**	**99.7**	**99.6**	**99.7**	**99.6**	**99.5**	**99.7**
Fe (apfu)	0.54	0.54	0.54	0.54	0.54	0.54	0.54
S	1.10	1.10	1.10	1.10	1.09	1.09	1.09
Cu	0.54	0.54	0.54	0.54	0.54	0.54	0.55
Mineral Formula	$Cu_{0.99}Fe_{0.98}S_{2.00}$	$Cu_{0.99}Fe_{0.97}S_{2.00}$	$Cu_{0.98}Fe_{0.97}S_{2.00}$	$Cu_{0.99}Fe_{0.97}S_{2.00}$	$Cu_{0.99}Fe_{0.99}S_{2.00}$	$Cu_{0.99}Fe_{0.98}S_{2.00}$	$Cu_{1.00}Fe_{0.98}S_{2.00}$

Sample Name	LD-10-32A_1020.71	LD-10-32A_1020.71	LD-10-32A_1020.71	LD-10-32A_1020.71	LD-10-32A_1020.71	LD-10-32A_1020.71	LD-09-28_588.95
Drill Hole	LD-10-32A	LD-10-32A	LD-10-32A	LD-10-32A	LD-10-32A	LD-10-32A	LD-09-28
Depth	1020.71	1020.71	1020.71	1020.71	1020.71	1020.71	588.95
Facies	Ccp-dom. St.	Ccp-dom. St.	Ccp-dom. St.	Ccp-dom. St.	Ccp-dom. St.	Ccp-dom. St.	Py-dom. St.
Probe analysis	194	195	196	197	198	199	162
Fe (wt%)	30.1	30.2	30.2	29.9	30.0	29.9	30.0
S	35.0	35.0	35.0	34.9	35.2	35.1	35.3
Cu	34.7	34.8	34.4	34.9	34.5	34.6	34.4
Total	**99.8**	**100.0**	**99.6**	**99.7**	**99.8**	**99.5**	**99.7**
Fe (apfu)	0.54	0.54	0.54	0.54	0.54	0.54	0.54
S	1.09	1.09	1.09	1.09	1.10	1.09	1.10
Cu	0.55	0.55	0.54	0.55	0.54	0.54	0.54
Mineral Formula	$Cu_{1.00}Fe_{0.99}S_{2.00}$	$Cu_{1.00}Fe_{0.99}S_{2.00}$	$Cu_{0.99}Fe_{0.99}S_{2.00}$	$Cu_{1.01}Fe_{0.98}S_{2.00}$	$Cu_{0.99}Fe_{0.98}S_{2.00}$	$Cu_{0.99}Fe_{0.98}S_{2.00}$	$Cu_{0.98}Fe_{0.98}S_{2.00}$

Table 2.5 cont: Electron microprobe analyses for chalcopyrite. Atomic proportions based on 4 atoms per formula unit and recalculated based on 2 sulfur per formula unit.

Sample Name	LD-09-28_588.95	LD-09-28_588.95	LD-09-28_588.95	LD-09-28_588.95	LD-09-28_588.95	LD-09-28_588.95	LD-09-28_588.95
Drill Hole	LD-09-28	LD-09-28	LD-09-28	LD-09-28	LD-09-28	LD-09-28	LD-09-28
Depth	588.95	588.95	588.95	588.95	588.95	588.95	588.95
Facies	Py-dom. St.	Py-dom. St.	Py-dom. St.	Py-dom. St.	Py-dom. St.	Py-dom. St.	Py-dom. St.
Probe analysis	163	164	165	166	167	169	173
Fe (wt%)	29.9	29.9	29.8	29.9	29.9	30.4	30.1
S	35.1	35.2	35.2	35.3	35.1	35.3	35.2
Cu	34.7	34.7	34.4	34.6	34.5	34.1	34.2
Total	**99.6**	**99.8**	**99.4**	**99.8**	**99.5**	**99.9**	**99.5**
Fe (apfu)	0.54	0.54	0.53	0.54	0.54	0.54	0.54
S	1.09	1.10	1.10	1.10	1.10	1.10	1.10
Cu	0.55	0.55	0.54	0.54	0.54	0.54	0.54
Mineral Formula	$Cu_{1.00}Fe_{0.98}S_{2.00}$	$Cu_{1.00}Fe_{0.98}S_{2.00}$	$Cu_{0.98}Fe_{0.97}S_{2.00}$	$Cu_{0.99}Fe_{0.97}S_{2.00}$	$Cu_{0.99}Fe_{0.98}S_{2.00}$	$Cu_{0.97}Fe_{0.99}S_{2.00}$	$Cu_{0.98}Fe_{0.98}S_{2.00}$

Sample Name	LD-09-28_588.95	LD-09-28_588.95	LD-09-25_835.20	LD-09-25_835.20	LD-09-25_835.20	LD-09-25_835.20	LD-09-25_835.20
Drill Hole	LD-09-28	LD-09-28	LD-09-25	LD-09-25	LD-09-25	LD-09-25	LD-09-25
Depth	588.95	588.95	835.2	835.2	835.2	835.2	835.2
Facies	Py-dom. St.	Py-dom. St.	Py-dom. St.	Py-dom. St.	Py-dom. St.	Py-dom. St.	Py-dom. St.
Probe analysis	177	178	322	323	324	325	326
Fe (wt%)	29.8	29.7	30.1	30.1	30.0	30.4	30.2
S	35.4	35.5	35.0	35.0	35.3	35.0	35.1
Cu	34.5	34.5	34.5	34.5	34.6	34.6	34.5
Total	**99.8**	**99.7**	**99.7**	**99.6**	**99.8**	**99.9**	**99.9**
Fe (apfu)	0.53	0.53	0.54	0.54	0.54	0.54	0.54
S	1.11	1.11	1.09	1.09	1.10	1.09	1.10
Cu	0.54	0.54	0.54	0.54	0.54	0.54	0.54
Mineral Formula	$Cu_{0.98}Fe_{0.97}S_{2.00}$	$Cu_{0.98}Fe_{0.96}S_{2.00}$	$Cu_{0.99}Fe_{0.99}S_{2.00}$	$Cu_{1.00}Fe_{0.99}S_{2.00}$	$Cu_{0.99}Fe_{0.98}S_{2.00}$	$Cu_{1.00}Fe_{1.00}S_{2.00}$	$Cu_{0.99}Fe_{0.99}S_{2.00}$

Table 2.5 cont: Electron microprobe analyses for chalcopyrite. Atomic proportions based on 4 atoms per formula unit and recalculated based on 2 sulfur per formula unit.

Sample Name	LD-09-24_753.90	LD-09-24_753.90	LD-09-24_753.90	LD-09-24_753.90	LD-09-24_753.90	LD-09-24_753.90	LD-09-24_753.90
Drill Hole	LD-09-24	LD-09-24	LD-09-24	LD-09-24	LD-09-24	LD-09-24	LD-09-24
Depth	753.9	753.9	753.9	753.9	753.9	753.9	753.9
Facies	Po-dom. SM	Po-dom. SM	Po-dom. SM	Po-dom. SM	Po-dom. SM	Po-dom. SM	Po-dom. SM
Probe analysis	200	201	202	203	204	205	206
Fe (wt%)	30.1	30.1	30.1	29.9	30.0	30.0	30.1
S	35.2	35.2	35.0	34.8	35.1	34.9	35.2
Cu	34.6	34.5	34.6	34.9	34.7	34.9	34.4
Total	**99.9**	**99.9**	**99.7**	**99.6**	**99.7**	**99.8**	**99.7**
Fe (apfu)	0.54	0.54	0.54	0.54	0.54	0.54	0.54
S	1.10	1.10	1.09	1.09	1.09	1.09	1.10
Cu	0.55	0.54	0.54	0.55	0.55	0.55	0.54
Mineral Formula	$Cu_{0.99}Fe_{0.98}S_{2.00}$	$Cu_{0.99}Fe_{0.98}S_{2.00}$	$Cu_{1.00}Fe_{0.99}S_{2.00}$	$Cu_{1.01}Fe_{0.99}S_{2.00}$	$Cu_{1.00}Fe_{0.98}S_{2.00}$	$Cu_{1.01}Fe_{0.99}S_{2.00}$	$Cu_{0.99}Fe_{0.98}S_{2.00}$

Sample Name	LD-10-41_221.25	LD-10-41_221.25	LD-10-41_221.25	LD-10-41_221.25	LD-10-41_221.25	LD-11-44_473.64	LD-11-44_473.64
Drill Hole	LD-10-41	LD-10-41	LD-10-41	LD-10-41	LD-10-41	LD-11-44	LD-11-44
Depth	221.25	221.25	221.25	221.25	221.25	473.64	473.64
Facies	Po-dom. SM	Po-dom. SM	Po-dom. SM	Po-dom. SM	Po-dom. SM	Ccp-dom. SM	Ccp-dom. SM
Probe analysis	215	216	217	218	219	307	309
Fe (wt%)	30.9	30.7	31.0	30.7	30.9	30.2	30.1
S	33.5	33.9	33.6	33.6	33.6	34.9	34.9
Cu	35.3	35.3	35.2	35.4	35.3	34.8	34.7
Total	**99.8**	**99.8**	**99.8**	**99.7**	**99.8**	**99.8**	**99.7**
Fe (apfu)	0.55	0.55	0.55	0.55	0.55	0.54	0.54
S	1.05	1.06	1.05	1.05	1.05	1.09	1.09
Cu	0.56	0.56	0.55	0.56	0.55	0.55	0.55
Mineral Formula	$Cu_{1.06}Fe_{1.06}S_{2.00}$	$Cu_{1.05}Fe_{1.04}S_{2.00}$	$Cu_{1.06}Fe_{1.06}S_{2.00}$	$Cu_{1.06}Fe_{1.05}S_{2.00}$	$Cu_{1.06}Fe_{1.05}S_{2.00}$	$Cu_{1.01}Fe_{0.99}S_{2.00}$	$Cu_{1.00}Fe_{0.99}S_{2.00}$

Table 2.5 cont: Electron microprobe analyses for chalcopyrite. Atomic proportions based on 4 atoms per formula unit and recalculated based on 2 sulfur per formula unit.

Sample Name	LD-11-44_473.64	LD-11-44_473.64	LD-10-38_679.10	LD-10-38_679.10	LD-10-38_679.10
Drill Hole	LD-11-44	LD-11-44	LD-10-38	LD-10-38	LD-10-38
Depth	473.64	473.64	679.1	679.1	679.1
Facies	Ccp-dom. SM	Ccp-dom. SM	Ccp-dom. SM	Ccp-dom. SM	Ccp-dom. SM
Probe analysis	311	313	315	317	321
Fe (wt%)	30.4	30.0	30.0	30.0	30.1
S	34.9	34.9	35.0	34.9	35.1
Cu	34.5	34.7	34.6	34.7	34.5
Total	**99.8**	**99.6**	**99.7**	**99.7**	**99.7**
Fe (apfu)	0.54	0.54	0.54	0.54	0.54
S	1.09	1.09	1.09	1.09	1.09
Cu	0.54	0.55	0.54	0.55	0.54
Mineral Formula	$Cu_{1.00}Fe_{1.00}S_{2.00}$	$Cu_{1.00}Fe_{0.99}S_{2.00}$	$Cu_{1.00}Fe_{0.99}S_{2.00}$	$Cu_{1.00}Fe_{0.99}S_{2.00}$	$Cu_{0.99}Fe_{0.99}S_{2.00}$

Table 2.6
Electron microprobe analyses for pyrrhotite. Atomic proportions based on 2 atoms per formula unit and recalculated based on 1 sulfur per formula unit.

Sample Name	LD-10-41_231.75	LD-10-41_231.75	LD-10-41_231.75	LD-10-41_231.75	LD-10-41_231.75	LD-10-41_231.75	LD-09-28_588.95
Drill Hole	LD-10-41	LD-10-41	LD-10-41	LD-10-41	LD-10-41	LD-10-41	LD-09-28
Depth	231.75	231.75	231.75	231.75	231.75	231.75	588.95
Facies	Ccp-dom. St.	Ccp-dom. St.	Ccp-dom. St.	Ccp-dom. St.	Ccp-dom. St.	Ccp-dom. St.	Py-dom. St
Probe analysis	150	152	154	156	158	160	168
Fe (wt%)	60.1	60.2	60.4	60.1	60.0	60.1	60.1
S	39.5	39.5	39.4	39.6	39.6	39.6	39.5
Total	**99.7**	**99.7**	**99.8**	**99.7**	**99.6**	**99.7**	**99.7**
Cu (ppm)	1347	-	-	-	-	-	-
Co	351	449	242	249	439	342	-
Ni	-	-	287	-	-	-	-
Fe (apfu)	1.08	1.08	1.08	1.08	1.07	1.08	1.08
S	1.23	1.23	1.23	1.24	1.24	1.24	1.23
Cu	-	-	-	-	-	-	-
Co	-	-	-	-	-	-	-
Ni	-	-	-	-	-	-	-
Mineral Formula	$Fe_{0.87}S_{1.00}$	$Fe_{0.88}S_{1.00}$	$Fe_{0.88}S_{1.00}$	$Fe_{0.87}S_{1.00}$	$Fe_{0.87}S_{1.00}$	$Fe_{0.87}S_{1.00}$	$Fe_{0.87}S_{1.00}$

Table 2.6 cont: Electron microprobe analyses for pyrrhotite. Atomic proportions based on 2 atoms per formula unit and recalculated based on 1 sulfur per formula unit.

Sample Name	LD-09-28_588.95	LD-09-28_588.95	LD-09-28_588.95	LD-09-28_588.95	LD-09-28_588.95	LD-09-28_588.95	LD-09-28_588.95
Drill Hole	LD-09-28	LD-09-28	LD-09-28	LD-09-28	LD-09-28	LD-09-28	LD-09-28
Depth	588.95	588.95	588.95	588.95	588.95	588.95	588.95
Facies	Py-dom. St	Py-dom. St	Py-dom. St	Py-dom. St	Py-dom. St	Py-dom. St	Py-dom. St
Probe analysis	170	171	172	174	175	176	179
Fe (wt%)	60.1	60.1	60.0	60.3	60.1	60.2	60.2
S	39.5	39.6	39.7	39.4	39.7	39.6	39.5
Total	**99.7**	**99.8**	**99.7**	**99.7**	**99.7**	**99.8**	**99.6**
Cu (ppm)	-	-	-	-	-	-	-
Co	-	-	-	-	-	-	-
Ni	-	-	301	262	286	-	-
Fe (apfu)	1.08	1.08	1.07	1.08	1.08	1.08	1.08
S	1.23	1.24	1.24	1.23	1.24	1.24	1.23
Cu	-	-	-	-	-	-	-
Co	-	-	-	-	-	-	-
Ni	-	-	-	-	-	-	-
Mineral Formula	$Fe_{0.87}S_{1.00}$	$Fe_{0.87}S_{1.00}$	$Fe_{0.87}S_{1.00}$	$Fe_{0.88}S_{1.00}$	$Fe_{0.87}S_{1.00}$	$Fe_{0.87}S_{1.00}$	$Fe_{0.88}S_{1.00}$

Table 2.6 cont: Electron microprobe analyses for pyrrhotite. Atomic proportions based on 2 atoms per formula unit and recalculated based on 1 sulfur per formula unit.

Sample Name	LD-10-32A_1020.71	LD-10-32A_1020.71	LD-10-32A_1020.71	LD-10-32A_1020.71	LD-10-32A_1020.71	LD-10-32A_1020.71	LD-10-32A_1020.71
Drill Hole	LD-10-32A	LD-10-32A	LD-10-32A	LD-10-32A	LD-10-32A	LD-10-32A	LD-10-32A
Depth	1020.21	1020.21	1020.21	1020.21	1020.21	1020.21	1020.21
Facies	Py-dom. St	Py-dom. St	Py-dom. St	Py-dom. St	Py-dom. St	Py-dom. St	Py-dom. St
Probe analysis	186	187	188	189	190	191	192
Fe (wt%)	59.9	60.1	60.0	60.0	60.1	59.9	59.9
S	39.8	39.5	39.6	39.7	39.6	39.5	39.8
Total	**99.7**	**99.6**	**99.6**	**99.7**	**99.7**	**99.4**	**99.7**
Cu (ppm)	-	-	-	0.07	-	779	-
Co	250	-	-	-	-	-	-
Ni	240	247	-	-	-	-	-
Fe (apfu)	1.07	1.08	1.07	1.07	1.08	1.07	1.07
S	1.24	1.23	1.24	1.24	1.24	1.23	1.24
Cu	-	-	-	-	-	-	-
Co	-	-	-	-	-	-	-
Ni	-	-	-	-	-	-	-
Mineral Formula	$Fe_{0.86}S_{1.00}$	$Fe_{0.87}S_{1.00}$	$Fe_{0.87}S_{1.00}$	$Fe_{0.87}S_{1.00}$	$Fe_{0.87}S_{1.00}$	$Fe_{0.87}S_{1.00}$	$Fe_{0.86}S_{1.00}$

Sample Name	LD-09-24_753.9	LD-09-24_753.9	LD-09-24_753.9	LD-09-24_753.9	LD-09-24_753.9	LD-09-24_753.9	LD-09-24_753.9
Drill Hole	LD-09-24	LD-09-24	LD-09-24	LD-09-24	LD-09-24	LD-09-24	LD-09-24
Depth	753.9	753.9	753.9	753.9	753.9	753.9	753.9
Facies	Po-dom. SM	Po-dom. SM	Po-dom. SM	Po-dom. SM	Po-dom. SM	Po-dom. SM	Po-dom. SM
Probe analysis	207	208	209	210	211	212	213
Fe (wt%)	60.1	60.4	60.3	60.2	59.8	60.4	60.0
S	39.7	39.3	39.3	39.3	39.4	39.0	39.5
Total	**99.8**	**99.8**	**99.6**	**99.5**	**99.2**	**99.4**	99.5
Cu (ppm)	-	-	-	-	1342	-	-
Co	419	501	458	366	973	847	598
Ni	374	324	296	244	220	327	372
Fe (apfu)	1.08	1.08	1.08	1.08	1.07	1.08	1.07
S	1.24	1.23	1.23	1.22	1.23	1.22	1.23
Cu	-	-	-	-	-	-	-
Co	-	-	-	-	-	-	-
Ni	-	-	-	-	-	-	-
Mineral Formula	$Fe_{0.87}S_{1.00}$	$Fe_{0.88}S_{1.00}$	$Fe_{0.88}S_{1.00}$	$Fe_{0.88}S_{1.00}$	$Fe_{0.87}S_{1.00}$	$Fe_{0.89}S_{1.00}$	$Fe_{0.87}S_{1.00}$

Table 2.6 cont: Electron microprobe analyses for pyrrhotite. Atomic proportions based on 2 atoms per formula unit and recalculated based on 1 sulfur per formula unit.

Sample Name	LD-10-41_221.25	LD-10-41_221.25	LD-10-41_221.25	LD-10-41_221.25	LD-10-41_221.25	LD-11-44_473.64	LD-11-44_473.64
Drill Hole	LD-10-41	LD-10-41	LD-10-41	LD-10-41	LD-10-41	LD-11-44	LD-11-44
Depth	221.25	221.25	221.25	221.25	221.25	473.64	473.64
Facies	Po-dom. SM	Po-dom. SM	Po-dom. SM	Po-dom. SM	Po-dom. SM	Ccp-dom. SM	Ccp-dom. SM
Probe analysis	220	221	222	223	224	306	308
Fe (wt%)	60.2	60.0	59.9	60.3	60.2	60.7	61.1
S	39.3	39.4	39.3	39.2	39.3	38.9	38.6
Total	**99.4**	**99.4**	**99.2**	**99.5**	**99.5**	**99.7**	**99.8**
Cu (ppm)	-	-	-	-	-	-	-
Co	2711	2897	2787	2771	3050	1214	998
Ni	519	547	338	292	234	-	-
Fe (apfu)	1.08	1.08	1.07	1.08	1.08	1.09	1.09
S	1.23	1.23	1.23	1.22	1.23	1.21	1.21
Cu	-	-	-	-	-	-	-
Co	-	-	-	-	-	-	-
Ni	-	-	-	-	-	-	-
Mineral Formula	$Fe_{0.88}S_{1.00}$	$Fe_{0.88}S_{1.00}$	$Fe_{0.87}S_{1.00}$	$Fe_{0.88}S_{1.00}$	$Fe_{0.88}S_{1.00}$	$Fe_{0.90}S_{1.00}$	$Fe_{0.91}S_{1.00}$

Sample Name	LD-11-44_473.64	LD-11-44_473.64	LD-10-38_679.10	LD-10-38_679.10	LD-10-38_679.10	LD-10-38_679.10	LD-09-25_707.23
Drill Hole	LD-11-44	LD-11-44	LD-10-38	LD-10-38	LD-10-38	LD-10-38	LD-09-25
Depth	473.64	473.64	679.1	679.1	679.1	679.1	707.23
Facies	Ccp-dom. SM	Ccp-dom. SM	Ccp-dom. SM	Ccp-dom. SM	Ccp-dom. SM	Ccp-dom. SM	Py-Po-Sp
Probe analysis	310	312	314	316	318	320	180
Fe (wt%)	60.6	60.5	60.1	60.4	60.4	60.5	60.3
S	39.0	39.1	39.6	39.2	39.2	39.2	39.3
Total	**99.6**	**99.7**	**99.7**	**99.6**	**99.6**	**99.7**	**99.6**
Cu (ppm)	-	-	-	-	-	-	-
Co	1157	695	886	797	797	1005	-
Ni	-	-	-	-	-	-	-
Fe (apfu)	1.08	1.08	1.08	1.08	1.08	1.08	1.08
S	1.22	1.22	1.23	1.22	1.22	1.22	1.23
Cu	-	-	-	-	-	-	-
Co	-	-	-	-	-	-	-
Ni	-	-	-	-	-	-	-
Mineral Formula	$Fe_{0.89}S_{1.00}$	$Fe_{0.89}S_{1.00}$	$Fe_{0.87}S_{1.00}$	$Fe_{0.89}S_{1.00}$	$Fe_{0.89}S_{1.00}$	$Fe_{0.89}S_{1.00}$	$Fe_{0.88}S_{1.00}$

Table 2.6 cont: Electron microprobe analyses for pyrrhotite. Atomic proportions based on 2 atoms per formula unit and recalculated based on 1 sulfur per formula unit.

Sample Name	LD-09-25_707.23	LD-09-25_707.23	LD-09-25_707.23	LD-09-25_707.23	LD-09-25_707.23
Drill Hole	LD-09-25	LD-09-25	LD-09-25	LD-09-25	LD-09-25
Depth	707.23	707.23	707.23	707.23	707.23
Facies	Py-Sp-Po	Py-Sp-Po	Py-Sp-Po	Py-Sp-Po	Py-Sp-Po
Probe analysis	181	182	183	184	185
Fe (wt%)	60.6	60.1	60.1	60.4	60.5
S	39.1	39.5	39.5	39.4	39.3
Total	**99.7**	**99.6**	**99.6**	**99.8**	**99.8**
Cu (ppm)	-	-	-	-	-
Co	-	-	-	-	-
Ni	-	263	346	-	-
Fe (apfu)	1.09	1.08	1.08	1.08	1.08
S	1.22	1.23	1.23	1.23	1.23
Cu	-	-	-	-	-
Co	-	-	-	-	-
Ni	-	-	-	-	-
Mineral Formula	$Fe_{0.89}S_{1.00}$	$Fe_{0.87}S_{1.00}$	$Fe_{0.87}S_{1.00}$	$Fe_{0.88}S_{1.00}$	$Fe_{0.88}S_{1.00}$

Table 2.7
Electron microprobe analyses for pyrite. Atomic proportions based on 3 atoms per formula unit and recalculated based on 2 sulfur per formula unit.

Sample Name	LD-09-24_753.9	LD-09-24_753.9	LD-09-24_753.9	LD-09-24_753.9	LD-10-41_221.25	LD-10-41_221.25	LD-10-41_221.25	LD-10-41_221.25
Drill Hole	LD-09-24	LD-09-24	LD-09-24	LD-09-24	LD-10-41	LD-10-41	LD-10-41	LD-10-41
Depth	753.9	753.9	753.9	753.9	221.25	221.25	221.25	221.25
Facies	Po-dom. SM	Po-dom. SM	Po-dom. SM	Po-dom. SM	Po-dom. SM	Po-dom. SM	Po-dom. SM	Po-dom. SM
Probe analysis	111	112	113	114	115	116	117	118
Fe (wt%)	43.0	45.9	45.6	45.6	45.9	45.7	45.9	45.5
S	53.0	53.8	54.0	53.8	53.8	54.0	54.0	54.1
Zn	3.7	-	0.2	-	-	-	-	-
Total	**99.7**	**99.7**	**99.8**	**99.5**	**99.6**	**99.6**	**99.9**	**99.6**
Cu (ppm)	898	-	-	1014	-	-	-	-
Co	-	-	-	2401	-	776	-	-
Ni	-	-	-	626	-	-	-	-
Fe (apfu)	0.77	0.82	0.82	0.82	0.82	0.82	0.82	0.82
S	1.65	1.68	1.68	1.68	1.68	1.68	1.68	1.69
Zn	0.06	-	-	-	-	-	-	-
Cu	-	-	-	-	-	-	-	-
Co	-	-	-	-	-	-	-	-
Ni	-	-	-	-	-	-	-	-
Mineral Formula	$Fe_{0.93}S_{2.00}$	$Fe_{0.98}S_{2.00}$	$Fe_{0.97}S_{2.00}$	$Fe_{0.97}S_{2.00}$	$Fe_{0.98}S_{2.00}$	$Fe_{0.97}S_{2.00}$	$Fe_{0.98}S_{2.00}$	$Fe_{0.97}S_{2.00}$

Table 2.7 cont: Electron microprobe analyses for pyrite. Atomic proportions based on 3 atoms per formula unit and recalculated based on 2 sulfur per formula unit.

Sample Name	LD-10-41_221.25	LD-10-32A_1020.21	LD-10-32A_1020.21	LD-10-32A_1020.21	LD-10-41_231.75	LD-10-41_231.75	LD-10-41_231.75
Drill Hole	LD-10-41	LD-10-32A	LD-10-32A	LD-10-32A	LD-10-41	LD-10-41	LD-10-41
Depth	221.25	1020.21	1020.21	1020.21	231.75	231.75	231.75
Facies	Po-dom. SM	Ccp-dom. St.	Ccp-dom. St.	Ccp-dom. St.	Ccp-dom. St.	Ccp-dom. St.	Ccp-dom. St.
Probe analysis	119	120	121	122	123	124	125
Fe (wt%)	45.6	45.9	46.0	45.6	45.6	44.8	45.5
S	54.1	53.9	53.9	54.0	54.2	53.8	54.0
Zn	-	-	-	-	-	0.8	0.1
Total	**99.7**	**99.8**	**99.8**	**99.7**	**99.9**	**99.4**	**99.5**
Cu (ppm)	-	-	-	-	-	1504	-
Co	-	-	-	-	-	2261	2622
Ni	-	-	-	-	-	-	-
Fe (apfu)	0.82	0.82	0.82	0.82	0.82	0.80	0.82
S	1.69	1.68	1.68	1.69	1.69	1.68	1.69
Zn	-	-	-	-	-	0.01	-
Cu	-	-	-	-	-	-	-
Co	-	-	-	-	-	-	-
Ni	-	-	-	-	-	-	-
Mineral Formula	$Fe_{0.97}S_{2.00}$	$Fe_{0.98}S_{2.00}$	$Fe_{0.98}S_{2.00}$	$Fe_{0.97}S_{2.00}$	$Fe_{0.97}S_{2.00}$	$Fe_{0.96}S_{2.00}$	$Fe_{0.97}S_{2.00}$

Table 2.7 cont: Electron microprobe analyses for pyrite. Atomic proportions based on 3 atoms per formula unit and recalculated based on 2 sulfur per formula unit.

Sample Name	LD-10-41_231.75	LD-10-41_231.75	LD-10-41_231.75	LD-10-41_231.75	LD-09-25_707.23	LD-09-25_707.23	LD-09-25_707.23
Drill Hole	LD-10-41	LD-10-41	LD-10-41	LD-10-41	LD-09-25	LD-09-25	LD-09-25
Depth	231.75	231.75	231.75	231.75	707.23	707.23	707.23
Facies	Ccp-dom. St.	Ccp-dom. St.	Ccp-dom. St.	Ccp-dom. St.	Py-Sp-Po	Py-Sp-Po	Py-Sp-Po
Probe analysis	126	127	128	129	130	131	132
Fe (wt%)	45.9	45.4	44.9	45.2	45.8	45.9	45.8
S	53.9	53.8	53.9	54.1	53.9	53.9	54.0
Zn	-	-	-	-	-	-	-
Total	**99.8**	**99.3**	**98.8**	**99.2**	**99.8**	**99.8**	**99.9**
Cu (ppm)	-	-	-	-	-	-	-
Co	-	3351	7762	5261	-	-	-
Ni	-	-	-	-	-	-	-
Fe (apfu)	0.82	0.81	0.81	0.81	0.82	0.82	0.82
S	1.68	1.68	1.68	1.69	1.68	1.68	1.69
Zn	-	-	-	-	-	-	-
Cu	-	-	-	-	-	-	-
Co	-	-	0.01	-	-	-	-
Ni	-	-	-	-	-	-	-
Mineral Formula	$Fe_{0.98}S_{2.00}$	$Fe_{0.97}S_{2.00}$	$Fe_{0.96}S_{2.00}$	$Fe_{0.96}S_{2.00}$	$Fe_{0.98}S_{2.00}$	$Fe_{0.98}S_{2.00}$	$Fe_{0.97}S_{2.00}$

Table 2.7 cont: Electron microprobe analyses for pyrite. Atomic proportions based on 3 atoms per formula unit and recalculated based on 2 sulfur per formula unit.

Sample Name	LD-09-25_707.23	LD-09-25_707.23	LD-09-28_588.95	LD-09-28_588.95	LD-09-28_588.95	LD-09-25_835.20	LD-09-25_835.20
Drill Hole	LD-09-25	LD-09-25	LD-09-28	LD-09-28	LD-09-28	LD-09-25	LD-09-25
Depth	707.23	707.23	588.95	588.95	588.95	835.2	835.2
Facies	Py-Sp-Po	Py-Sp-Po	Py-dom. St.	Py-dom. St.	Py-dom. St.	Py-dom. St.	Py-dom. St.
Probe analysis	133	134	135	136	137	339	340
Fe (wt%)	45.9	45.5	45.6	45.4	45.6	46.2	46.0
S	54.0	54.2	54.1	53.9	54.1	53.5	53.7
Zn	-	-	-	-	-	-	-
Total	**99.9**	**99.8**	**99.7**	**99.3**	**99.7**	**99.7**	**99.7**
Cu (ppm)							
Co	-	-	-	-	-	-	-
Ni	-	-	-	3370	-	-	-
	-	-	-	-	-	-	-
Fe (apfu)	0.82	0.82	0.82	0.81	0.82	0.83	0.83
S	1.68	1.69	1.69	1.68	1.69	1.67	1.67
Zn	-	-	-	-	-	-	-
Cu	-	-	-	-	-	-	-
Co	-	-	-	-	-	-	-
Ni	-	-	-	-	-	-	-
Mineral Formula	$Fe_{0.98}S_{2.00}$	$Fe_{0.96}S_{2.00}$	$Fe_{0.97}S_{2.00}$	$Fe_{0.97}S_{2.00}$	$Fe_{0.97}S_{2.00}$	$Fe_{0.99}S_{2.00}$	$Fe_{0.98}S_{2.00}$

Table 2.7 cont: Electron microprobe analyses for pyrite. Atomic proportions based on 3 atoms per formula unit and recalculated based on 2 sulfur per formula unit.

Sample Name	LD-09-25_835.20	LD-09-25_835.20	LD-10-38_679.10	LD-10-38_679.10	LD-10-38_679.10	LD-10-38_679.10	LD-11-44_473.64
Drill Hole	LD-09-25	LD-09-25	LD-10-38	LD-10-38	LD-10-38	LD-10-38	LD-11-44
Depth	835.2	835.2	679.1	679.1	679.1	679.1	473.64
Facies	Py-dom. St.	Py-dom. St.	Ccp-dom. SM	Ccp-dom. SM	Ccp-dom. SM	Ccp-dom. SM	Ccp-dom. SM
Probe analysis	341	342	331	332	333	334	335
Fe (wt%)	46.3	46.1	46.3	46.2	46.4	46.5	46.2
S	53.4	53.6	53.5	53.5	53.4	53.3	53.7
Zn	-	-	-	-	-	-	-
Total	**99.7**	**99.7**	**99.7**	**99.7**	**99.8**	**99.7**	**99.9**
Cu (ppm)	-	-	-	-	-	700	-
Co	-	-	1757	-	-	-	-
Ni	-	-	-	-	-	-	-
Fe (apfu)	0.83	0.83	0.83	0.83	0.83	0.83	0.83
S	1.67	1.67	1.67	1.67	1.67	1.66	1.68
Zn	-	-	-	-	-	-	-
Cu	-	-	-	-	-	-	-
Co	-	-	-	-	-	-	-
Ni	-	-	-	-	-	-	-
Mineral Formula	$Fe_{1.00}S_{2.00}$	$Fe_{0.99}S_{2.00}$	$Fe_{0.99}S_{2.00}$	$Fe_{0.99}S_{2.00}$	$Fe_{1.00}S_{2.00}$	$Fe_{1.00}S_{2.00}$	$Fe_{0.99}S_{2.00}$

Table 2.7 cont: Electron microprobe analyses for pyrite. Atomic proportions based on 3 atoms per formula unit and recalculated based on 2 sulfur per formula unit.

Sample Name	LD-11-44_473.64	LD-11-44_473.64	LD-11-44_473.64
Drill Hole	LD-11-44	LD-11-44	LD-11-44
Depth	473.64	473.64	473.64
Facies	Ccp-dom. SM	Ccp-dom. SM	Ccp-dom. SM
Probe analysis	336	337	338
Fe (wt%)	46.2	46.3	46.2
S	53.7	53.4	53.3
Zn	-	-	-
Total	**99.8**	**99.7**	**99.6**
Cu (ppm)	-	-	-
Co	337	-	-
Ni	-	-	-
Fe (apfu)	0.83	0.83	0.83
S	1.67	1.66	1.66
Zn	-	-	-
Cu	-	-	-
Co	-	-	-
Ni	-	-	-
Mineral Formula	$Fe_{0.99}S_{2.00}$	$Fe_{1.00}S_{2.00}$	$Fe_{1.00}S_{2.00}$

Table 2.8
Electron microprobe analyses for sphalerite. Atomic proportions based on 2 atoms per formula unit and recalculated based on 1 sulfur per formula unit.

Sample Name	LD-10-41_221.25	LD-10-41_221.25	LD-10-41_221.25	LD-10-41_221.25	LD-10-41_221.25	LD-10-41_221.25	LD-10-41_221.25	LD-10-41_221.25
Drill Hole	LD-10-41	LD-10-41	LD-10-41	LD-10-41	LD-10-41	LD-10-41	LD-10-41	LD-10-41
Depth	221.25	221.25	221.25	221.25	221.25	221.25	221.25	221.25
Facies	Po-dom. SM	Po-dom. SM	Po-dom. SM	Po-dom. SM	Po-dom. SM	Po-dom. SM	Po-dom. SM	Po-dom. SM
Probe analysis	230	231	232	233	234	235	242	243
Fe (wt%)	7.0	7.7	6.6	6.6	6.4	6.7	6.2	6.5
S	33.0	33.0	33.0	33.2	33.2	33.3	33.3	33.0
Zn	59.2	58.2	58.9	59.0	60.0	59.2	58.3	58.5
Cu	0.72	0.72	1.10	1.02	0.19	0.70	2.02	1.91
Total	**99.9**	**99.6**	**99.7**	**99.7**	**99.8**	**99.9**	**99.9**	**99.8**
Co (ppm)	223	311	388	359	397	318	453	503
Ni	-	-	-	-	-	-	-	-
Fe (apfu)	0.13	0.14	0.12	0.12	0.11	0.12	0.11	0.12
S	1.00	1.03	1.03	1.04	1.04	1.04	1.04	1.03
Zn	0.90	0.89	0.90	0.90	0.92	0.91	0.89	0.89
Cu	0.01	0.01	0.02	0.02	-	0.01	0.03	0.03
Co	-	-	-	-	-	-	-	-
Ni	-	-	-	-	-	-	-	-
Mineral Formula	$Zn_{0.88}Fe_{0.12}S_{1.00}$	$Zn_{0.87}Fe_{0.13}S_{1.00}$	$Zn_{0.88}Fe_{0.12}S_{1.00}$	$Zn_{0.87}Fe_{0.11}S_{1.00}$	$Zn_{0.89}Fe_{0.11}S_{1.00}$	$Zn_{0.87}Fe_{0.12}S_{1.00}$	$Zn_{0.86}Fe_{0.11}S_{1.00}$	$Zn_{0.87}Fe_{0.11}S_{1.00}$

Table 2.8 cont: Electron microprobe analyses for sphalerite. Atomic proportions based on 2 atoms per formula unit and recalculated based on 1 sulfur per formula unit.

Sample Name	LD-10-41_221.25	LD-10-41_221.25	LD-10-41_221.25	LD-09-25_707.23	LD-09-25_707.23	LD-09-25_707.23	LD-09-25_707.23	LD-09-25_707.23
Drill Hole	LD-10-41	LD-10-41	LD-10-41	LD-09-25	LD-09-25	LD-09-25	LD-09-25	LD-09-25
Depth	221.25	221.25	221.25	707.23	707.23	707.23	707.23	707.23
Facies	Po-dom. SM	Po-dom. SM	Po-dom. SM	Py-Sp-Po	Py-Sp-Po	Py-Sp-Po	Py-Sp-Po	Py-Sp-Po
Probe analysis	244	245	246	236	237	238	239	240
Fe (wt%)	48.6	6.0	6.9	6.8	6.6	6.6	6.5	6.5
S	37.7	33.1	32.9	33.4	33.7	33.8	33.6	33.4
Zn	13.0	59.5	59.2	59.7	59.5	59.4	59.6	59.7
Cu	0.42	1.11	0.73	-	-	0.07	-	-
Total	**99.7**	**99.8**	**99.7**	**99.8**	**99.8**	**99.9**	**99.7**	**99.7**
Co (ppm)	524	428	410	142	-	-	243	-
Ni	-	-	-	-	-	-	-	-
Fe (apfu)	0.87	0.11	0.12	0.12	0.12	0.12	0.12	0.12
S	1.18	1.03	1.03	1.04	1.05	1.05	1.05	1.04
Zn	0.20	0.91	0.91	0.91	0.91	0.91	0.91	0.91
Cu	-	0.02	0.01	-	-	-	-	-
Co	-	-	-	-	-	-	-	-
Ni	-	-	-	-	-	-	-	-
Mineral Formula	$Zn_{0.17}Fe_{0.74}S_{1.00}$	$Zn_{0.88}Fe_{0.10}S_{1.00}$	$Zn_{0.88}Fe_{0.12}S_{1.00}$	$Zn_{0.88}Fe_{0.12}S_{1.00}$	$Zn_{0.87}Fe_{0.11}S_{1.00}$	$Zn_{0.86}Fe_{0.11}S_{1.00}$	$Zn_{0.87}Fe_{0.11}S_{1.00}$	$Zn_{0.88}Fe_{0.11}S_{1.00}$

Table 2.8 cont: Electron microprobe analyses for sphalerite. Atomic proportions based on 2 atoms per formula unit and recalculated based on 1 sulfur per formula unit.

Sample Name	LD-09-25_707.23	LD-09-28_588.95	LD-09-28_588.95	LD-09-28_588.95	LD-09-28_588.95	LD-09-28_588.95	LD-11-44_473.64	LD-11-44_473.64
Drill Hole	LD-09-25	LD-09-28	LD-09-28	LD-09-28	LD-09-28	LD-09-28	LD-11-44	LD-11-44
Depth	707.23	588.95	588.95	588.95	588.95	588.95	473.64	473.64
Facies	Py-Sp-Po	Py-dom. St.	Py-dom. St.	Py-dom. St.	Py-dom. St.	Py-dom. St.	Ccp-dom. SM	Ccp-dom. SM
Probe analysis	241	247	248	249	250	251	252	253
Fe (wt%)	6.5	5.6	6.3	6.8	9.7	5.9	7.7	5.5
S	33.3	33.3	33.2	33.2	35.1	33.4	32.9	33.3
Zn	59.8	60.1	60.1	59.4	54.4	59.8	58.4	60.1
Cu	-	0.91	0.32	0.48	0.09	0.67	0.71	0.69
Total	**99.6**	**99.9**	**99.9**	**99.9**	**99.4**	**99.8**	**99.8**	**99.7**
Co (ppm)	-	200	211	240	1,006	-	896	958
Ni	-	-	-	-	-	-	-	151
Fe (apfu)	0.12	0.10	0.11	0.12	0.17	0.11	0.14	0.10
S	1.04	1.04	1.03	1.04	1.10	1.04	1.03	1.04
Zn	0.91	0.92	0.92	0.91	0.83	0.92	0.89	0.92
Cu	-	0.01	-	-	-	0.01	0.01	0.01
Co	-	-	-	-	-	-	-	-
Ni	-	-	-	-	-	-	-	-
Mineral Formula	$Zn_{0.88}Fe_{0.11}S_{1.00}$	$Zn_{0.88}Fe_{0.10}S_{1.00}$	$Zn_{0.89}Fe_{0.10}S_{1.00}$	$Zn_{0.88}Fe_{0.12}S_{1.00}$	$Zn_{0.76}Fe_{0.16}S_{1.00}$	$Zn_{0.88}Fe_{0.10}S_{1.00}$	$Zn_{0.87}Fe_{0.13}S_{1.00}$	$Zn_{0.88}Fe_{0.10}S_{1.00}$

Table 2.8 cont: Electron microprobe analyses for sphalerite. Atomic proportions based on 2 atoms per formula unit and recalculated based on 1 sulfur per formula unit.

Sample Name	LD-11-44_473.64	LD-11-44_473.64	LD-11-44_473.64	LD-11-44_473.64	LD-11-44_473.64	LD-11-44_473.64	LD-11-44_473.64	LD-11-44_473.64
Drill Hole	LD-11-44	LD-11-44	LD-11-44	LD-11-44	LD-11-44	LD-11-44	LD-11-44	LD-11-44
Depth	473.64	473.64	473.64	473.64	473.64	473.64	473.64	473.64
Facies	Ccp-dom. SM	Ccp-dom. SM	Ccp-dom. SM	Ccp-dom. SM	Ccp-dom. SM	Ccp-dom. SM	Ccp-dom. SM	Ccp-dom. SM
Probe analysis	254	255	256	257	258	259	260	261
Fe (wt%)	6.9	5.6	5.5	6.5	5.7	6.3	5.2	5.7
S	33.1	33.1	33.5	33.2	33.7	33.4	33.6	33.3
Zn	59.4	60.3	60.2	59.2	59.4	59.6	60.6	60.3
Cu	0.34	0.73	0.60	0.72	0.92	0.30	0.38	0.42
Total	**99.8**	**99.7**	**99.7**	**99.6**	**99.8**	**99.6**	**99.8**	**99.7**
Co (ppm)	879	980	859	915	621	820	855	788
Ni	-	-	-	-	-	-	-	-
Fe (apfu)	0.12	0.10	0.10	0.12	0.10	0.11	0.09	0.10
S	1.03	1.03	1.04	1.04	1.05	1.04	1.05	1.04
Zn	0.91	0.92	0.92	0.90	0.91	0.91	0.93	0.92
Cu	-	-	-	0.01	0.02	-	-	-
Co	-	-	-	-	-	-	-	-
Ni	-	-	-	-	-	-	-	-
Mineral Formula	$Zn_{0.88}Fe_{0.12}S_{1.00}$	$Zn_{0.89}Fe_{0.10}S_{1.00}$	$Zn_{0.88}Fe_{0.09}S_{1.00}$	$Zn_{0.87}Fe_{0.11}S_{1.00}$	$Zn_{0.86}Fe_{0.10}S_{1.00}$	$Zn_{0.87}Fe_{0.11}S_{1.00}$	$Zn_{0.89}Fe_{0.09}S_{1.00}$	$Zn_{0.89}Fe_{0.10}S_{1.00}$

Table 2.8 cont: Electron microprobe analyses for sphalerite. Atomic proportions based on 2 atoms per formula unit and recalculated based on 1 sulfur per formula unit.

Sample Name	LD-11-44_473.64	LD-11-44_473.64	LD-10-38_679.10	LD-10-38_679.10	LD-10-38_679.10	LD-10-38_679.10	LD-10-38_679.10	LD-10-38_679.10
Drill Hole	LD-11-44	LD-11-44	LD-10-38	LD-10-38	LD-10-38	LD-10-38	LD-10-38	LD-10-38
Depth	473.64	473.64	679.10	679.10	679.10	679.10	679.10	679.10
Facies	Ccp-dom. SM	Ccp-dom. SM	Ccp-dom. SM	Ccp-dom. SM	Ccp-dom. SM	Ccp-dom. SM	Ccp-dom. SM	Ccp-dom. SM
Probe analysis	262	263	264	265	266	267	268	269
Fe (wt%)	5.8	5.2	6.9	6.7	5.8	6.6	6.3	6.5
S	33.0	33.3	33.2	33.4	33.3	32.6	33.2	33.3
Zn	60.4	60.8	58.6	58.0	59.0	59.7	59.7	59.6
Cu	0.34	0.56	1.16	1.61	1.46	0.87	0.58	0.39
Total	**99.5**	**99.8**	**99.9**	**99.7**	**99.7**	**99.8**	**99.7**	**99.8**
Co (ppm)	891	922	649	610	520	536	791	618
Ni	-	-	-	-	-	-	183	-
Fe (apfu)	0.10	0.09	0.12	0.12	0.10	0.12	0.11	0.12
S	1.03	1.04	1.04	1.04	1.04	1.02	1.03	1.04
Zn	0.92	0.93	0.90	0.89	0.90	0.91	0.91	0.91
Cu	-	-	0.02	0.03	0.02	0.01	-	-
Co	-	-	-	-	-	-	-	-
Ni	-	-	-	-	-	-	-	-
Mineral Formula	$Zn_{0.90}Fe_{0.10}S_{1.00}$	$Zn_{0.90}Fe_{0.09}S_{1.00}$	$Zn_{0.87}Fe_{0.12}S_{1.00}$	$Zn_{0.85}Fe_{0.11}S_{1.00}$	$Zn_{0.87}Fe_{0.10}S_{1.00}$	$Zn_{0.90}Fe_{0.12}S_{1.00}$	$Zn_{0.88}Fe_{0.11}S_{1.00}$	$Zn_{0.88}Fe_{0.11}S_{1.00}$

Table 2.8 cont: Electron microprobe analyses for sphalerite. Atomic proportions based on 2 atoms per formula unit and recalculated based on 1 sulfur per formula unit.

Sample Name	LD-10-38_679.10
Drill Hole	LD-10-38
Depth	679.10
Facies	Ccp-dom. SM
Probe analysis	270
Fe (wt%)	6.8
S	33.8
Zn	58.1
Cu	0.99
Total	**99.7**
Co (ppm)	625
Ni	-
Fe (apfu)	0.12
S	1.05
Zn	0.89
Cu	0.02
Co	-
Ni	-
Mineral Formula	$Zn_{0.84}Fe_{0.12}S_{1.00}$

Table 2.9
Electron microprobe analyses for cobaltite. Atomic proportions based on 3 atoms per formula unit and recalculated based on 1 sulfur per formula unit.

Sample Name	LD-10-38_679.10	LD-10-38_679.10	LD-10-38_679.10	LD-10-38_679.10	LD-10-38_679.10	LD-10-38_679.10
Drill Hole	LD-10-38	LD-10-38	LD-10-38	LD-10-38	LD-10-38	LD-10-38
Depth	679.10	679.10	679.10	679.10	679.10	679.10
Facies	Ccp-dom. SM	Ccp-dom. SM	Ccp-dom. SM	Ccp-dom. SM	Ccp-dom. SM	Ccp-dom. SM
Probe analysis	275	276	277	278	279	280
Fe (wt%)	6.8	8.8	5.2	3.2	5.8	2.8
S	23.3	26.4	23.7	23.6	24.6	23.3
As	40.5	36.8	40.6	42.1	40.0	42.9
Co	28.7	27.1	28.7	29.4	28.9	29.7
Total	**99.4**	**99.2**	**98.3**	**98.5**	**99.4**	**98.8**
Cu (ppm)	2,273	5119	10,705	4,612	3,666	972
Zn	-	-	-	-	-	-
Te	-	-	-	-	-	-
Ni	679	304	2,775	9,719	670	9,189
Se	-	-	-	-	-	-
Fe (apfu)	0.12	0.16	0.09	0.06	0.10	0.05
S	0.73	0.82	0.74	0.74	0.77	0.73
As	0.54	0.49	0.54	0.56	0.53	0.57
Co	0.49	0.46	0.49	0.50	0.49	0.50
Cu	-	-	0.02	-	-	-
Zn	-	-	-	-	-	-
Te	-	-	-	-	-	-
Ni	-	-	-	0.02	-	0.02
Se	-	-	-	-	-	-
Mineral Formula	$(Co_{0.67},Fe_{0.17})As_{0.74}S_{1.00}$	$(Co_{0.56},Fe_{0.19})As_{0.60}S_{1.00}$	$(Co_{0.66},Fe_{0.13})As_{0.73}S_{1.00}$	$(Co_{0.68},Fe_{0.08})As_{0.76}S_{1.00}$	$(Co_{0.64},Fe_{0.14})As_{0.70}S_{1.00}$	$(Co_{0.69},Fe_{0.07})As_{0.79}S_{1.00}$

Table 2.9 cont: Electron microprobe analyses for cobaltite. Atomic proportions based on 3 atoms per formula unit and recalculated based on 1 sulfur per formula unit.

Sample Name	LD-10-38_679.10	LD-10-38_679.10	LD-10-38_679.10	LD-10-38_679.10	LD-10-38_679.10	LD-11-44_473.64
Drill Hole	LD-10-38	LD-10-38	LD-10-38	LD-10-38	LD-10-38	LD-11-44
Depth	679.10	679.10	679.10	679.10	679.10	473.64
Facies	Ccp-dom. SM	Ccp-dom. SM	Ccp-dom. SM	Ccp-dom. SM	Ccp-dom. SM	Ccp-dom. SM
Probe analysis	281	282	283	284	285	287
Fe (wt%)	7.5	9.1	9.4	8.2	45.0	9.2
S	27.4	24.1	23.8	22.5	53.1	22.5
As	37.9	38.8	39.1	40.5	-	40.2
Co	26.8	27.6	27.3	27.4	1.52	27.6
Total	**99.7**	**99.7**	**99.7**	**98.9**	**99.7**	**99.7**
Cu (ppm)	1,706	1,007	1,338	6,913	940	1,064
Zn	-	-	-	-	-	-
Te	-	-	-	-	-	-
Ni	352	545	208	1,965	-	-
Se	-	-	-	-	-	-
Fe (apfu)	0.13	0.16	0.17	0.15	0.81	0.17
S	0.86	0.75	0.74	0.70	1.66	0.70
As	0.51	0.52	0.52	0.54	-	0.54
Co	0.46	0.47	0.46	0.47	0.03	0.47
Cu	-	0.02	-	0.01	-	-
Zn	-	-	-	-	-	-
Te	-	-	-	-	-	-
Ni	-	-	-	-	-	-
Se	-	-	-	-	-	-
Mineral Formula	$(Co_{0.53},Fe_{0.16})As_{0.59}S_{1.00}$	$(Co_{0.62},Fe_{0.22})As_{0.69}S_{1.00}$	$(Co_{0.62},Fe_{0.23})As_{0.70}S_{1.00}$	$(Co_{0.66},Fe_{0.21})As_{0.77}S_{1.00}$	$(Co_{0.02},Fe_{0.49})As_{0.00}S_{1.00}$	$(Co_{0.67},Fe_{0.24})As_{0.76}S_{1.00}$

Table 2.9 cont: Electron microprobe analyses for cobaltite. Atomic proportions based on 3 atoms per formula unit and recalculated based on 1 sulfur per formula unit.

Sample Name	LD-11-44_473.64	LD-11-44_473.64	LD-09-26_835.20	LD-08-11_530.15	LD-10-41_221.25	LD-10-41_221.25
Drill Hole	LD-11-44	LD-11-44	LD-09-26	LD-08-11	LD-10-41	LD-10-41
Depth	473.64	473.64	835.20	530.15	221.25	221.25
Facies	Ccp-dom. SM	Ccp-dom. SM	Py-dom. St.	Po-dom. SM	Po-dom. SM	Po-dom. SM
Probe analysis	288	289	286	290	291	292
Fe (wt%)	7.1	10.1	46.6	7.0	4.6	7.9
S	22.6	23.6	53.0	23.9	23.3	27.4
As	40.1	38.7	-	40.6	40.8	37.5
Co	28.6	27.1	-	28.1	29.0	26.3
Total	**98.5**	**99.7**	**99.6**	**99.8**	**97.9**	**99.2**
Cu (ppm)	11,231	188	835	-	12,278	5,921
Zn	-	-	-	-	-	-
Te	-	-	-	-	-	-
Ni	434	1,741	-	-	4,017	-
Se	-	-	-	-	-	-
Fe (apfu)	0.13	0.18	0.84	0.13	0.08	0.14
S	0.71	0.74	1.65	0.75	0.73	0.86
As	0.54	0.52	-	0.54	0.55	0.50
Co	0.49	0.46	-	0.48	0.49	0.45
Cu	0.02	-	-	-	0.02	-
Zn	-	-	-	-	-	-
Te	-	-	-	-	-	-
Ni	-	-	-	-	-	-
Se	-	-	-	-	-	-
Mineral Formula	$(Co_{0.69},Fe_{0.18})As_{0.76}S_{1.00}$	$(Co_{0.62},Fe_{0.25})As_{0.70}S_{1.00}$	$(Co_{0.00},Fe_{0.51})As_{0.00}S_{1.00}$	$(Co_{0.64},Fe_{0.17})As_{0.73}S_{1.00}$	$(Co_{0.68},Fe_{0.12})As_{0.75}S_{1.00}$	$(Co_{0.52},Fe_{0.17})As_{0.59}S_{1.00}$

Table 2.9 cont: Electron microprobe analyses for cobaltite. Atomic proportions based on 3 atoms per formula unit and recalculated based on 1 sulfur per formula unit.

Sample Name	LD-10-41_221.25	LD-10-41_221.25	LD-10-41_221.25	LD-10-41_221.25	LD-10-41_221.25	LD-10-41_221.25
Drill Hole	LD-10-41	LD-10-41	LD-10-41	LD-10-41	LD-10-41	LD-10-41
Depth	221.25	221.25	221.25	221.25	221.25	221.25
Facies	Po-dom. SM	Po-dom. SM	Po-dom. SM	Po-dom. SM	Po-dom. SM	Po-dom. SM
Probe analysis	293	294	295	296	297	298
Fe (wt%)	5.8	7.5	3.2	4.4	7.5	8.2
S	25.7	24.4	23.0	23.3	23.7	23.3
As	39.6	39.3	42.9	41.8	39.8	40.1
Co	28.1	27.7	29.9	28.9	28.2	27.8
Total	**99.4**	**99.1**	**99.2**	**98.5**	**99.4**	**99.6**
Cu (ppm)	-	5,068	-	4,383	2,934	2,796
Zn	-	-	-	-	-	-
Te	-	-	-	-	-	-
Ni	864	-	4,300	8,703	1,005	-
Se	-	-	-	-	-	-
Fe (apfu)	0.10	0.13	0.06	0.08	0.14	0.15
S	0.80	0.76	0.72	0.73	0.74	0.73
As	0.53	0.53	0.57	0.56	0.53	0.54
Co	0.48	0.47	0.51	0.49	0.48	0.47
Cu	-	-	-	-	-	-
Zn	-	-	-	-	-	-
Te	-	-	-	-	-	-
Ni	-	-	-	0.02	-	-
Se	-	-	-	-	-	-
Mineral Formula	$(Co_{0.60},Fe_{0.13})As_{0.66}S_{1.00}$	$(Co_{0.62},Fe_{0.18})As_{0.69}S_{1.00}$	$(Co_{0.71},Fe_{0.08})As_{0.80}S_{1.00}$	$(Co_{0.68},Fe_{0.11})As_{0.77}S_{1.00}$	$(Co_{0.65},Fe_{0.18})As_{0.72}S_{1.00}$	$(Co_{0.65},Fe_{0.20})As_{0.73}S_{1.00}$

Table 2.9 cont: Electron microprobe analyses for cobaltite. Atomic proportions based on 3 atoms per formula unit and recalculated based on 1 sulfur per formula unit.

Sample Name	LD-10-41_221.25	LD-10-41_221.25
Drill Hole	LD-10-41	LD-10-41
Depth	221.25	221.25
Facies	Po-dom. SM	Po-dom. SM
Probe analysis	299	300
Fe (wt%)	2.4	2.6
S	23.8	23.3
As	42.1	42.6
Co	30.3	29.9
Total	**98.7**	**98.5**
Cu (ppm)	2,240	4,015
Zn	-	1,703
Te	2,592	-
Ni	5,235	4,707
Se	-	2,289
Fe (apfu)	0.04	0.05
S	0.74	0.73
As	0.56	0.57
Co	0.51	0.51
Cu	-	-
Zn	-	-
Te	-	-
Ni	-	-
Se	-	-
Mineral Formula	$(Co_{0.69},Fe_{0.06})As_{0.76}S_{1.00}$	$(Co_{0.70},Fe_{0.06})As_{0.78}S_{1.00}$

Table 2.10
$\delta^{34}S$-values for chalcopyrite, pyrrhotite, and pyrite from the Little Deer VMS deposit obtained via SIMS.

Sample	Mineralization Style	Ccp ID	$\delta^{34}S$ (Ccp)	Po ID	$\delta^{34}S$ (Po)	Py ID	$\delta^{34}S$ (Py)
LD-10-41 (221.25-221.45)	Po-dominated Semi-Massive	Ccp 001	1.9			Py 002	-5.6
		Ccp 002	10.5			Py 004	5.0
						Py 005	9.8
						Py 006	6.3
LD-10-41 (231.75-231.91)	Ccp-dominated Stringers	Ccp 001	4.3	Po 1c	1.6	Py 001	6.3
		Ccp 002	1.9	Po 002	3.5	Py 002	2.2
						Py 003	3.8
						Py 004	1.7
						Py 005	15.2
						Py 006	3.8
						Py 007	2.3
LD-08-11 (530.15-530.40)	Po-dominated Semi-Massive	Ccp 002	5.8	Po 001b	0.2	Py 001	1.5
		Ccp 003	0.6	Po 003b	-0.3	Py 002	2.3
						Py 003	2.9
LD-98-7A (537.52-537.67)	Py-dominated Stringers					Py 001	5.5
						Py 002	6.1
						Py 003	7.2
						Py 004	5.0
LD-09-28 (588.95-589.25)	Py-dominated Stringers	Ccp 001	6.6			Py 001	6.8
						Py 002	4.6
						Py 003	4.7
						Py 004	4.3
						Py 005	3.4
						Py 006	6.3
LD-09-25 (705.75-705.85)	Disseminated Py	Ccp 002	4.0	Po 001	3.7	Py 001	3.4
		Ccp 003	3.4	Po 002	6.0	Py 003	3.8
		Ccp 004	4.4	Po 003	4.7	Py 005	3.2

Table 2.10 cont: $\delta^{34}S$-values for chalcopyrite, pyrrhotite, and pyrite from the Little Deer VMS deposit obtained via SIMS.

Sample	Mineralization Style	Ccp ID	$\delta^{34}S$ (Ccp)	Po ID	$\delta^{34}S$ (Po)	Py ID	$\delta^{34}S$ (Py)
LD-09-10A (806.37) (1)	Po-dom. Semi-Massive	Ccp 005 Ccp 009	1.5 3.0	Po 002 Po 003 Po 005 Po 007	4.4 4.9 5.6 3.7	Py 002 Py 003 Py 004 Py 005 Py 006 Py 007	4.1 5.2 4.1 2.9 2.9 1.8
LD-09-10A (806.37) (2)	Ccp-dom. Semi-Massive	Ccp 001 Ccp 002 Ccp 004 Ccp 005 Ccp 006	3.1 3.5 3.4 3.3 3.3				
		Average 3.8		**Average 3.5**		**Average 4.3**	
		Overall average for Little Deer: □^{34}S 3.9					

Table 2.11
$\delta^{34}S$-ranges for chalcopyrite, pyrrhotite, and pyrite related to the five different ore types (representing variants of the three facies established at Little Deer) analysed: chalcopyrite-dominated semi-massive sulfides; pyrrhotite-dominated semi-massive sulfides chalcopyrite-dominated stringers; pyrite-dominated stringers and disseminated pyrite.

Facies Style	No. analyses	Ccp	No. analyses	Po	No. analyses	Py
Ccp-dom. Semi-Massive	5	3.1 - 3.5	0	-	0	-
Po-dom. Semi-Massive	6	0.6 - 10.5	6	-0.3 - 5.6	12	-5.6 to 9.8
Ccp-dom. Stringers	2	1.9 - 4.3	2	1.6 - 3.5	7	1.7 - 15.2
Py-dom. Stringers	1	6.6	0	-	10	3.4 - 7.2
Disseminated Py	3	3.4 - 4.4	3	3.7 - 6	3	3.2 -3.8

Table 2.12
Calculated $\delta^{34}S$-values for chalcopyrite, pyrrhotite and pyrite when $\delta^{34}S$-values for seawater sulfate (SO_4) are 28, 29 and 30‰ respectively.

$\delta^{34}S$ (SO_4) : 28			(Eq. 9) $\delta^{34}S$ (Ccp) = - 0.05 ($10^6/T^2$) + $\delta^{34}S$ (H_2S)					
f	**$\delta^{34}S$ (SO_4) (Eq. 11)**	**$\delta^{34}S$ (H_2S) (Eq. 10)**	**T (°C)**	**T (K)**	**$\delta^{34}S$ (Ccp) if $\delta^{34}S$ (H_2S) = 3.0**	**$\delta^{34}S$ (Ccp) if $\delta^{34}S$ (H_2S) = 5.7**	**$\delta^{34}S$ (Ccp) if $\delta^{34}S$ (H_2S) = 11.5**	**$\delta^{34}S$ (Ccp) if $\delta^{34}S$ (H_2S) = 0**
1.0	28.00	3.0	250	523	2.8	5.5	11.3	-0.2
0.9	30.71	5.7	275	548	2.8	5.5	11.3	-0.2
0.8	36.47	11.5	300	573	2.8	5.6	11.3	-0.2
			325	598	2.9	5.6	11.3	-0.1
			350	623	2.9	5.6	11.3	-0.1
$\delta^{34}S$ (SO_4) : 29			(Eq. 9) $\delta^{34}S$ (Ccp) = - 0.05 ($10^6/T^2$) + $\delta^{34}S$ (H_2S)					
f	**$\delta^{34}S$ (SO_4) (Eq. 11)**	**$\delta^{34}S$ (H_2S) (Eq. 10)**	**T (°C)**	**T (K)**	**$\delta^{34}S$ (Ccp) if $\delta^{34}S$ (H_2S) = 4.0**	**$\delta^{34}S$ (Ccp) if $\delta^{34}S$ (H_2S) = 6.7**	**$\delta^{34}S$ (Ccp) if $\delta^{34}S$ (H_2S) = 12.5**	**$\delta^{34}S$ (Ccp) if $\delta^{34}S$ (H_2S) = 0**
1.0	29.00	4.00	250	523	3.8	6.5	12.3	-0.2
0.9	31.71	6.7	275	548	3.8	6.5	12.3	-0.2
0.8	37.48	12.5	300	573	3.8	6.6	12.3	-0.2
			325	598	3.9	6.6	12.3	-0.1
			350	623	3.9	6.6	12.4	-0.1
$\delta^{34}S$ (SO_4) : 30			(Eq. 9) $\delta^{34}S$ (Ccp) = - 0.05 ($10^6/T^2$) + $\delta^{34}S$ (H_2S)					
f	**$\delta^{34}S$ (SO_4) (Eq. 11)**	**$\delta^{34}S$ (H_2S) (Eq. 10)**	**T (°C)**	**T (K)**	**$\delta^{34}S$ (Ccp) if $\delta^{34}S$ (H_2S) = 5.0**	**$\delta^{34}S$ (Ccp) if $\delta^{34}S$ (H_2S) = 7.7**	**$\delta^{34}S$ (Ccp) if $\delta^{34}S$ (H_2S) = 13.5**	**$\delta^{34}S$ (Ccp) if $\delta^{34}S$ (H_2S) = 0**
1.0	30.00	5.00	250	523	4.8	7.5	13.3	-0.2
0.9	32.71	7.7	275	548	4.8	7.6	13.3	-0.2
0.8	38.49	13.5	300	573	4.8	7.6	13.3	-0.2
			325	598	4.9	7.6	13.4	-0.1
			350	623	4.9	7.6	13.4	-0.1

Table 2.12 cont: Calculated $\delta^{34}S$-values for chalcopyrite, pyrrhotite and pyrite when $\delta^{34}S$-values for seawater sulfate (SO_4) are 28, 29 and 30‰ respectively.

$\delta^{34}S$ (SO_4) : 28			(Eq. 9) $\delta^{34}S$ (Po) = 0.10 ($10^6/T^2$) + $\delta^{34}S$ (H_2S)					
f	**$\delta^{34}S$ (SO_4) (Eq. 11)**	**$\delta^{34}S$ (H_2S) (Eq. 10)**	**T (°C)**	**T (K)**	**$\delta^{34}S$ (Po) if $\delta^{34}S$ (H_2S) = 3.0**	**$\delta^{34}S$ (Po) if $\delta^{34}S$ (H_2S) = 5.7**	**$\delta^{34}S$ (Po) if $\delta^{34}S$ (H_2S) = 11.5**	**$\delta^{34}S$ (Po) if $\delta^{34}S$ (H_2S) = 0**
1.0	28.00	3.0	250	523	3.4	6.1	11.8	0.4
0.9	30.71	5.7	275	548	3.3	6.0	11.8	0.3
0.8	36.47	11.5	300	573	3.3	6.0	11.8	0.3
			325	598	3.3	6.0	11.8	0.3
			350	623	3.3	6.0	11.7	0.3
$\delta^{34}S$ (SO_4) : 29			(Eq. 9) $\delta^{34}S$ (Po) = 0.10 ($10^6/T^2$) + $\delta^{34}S$ (H_2S)					
f	**$\delta^{34}S$ (SO_4) (Eq. 11)**	**$\delta^{34}S$ (H_2S) (Eq. 10)**	**T (°C)**	**T (K)**	**$\delta^{34}S$ (Po) if $\delta^{34}S$ (H_2S) = 4.0**	**$\delta^{34}S$ (Po) if $\delta^{34}S$ (H_2S) = 6.7**	**$\delta^{34}S$ (Po) if $\delta^{34}S$ (H_2S) = 12.5**	**$\delta^{34}S$ (Po) if $\delta^{34}S$ (H_2S) = 0**
1.0	29.00	4.0	250	523	4.4	7.1	12.9	0.4
0.9	31.71	6.7	275	548	4.3	7.0	12.8	0.3
0.8	37.48	12.5	300	573	4.3	7.0	12.8	0.3
			325	598	4.3	7.0	12.8	0.3
			350	623	4.3	7.0	12.7	0.3
$\delta^{34}S$ (SO_4) : 30			(Eq. 9) $\delta^{34}S$ (Po) = 0.10 ($10^6/T^2$) + $\delta^{34}S$ (H_2S)					
f	**$\delta^{34}S$ (SO_4) (Eq. 11)**	**$\delta^{34}S$ (H_2S) (Eq. 10)**	**T (°C)**	**T (K)**	**$\delta^{34}S$ (Po) if $\delta^{34}S$ (H_2S) = 5.0**	**$\delta^{34}S$ (Po) if $\delta^{34}S$ (H_2S) = 7.7**	**$\delta^{34}S$ (Po) if $\delta^{34}S$ (H_2S) = 13.5**	**$\delta^{34}S$ (Po) if $\delta^{34}S$ (H_2S) = 0**
1.0	30.00	5.0	250	523	5.4	8.1	13.9	0.4
0.9	32.71	7.7	275	548	5.3	8.0	13.8	0.3
0.8	38.49	13.5	300	573	5.3	8.0	13.8	0.3
			325	598	5.3	8.0	13.8	0.3
			350	623	5.3	8.0	13.8	0.3

Table 2.12 cont: Calculated $\delta^{34}S$-values for chalcopyrite, pyrrhotite and pyrite when $\delta^{34}S$-values for seawater sulfate (SO_4) are 28, 29 and 30‰ respectively.

$\delta^{34}S$ (SO_4) : 28			(Eq. 9) $\delta^{34}S$ (Py) = 0.40 ($10^6/T^2$) + $\delta^{34}S$ (H_2S)					
f	**$\delta^{34}S$ (SO_4) (Eq. 11)**	**$\delta^{34}S$ (H_2S) (Eq. 10)**	**T (°C)**	**T (K)**	**$\delta^{34}S$ (Py) if $\delta^{34}S$ (H_2S) = 3.0**	**$\delta^{34}S$ (Py) if $\delta^{34}S$ (H_2S) = 5.7**	**$\delta^{34}S$ (Py) if $\delta^{34}S$ (H_2S) = 11.5**	**$\delta^{34}S$ (Py) if $\delta^{34}S$ (H_2S) = 0**
1.0	28.00	3.0	250	523	4.5	7.2	12.9	1.5
0.9	30.71	5.7	275	548	4.3	7.0	12.8	1.3
0.8	36.47	11.5	300	573	4.2	6.9	12.7	1.2
			325	598	4.1	6.8	12.6	1.1
			350	623	4.0	6.7	12.5	1.0
$\delta^{34}S$ (SO_4) : 29			(Eq. 9) $\delta^{34}S$ (Py) = 0.40 ($10^6/T^2$) + $\delta^{34}S$ (H_2S)					
f	**$\delta^{34}S$ (SO_4) (Eq. 11)**	**$\delta^{34}S$ (H_2S) (Eq. 10)**	**T (°C)**	**T (K)**	**$\delta^{34}S$ (Py) if $\delta^{34}S$ (H_2S) = 4.0**	**$\delta^{34}S$ (Py) if $\delta^{34}S$ (H_2S) = 6.7**	**$\delta^{34}S$ (Py) if $\delta^{34}S$ (H_2S) = 12.5**	**$\delta^{34}S$ (Py) if $\delta^{34}S$ (H_2S) = 0**
1.0	29.00	4.0	250	523	5.5	8.2	13.9	1.5
0.9	31.71	6.7	275	548	5.3	8.0	13.8	1.3
0.8	37.48	12.5	300	573	5.2	7.9	13.7	1.2
			325	598	5.1	7.8	13.6	1.1
			350	623	5.0	7.7	13.5	1.0
$\delta^{34}S$ (SO_4) : 30			(Eq. 9) $\delta^{34}S$ (Py) = 0.40 ($10^6/T^2$) + $\delta^{34}S$ (H_2S)					
f	**$\delta^{34}S$ (SO_4) (Eq. 11)**	**$\delta^{34}S$ (H_2S) (Eq. 10)**	**T (°C)**	**T (K)**	**$\delta^{34}S$ (Py) if $\delta^{34}S$ (H_2S) = 5.0**	**$\delta^{34}S$ (Py) if $\delta^{34}S$ (H_2S) = 7.7**	**$\delta^{34}S$ (Py) if $\delta^{34}S$ (H_2S) = 13.5**	**$\delta^{34}S$ (Py) if $\delta^{34}S$ (H_2S) = 0**
1.0	30.00	5.0	250	523	6.5	7.9	15.0	1.5
0.9	32.71	7.7	275	548	6.3	7.8	14.8	1.3
0.8	38.49	13.5	300	573	6.2	7.8	14.7	1.2
			325	598	6.1	7.8	14.6	1.1
			350	623	6.0	7.8	14.5	1.0

Chapter 3

[3.1] Summary

The Little Deer deposit, Springdale Peninsula, north-central Newfoundland, is a mafic-(Cyprus)-type VMS deposit hosted in a northern Appalachian ophiolite terrain; as a past-producer (Cu), Little Deer is currently the focus of extensive exploration. Recent exploration has presented a renewed opportunity to study the Little Deer deposit and obtain a better understanding of ophiolite-hosted VMS mineralization in the northern Appalachians.

The main conclusions of this study are:

1) The Little Deer VMS deposit is an Appalachian mafic-(Cyprus)-style VMS deposit consisting of a Cu-dominated VMS stockwork with occasional semi-massive to massive sulfide horizons. The deposit formed from high temperature (>300°C) VMS-related fluids via zone refining or boiling. The metal assemblages and bulk mineralogy of the ores is interpreted to represent primary VMS mineralization; however, the ores have been significantly texturally modified during metamorphism and deformation leading to abundant textural remobilization and recrystallization, including the formation of secondary minerals (e.g., cobaltite and telluride phases).

2) Based on $\delta^{34}S$-values for chalcopyrite, pyrrhotite and pyrite, it is suggested that reduced sulfur in sulfides from Little Deer was principally derived through TSR of Late Cambrian seawater sulfate, with or without an input of leached igneous sulfur from surrounding basaltic/ultramafic rocks. The $\delta^{34}S$-values obtained at Little Deer are within the range observed for Late Cambrian VMS deposits globally, suggesting that TSR was an important global mechanism for the production of reduced sulfur during Late Cambrian VMS formation.

3) The mineralogy, paragenesis, and textural evolution of the sulfides at Little Deer is similar to the massive sulfide deposits of the Italian Apennines; the Norwegian Caledonides and the VMS deposits of Cyprus. On a regional scale, Little Deer mineralization is similar to VMS accumulations at Betts Cove, Tilt Cove, Colchester Little Bay and Whalesback.

[3.2] Directions for Future Research

Although this thesis has provided and contributed to the understanding of the geology, mineralogy and sulfur isotope geochemistry of the Little Deer VMS deposit, potential areas for future research include:

1) This project utilizes the graphically logged mineralized horizons of 30 diamond drill cores, taken from across the Little Deer deposit, that document the mineralogy, mineral assemblages, mineral textures and mineralization styles present at Little Deer (Appendix A.1). Further graphic logs are suggested so that a greater understanding regarding the spatial distribution of the above can be determined. This may strengthen and develop the relationships established by the 3D metal zoning model and may also highlight areas of exploration interest that could be of benefit to future drilling programs at Little Deer.

2) Supplementary sulfur isotope work is recommended in order to further constrain $\delta^{34}S$-values at Little Deer. This could highlight whether the -5.6‰ value, obtained for a single pyrite crystal, was an anomaly or an indication for an alternate source for sulfur (possibly biogenic or sulfide oxidation) at Little Deer.

3) Obtaining bulk rock data on the ultramafics of the Lushs Bight Group may definitively establish whether they are a likely source for the trace metals found in the trace phase suite present at Little Deer.

4) If possible, the structure of the Little Deer-Whalesback area should be constrained. This may yield information regarding the possibility of a Little Deer massive sulfide lens, if in existence, and could also highlight the controls that structure had/may have had upon primary VMS sulfide mineralization.

Appendix A

Table A.1
Samples analyzed for Little Deer: 99 representative Little Deer samples were analyzed using standard transmitted and reflected light petrography; 43 samples from this 99 were analyzed using the SEM.

Drill Hole	From (m)	To (m)	Sample	Description	Style Of Mineralization
LD-98-07A	527	626.55	LD-98-07A (539.70-539.9)	Fe Rich Horizon w/ Jasper	Disseminated
			LD-98-07A (597.25-597.4)	Py Por + Po + Sp	Stringer
LD-98-07D	590.04	805.5	LD-98-07D (602.85-603.0)	Equal Po + Ccp w/ Py Assoc. w/ Qtz veins	Stringer
			LD-98-07D (617.75-617.90)	Dyke	
			LD-98-07D (671.60-672.70)	Po Dominated	Stringer
LD-00-12A	675.75	797.65	LD-00-12A (680.36-680.50)	Remobilized Ccp	Stringer
			LD-00-12A (706.65-706.90)	Remobilized Ccp + Po	Stringer
			LD-00-12A (789.65-789.73)	Ccp + Py +Po	Semi-Massive
			LD-00-12A (792.15-792.25)	Po + Py	Stringer
			LD-00-12A (796.60-796.80)	Qtz + Po + Sp	Stringer
LD-07-01A	676.43	768.3	LD-07-01A (682.0-682.3)	Ccp Dominated Pillow Lava?	Stringer
			LD-07-01A (697.9-698.0)	Po Dominated	Semi-Massive
			LD-07-01A (740.6-740.9)	Py Por Dominated + Ep + Po (cherry)	Stringer
			LD-07-01A (751.4-751.5)	Po Dominated (Cherry)	Stringer
			LD-07-01A (757.35-757.50)	Po/Sp?	Stringer
			LD-07-01A (765.2-765.4)	Py Por Dominated	Stringer
LD-07-06	538.36	558.59	LD-07-06 (541.6-542.0)	Equal Ccp + Po	Stringer
LD-07-07	408.22	424	LD-07-07 (409.8-409.95)	Ccp Dominated (Primary?)	Stringer
LD-07-08	612.13	638.3	LD-07-08 (631.45-631.7)	Epidote + Sp	Stringer
			LD-07-08 (636.8-637.0)	Dyke	
LD-08-10A	791.88	812.35	LD-08-10A (801.5-801.7)	Po + Py	Semi-Massive
LD-08-11	525.72	534.23	LD-08-11 (530.15-530.40)	Po Dominated	Semi-Massive Stringer
LD-08-14	479.42	718.8	LD-08-14 (482.5-482.75)	Py Dominated	Stringer
			LD-08-14 (705.25-705.35)	Fe Horizon	Stringer
LD-08-15	623.2	681.6	LD-08-15 (639.2-639.4)	Po Dominated	Stringer
			LD-08-15 (642.3-642.52)	Ccp Dominated	Stringer
			LD-08-15 (643.70-643.94	Po Dominated	Stringer

			LD-08-15 (647.14-647.30)	Ccp Dominated	Stringer
LD-08-16B	768.9	1071.1	LD-08-16B (777.55-777.80)	Py Por Pillow Lava?	Disseminated
			LD-08-16B (859.1-859.35)	Dyke	
			LD-08-16B (892.55-892.80)	Ccp Dominated	Stringer
LD-08-17	600.5	696.7	LD-08-17 (601.25-601.45)	Po Dominated	Stringer
			LD-08-17 (602.05-602.17)	Ccp Dominated	Semi-Massive
			LD-08-17 (633.5-633.8)	Remobilized Ccp	Stringer
			LD-08-17 (636.55-636.70)	Ccp Dominated	Stringer
			LD-08-17 (668.6-668.8)	Ccp Dominated	Semi-Massive
			LD-08-17 (670.0-670.2)	Po Dominated	Stringer
			LD-08-17 (695.32-695.60)	Po Dominated + Py Por	Stringer
LD-09-21	758.3	771	LD-09-21 (762.0-762.1)	Ccp Dominated	Semi-Massive
			LD-09-21 (766.63-766.80)	Ccp Dominated	Stringer
			LD-09-21 (768.59-768.96)	Po Dominated	Stringer
LD-09-22	692.8	828.9	LD-09-22 (694.23-694.45)	Py Por Replacing Po	Disseminated
			LD-09-22 (819.68-819.83)	Py Por + Sp	Stringer
LD-09-24	747.7	760.1	LD-09-24 (753.9-754.1)	Po Dominated	Semi-Massive
			LD-09-24 (754.82-755.04)	Po Dominated	Stringer
			LD-09-24 (756.9-757.1)	Dyke	
LD-09-25	689.43	839.4	LD-09-25 (835.20-835.39)	Py Dominated w/ Ccp	Stringer
LD-09-28	582.4	643.5	LD-09-28 (588.95-589.25)	Py Dominated w/ Po	Stringer
LD-09-30	682.5	718.8	LD-09-30 (700.25-700.50)	Ccp Dominated w/ Po Overprint	Stringer
			LD-09-30 (716.35-716.65)	Ccp going to Py	Stringer
LD-09-30A	842	854.3	LD-09-30A (851.65-851.88)	Py Por	Disseminated
LD-10-31	672.5	806.6	LD-10-31 (688.6-688.8)	Ccp Dominated	Semi-Massive
			LD-10-31 (689.7-689.9)	Dyke	
			LD-10-31 (694.0-694.25	Py + Po/Sp	Stringer
			LD-10-31 (704.7-704.9)	Py Por w/ Po	Stringer
			LD-10-31 (711.05-711.30)	Pillow Lava? w/ Sericite Alteration	Stringer
			LD-10-31 (724.55-724.7)	Dyke	
			LD-10-31 (741.0-741.15)	Ccp Dominated	Stringer
LD-10-32A	736.85	1016	LD-09-32A (740.39-740.48)	Ccp Dominated	Semi-Massive
LD-10-35	632.25	784.35	LD-10-35 (636.20-636.37)	Po Dominated banded w/ Ccp	Semi-Massive

			LD-10-35 (639.40-640.15)	Po Dominated w/ Ccp + Py Por	Stringer
			LD-10-35 (661.50-661.70)	Po Dominated	Stringer
			LD-10-35 (764.0-764.2)	Ccp Dominated	Stringer
			LD-10-35 (768.55-768.75)	Ccp Dominated w/ Po	Stringer
			LD-10-35 (776.2-776.0)	Ccp Dominated Flecks	Disseminated
			LD-10-35 (779.80-779.95)	Ccp Dominated	Stringer
LD-10-37	737.15	1137.5	LD-10-37 (743.1-743.3)	Ccp Dominated w/ Po	Stringer
			LD-10-37 (1104.5-1104.7)	Dyke	
			LD-10-37 (1114.0-1114.1)	Po Dominated	Stringer
LD-10-38	676.05	1001.5	LD-10-38 (679.1-679.4)	Ccp Dominated w/ Po	Semi-Massive Stringers
			LD-10-38 (906.25-906.35)	Remobilized Ccp Dominated	Stringer
			LD-10-38 (963.7-963.95)	Py Dominated	Stringer
			LD-10-38 (995.6-996.0)	Ccp Pillow Lava?	Stringer
LD-10-39	58.85	313.2	LD-10-39 (208.60-208.80)	Ccp Dominated	Semi-Massive
			LD-10-39 (215.2-215.4)	Po Dominated	Stringer
			LD-10-39 (240.7-240.85)	Py Por	Stringer
			LD-10-39 (274.6-274.8)	Py + Ccp	Stringer
			LD-10-39 (285.95-286.1)	Po Dom associated w/ Seri Alteration	Stringer
			LD-10-39 (297.40-297.55)	Py + Sp	Stringer
LD-10-41	179.1	240.95	LD-10-41 (202.2-202.3)	Banded Py Por w/ Ccp	Stringer
			LD-10-41 (202.8-203.0)	Remobilized Ccp	Stringer
			LD-10-41 (219.9-220.0)	Po Dominated	Semi-Massive
			LD-10-41 (220.9-221.15)	Equal Py, Po and Ccp	Stringer
			LD-10-41 (221.25-221.45)	Po Dominated	Semi-Massive
			LD-10-41 (230.2-230.3)	Po Dominated	Semi-Massive
			LD-10-41 (231.75-231.91)	Ccp Dominated	Stringer
			LD-10-41 (233.12-233.25)	Dyke	
			LD-10-41 (234.55-234.80)	Ccp at edge of Dyke	
			LD-10-41 (235.30-235.42)	Ccp Dominated	Semi-Massive
LD-11-44	412.4	484.6	LD-11-44 (414.4-414.5)	Py Dominated w/ Ccp	Semi-Massive
			LD-11-44 (415.28-415.35)	Ccp Dominated	Semi-Massive
			LD-11-44 (469.72-469.80)	Py Dominated	Disseminated
			LD-11-44 (469.9-470.0)	Ccp Dominated w/ Py	Semi-Massive
			LD-11-44 (473.64-473.73)	Ccp Dominated	Semi-Massive

LD-11-45	467.1	495.8	LD-11-45 (468.82-468.96)	Py + Ccp	Stringer
			LD-11-45 (469.49-469.57)	Py Por	Stringer
			LD-11-45 (493.64-493.82)	Po Dominated w/ Ccp	Semi-Massive

[A.1] Graphic Logs

This project utilizes the observations from fieldwork undertaken by the author in June - July 2011. During this field period, the mineralized horizons of 30 diamond drill cores, taken from across the Little Deer deposit, were graphically logged to document the mineralogy, mineral assemblages, mineral textures, mineralization styles and metal zoning in the Little Deer deposit.

A total of 145 representative samples of Little Deer mineralization and alteration phases were collected from 30 diamond drill cores.

- Log ID e.g., LD-07-06: LD - Little Deer

  07 - Year hole was drilled, i.e., 2007

  06 - Sixth hole drilled in the 2007 season

Key

Stratigraphy and Host Rocks

Host Rocks

Basalt

Intrusions

Porphyritic mafic/ andesitic dykes

Basaltic mafic dykes

Sulfide Facies

Pyrite Dominated Sulfides

Porphyroblasts

Pyrite only

Pyrite-dominated with pyrrhotite and chalcopyrite stringers

Pyrite-dominated with chalcopyrite stringers

Pyrite-dominated with pyrrhotite stringers

Semi-Massive

Pyrite dominated with semi-massive chalcopyrite

Chalcopyrite-Pyrrhotite Dominated Sulfides

Stringers

Chalcopyrite-dominated with pyrrhotite stringers and pyrite porphyroblasts

Chalcopyrite-dominated with pyrrhotite stringers

Pyrrhotite-dominated with chalcopyrite stringers and pyrite porphyroblasts

Pyrrhotite-dominated with chalcopyrite stringers

Pyrrhotite-dominated with pyrite porphyroblasts

Semi-Massive

Chalcopyrite dominated with semi-massive pyrrhotite +/- pyrite porphyroblasts

Pyrrhotite dominated with semi-massive chalcopyrite +/- pyrite porphyroblasts

Pyrite-Sphalerite-Pyrrhotite Dominated Sulfides

Disseminated pyrite-sphalerite-pyrrhotite

Disseminated pyrite-sphalerite-pyrrhotite + Fe-rich jasper horizons

Pyrrhotite stringers with sphalerite disseminations

Graphic Log Key A.1.1
Key for graphic logs

Key

Abbreviations

Mineralization	*Alteration*	*Rock Type*
Ccp = Chalcopyrite	Ca = Calcite	Arg = Argillite
Sp = Sphalerite	Ep = Epidote	L. Tuff = Lapilli Tuff
Py = Pyrite	Ser = Sericite	Tuff B. = Tuff Breccia
Po = Pyrrhotite	Qtz = Quartz	Flow = Flow
	Chl = Chlorite	Int = Intrusion
		Sulf = Massive Sulfide

Mineralization/Alteration Intensity

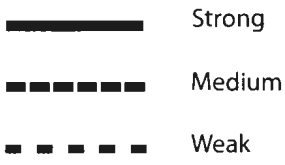

A.1.1 cont: Key for graphic logs

LD-98-07A

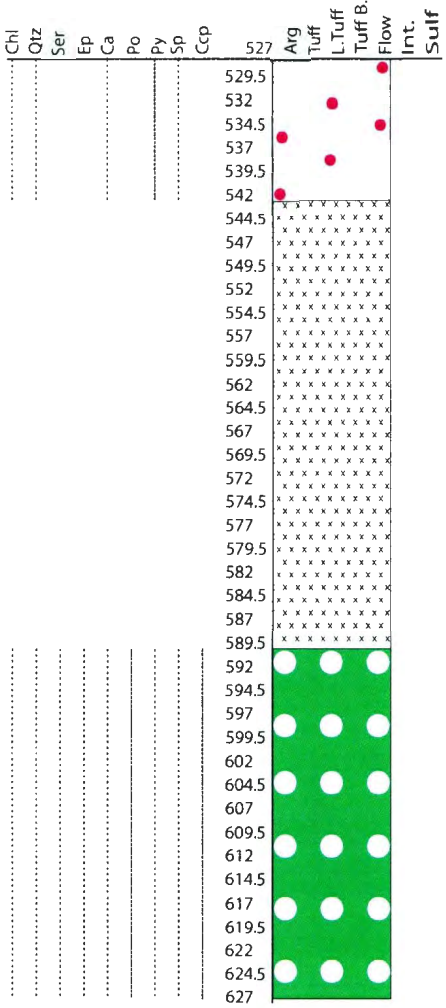

LD-98-07B

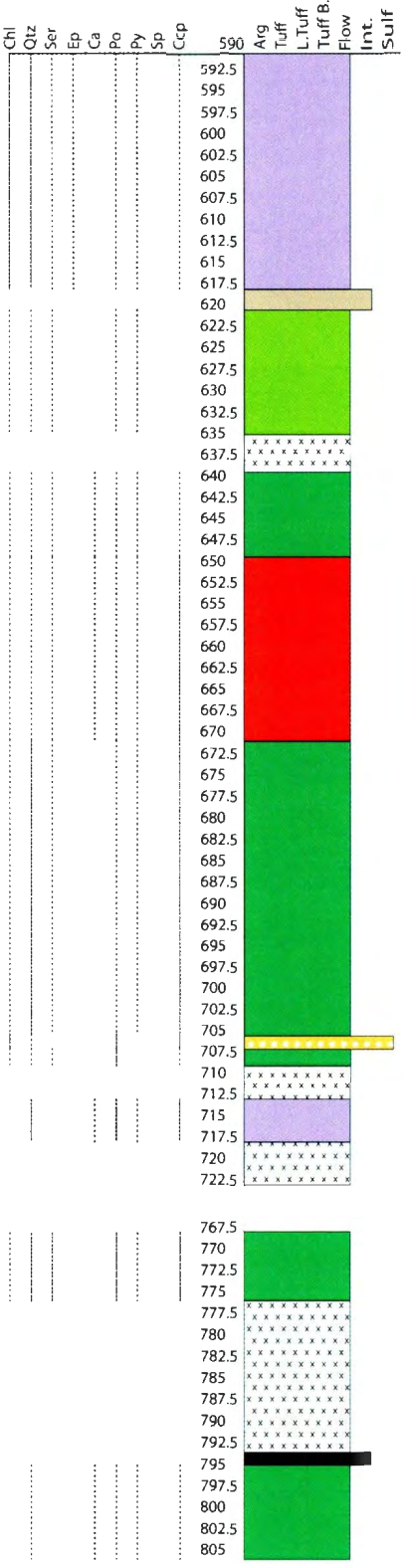

Graphic Logs A.1.2
Digitized graphic logs for Little Deer.

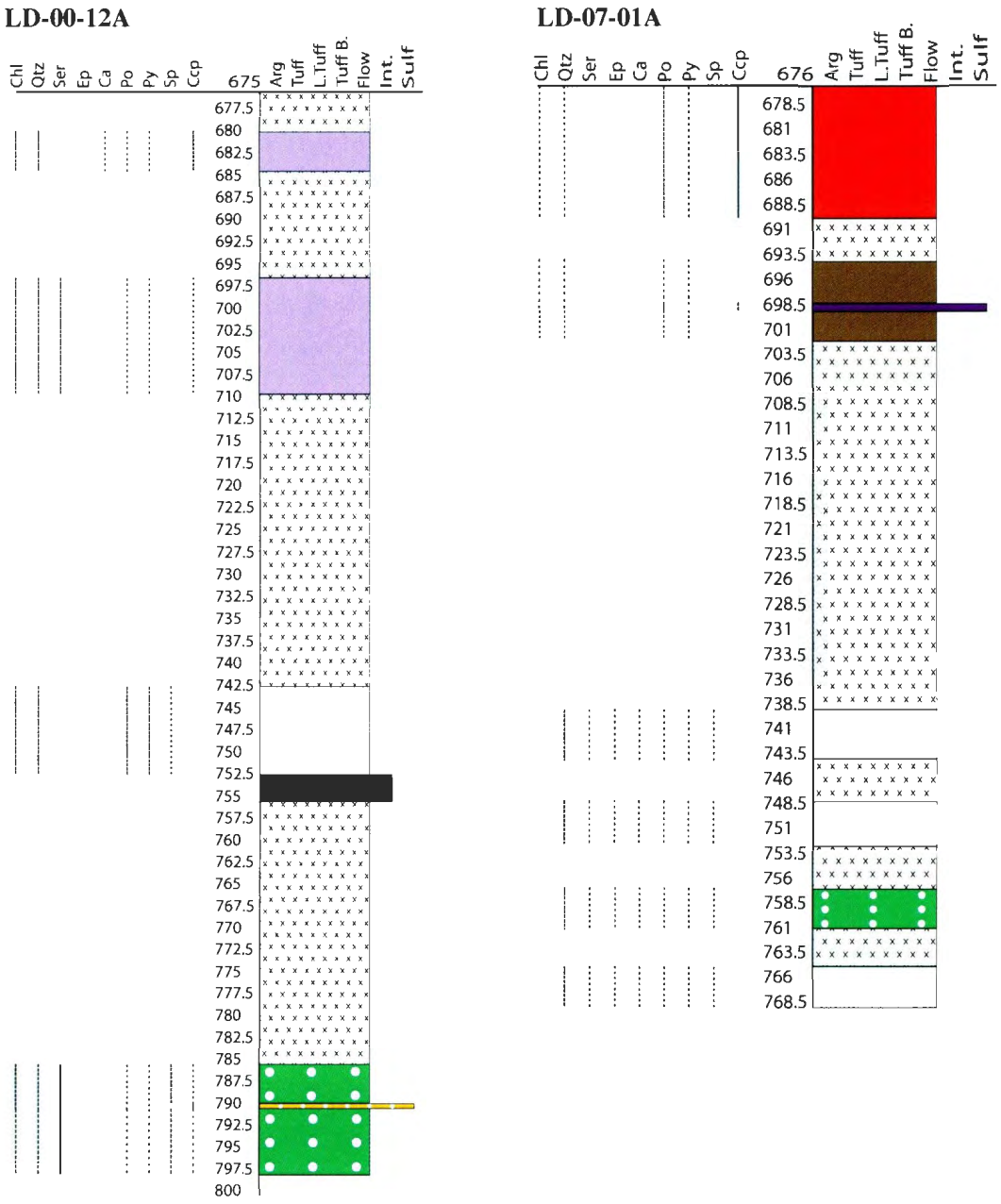

Graphic Logs A.1.2 cont: Digitized graphic logs for Little Deer.

LD-07-06

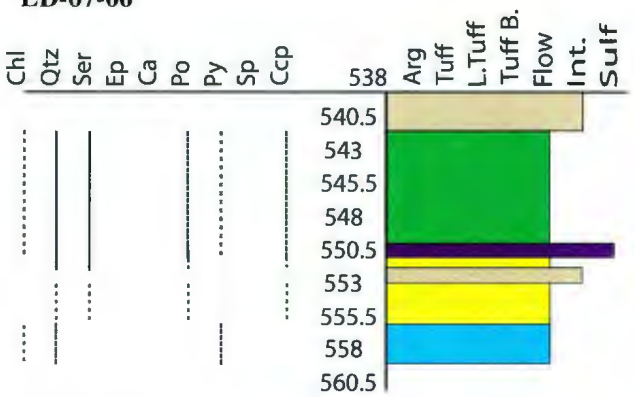

LD-07-07

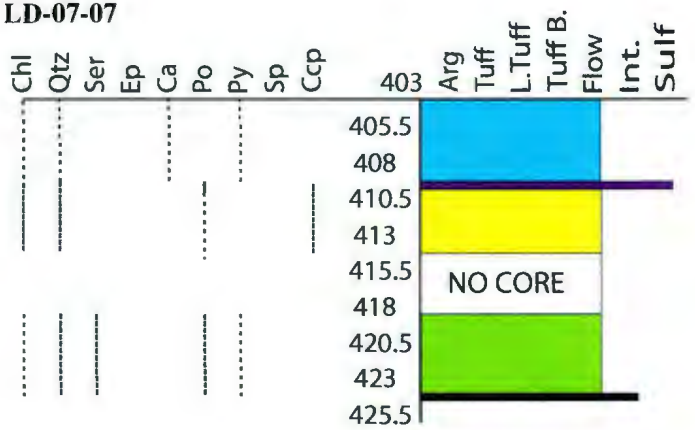

LD-07-08

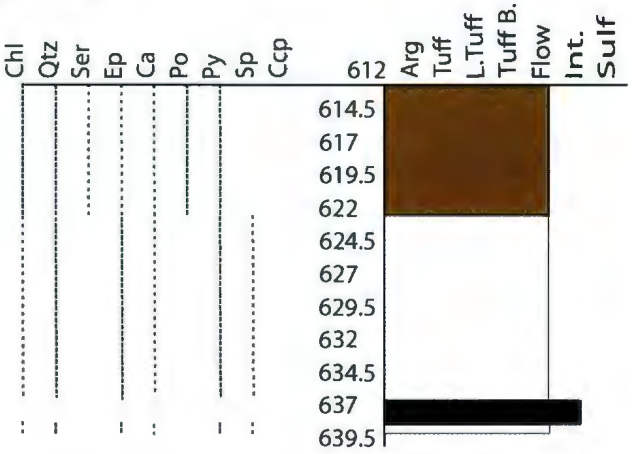

LD-08-10A

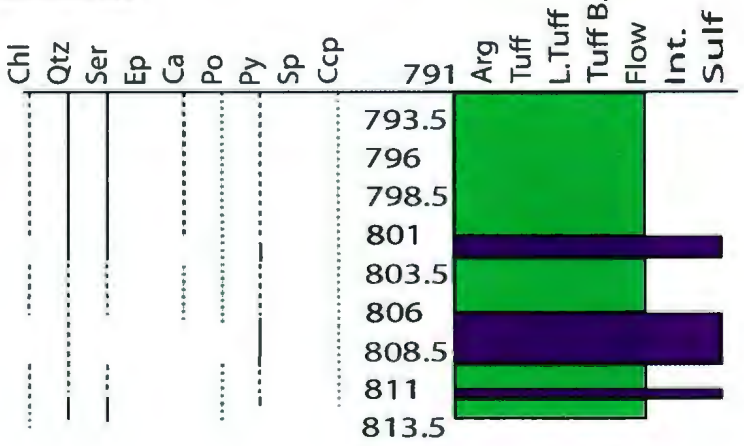

Graphic Logs A.1.2 cont: Digitized graphic logs for Little Deer.

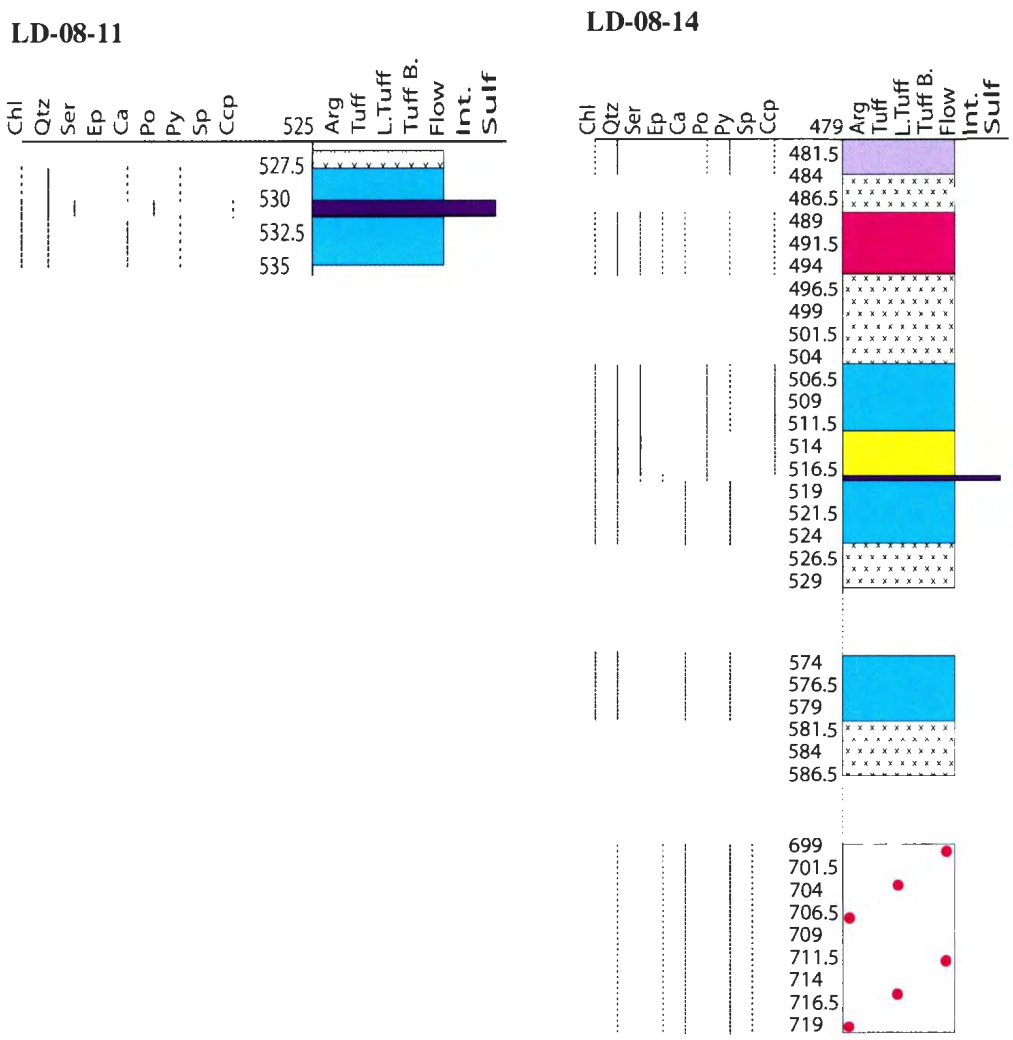

Graphic Logs A.1.2 cont: Digitized graphic logs for Little Deer.

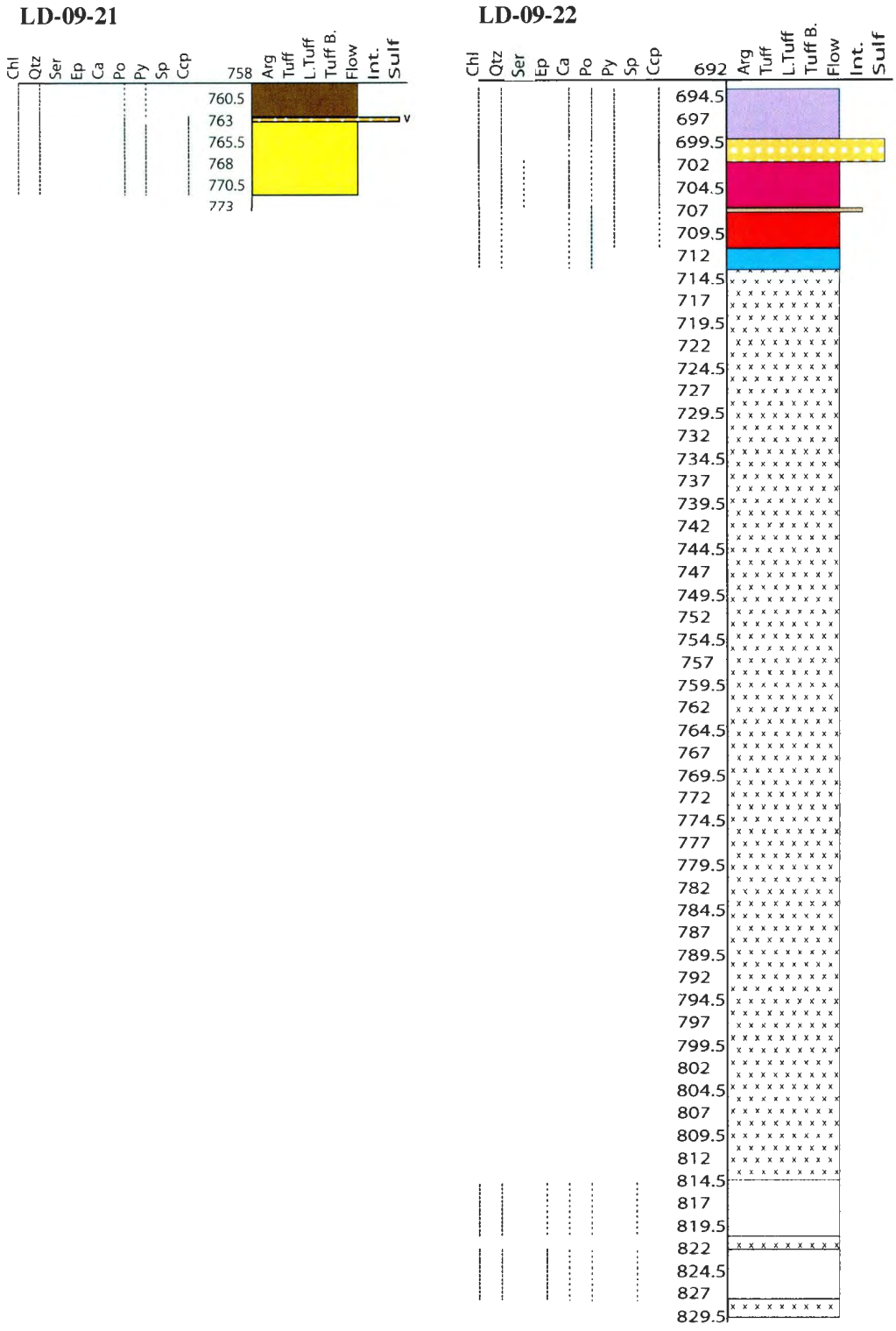

Graphic Logs A.1.2 cont: Digitized graphic logs for Little Deer.

LD-08-15A

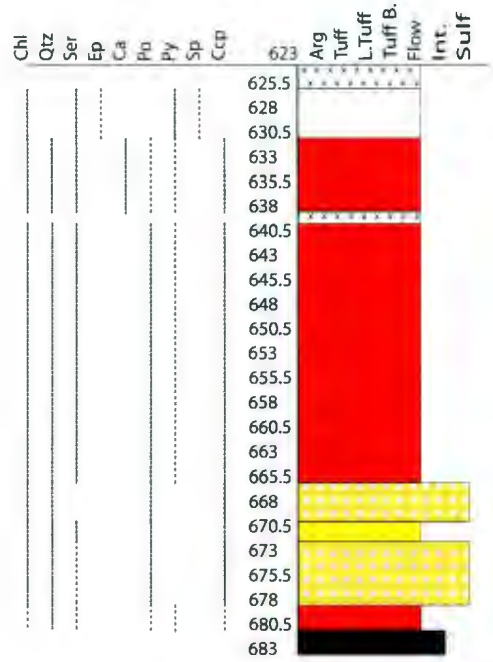

LD-08-16A

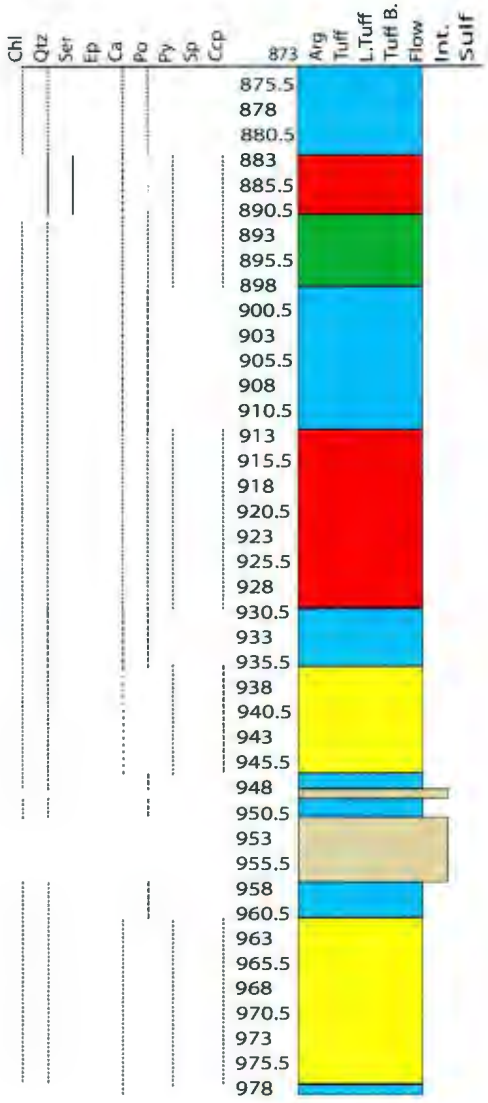

Graphic Logs A.1.2 cont: Digitized graphic logs for Little Deer.

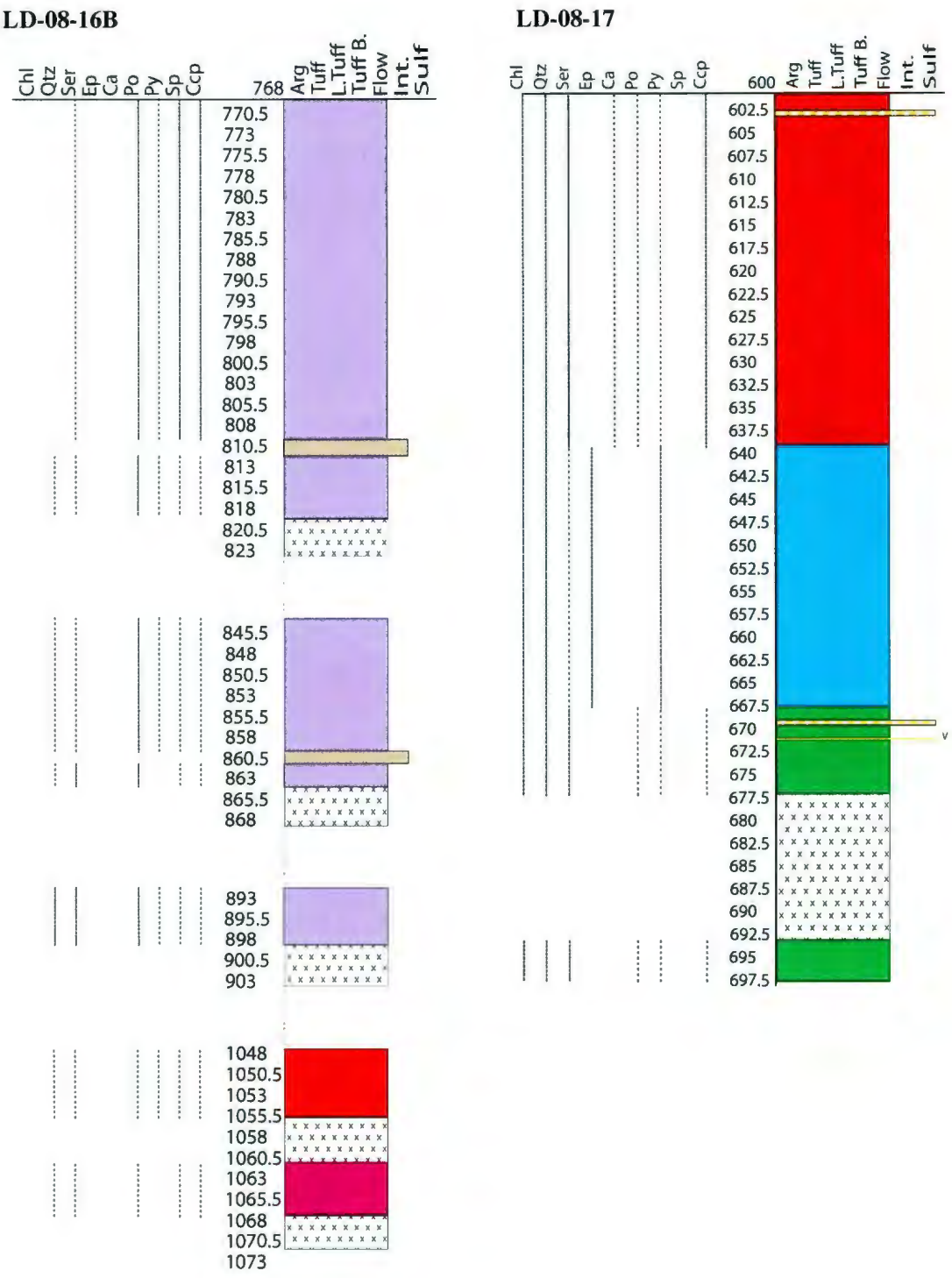

Graphic Logs A.1.2 cont: Digitized graphic logs for Little Deer.

LD-09-24

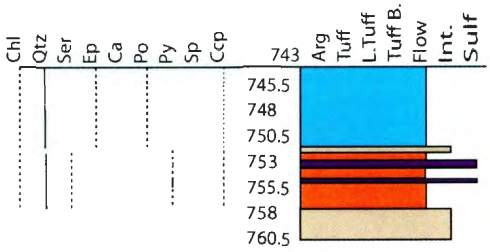

LD-09-25

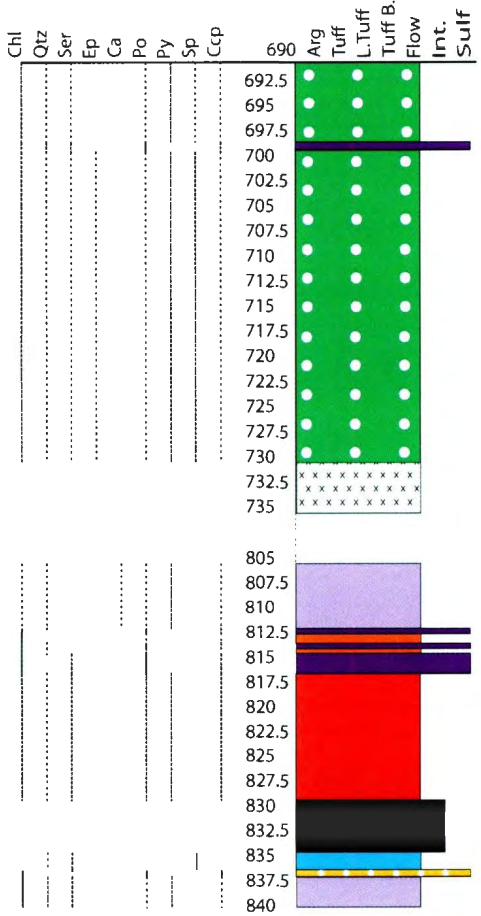

Graphic Logs A.1.2 cont: Digitized graphic logs for Little Deer.

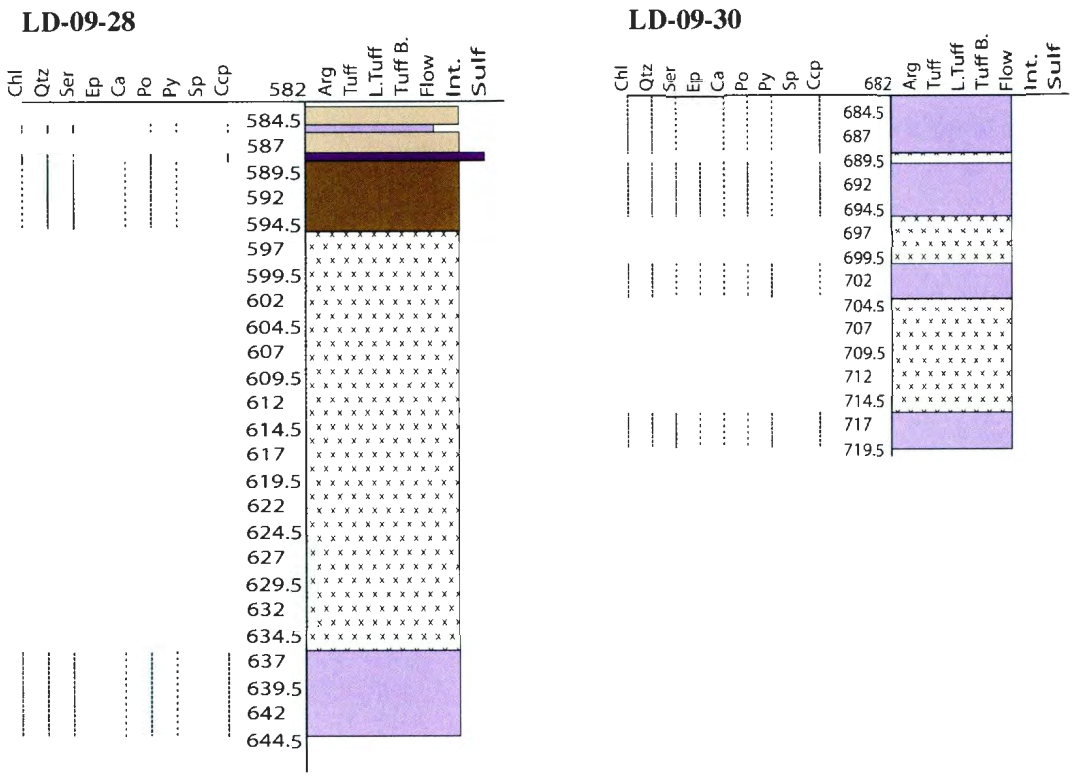

Graphic Logs A.1.2 cont: Digitized graphic logs for Little Deer.

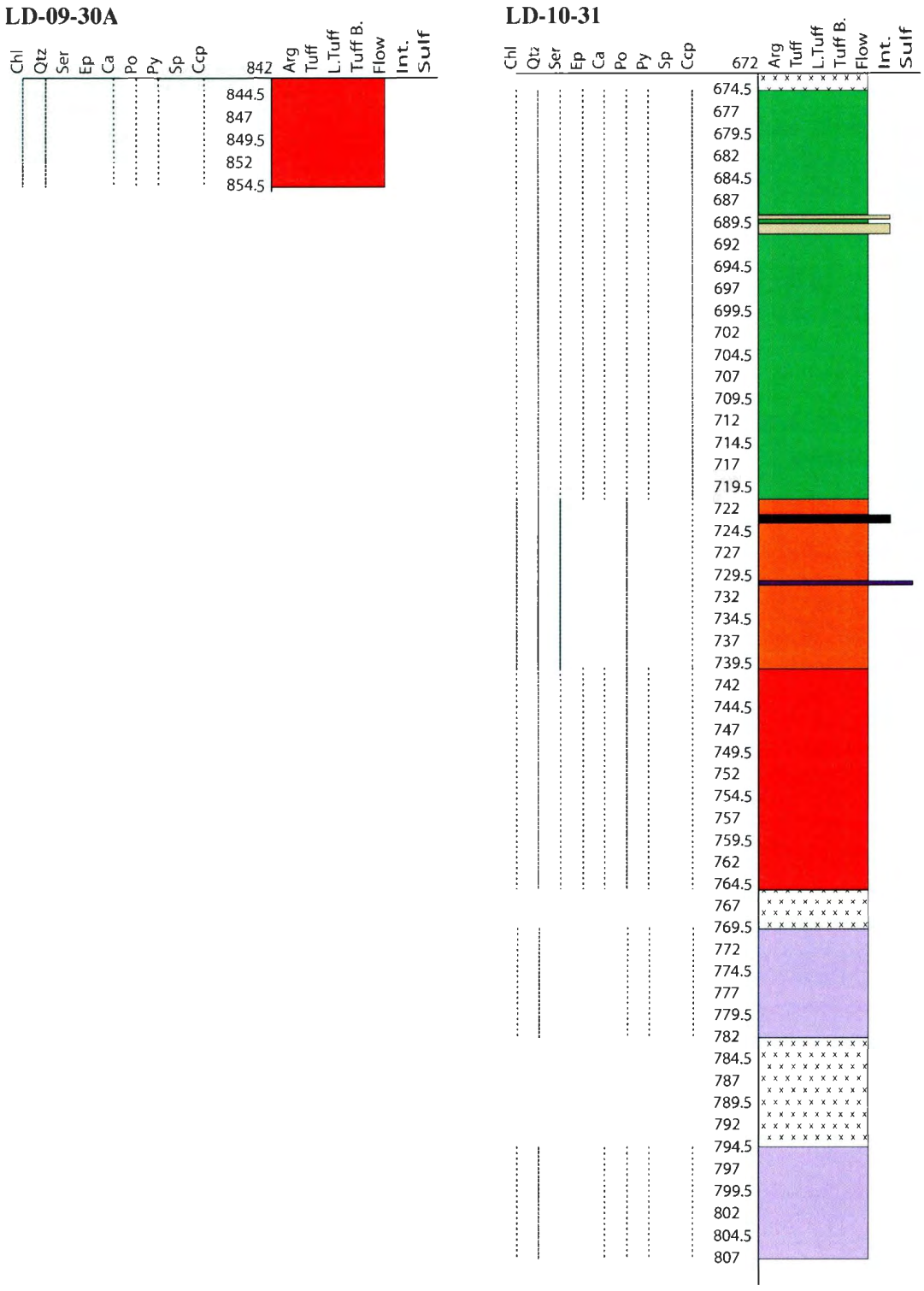

Graphic Logs A.1.2 cont: Digitized graphic logs for Little Deer.

LD-10-32A

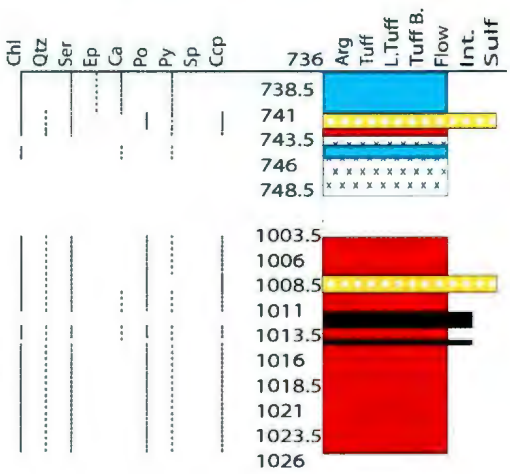

LD-10-35

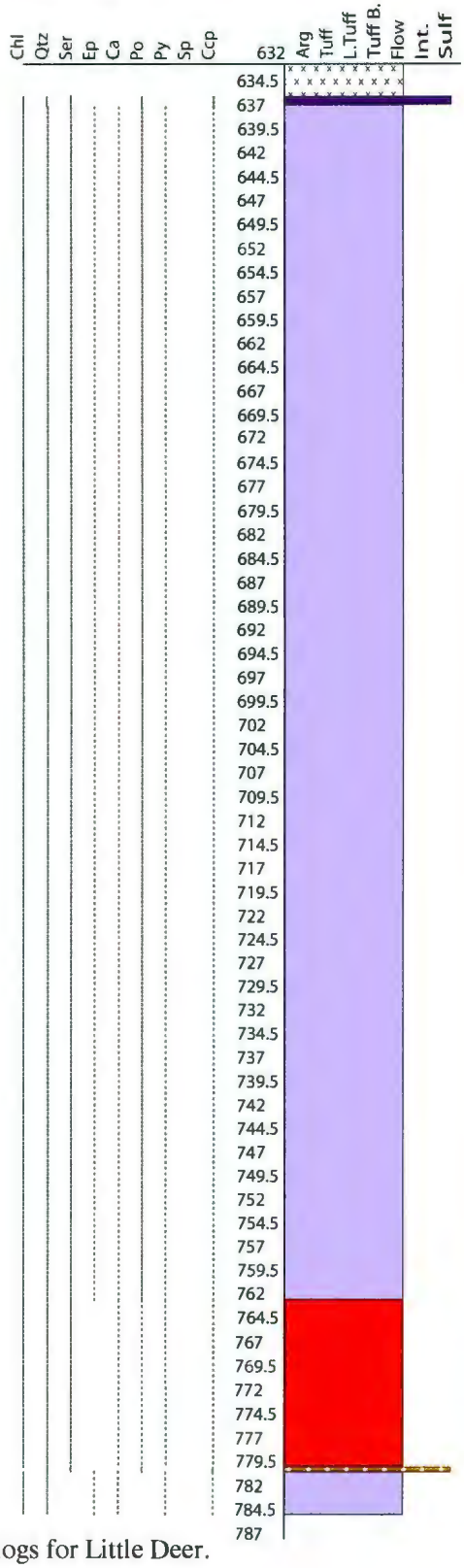

Graphic Logs A.1.2 cont: Digitized graphic logs for Little Deer.

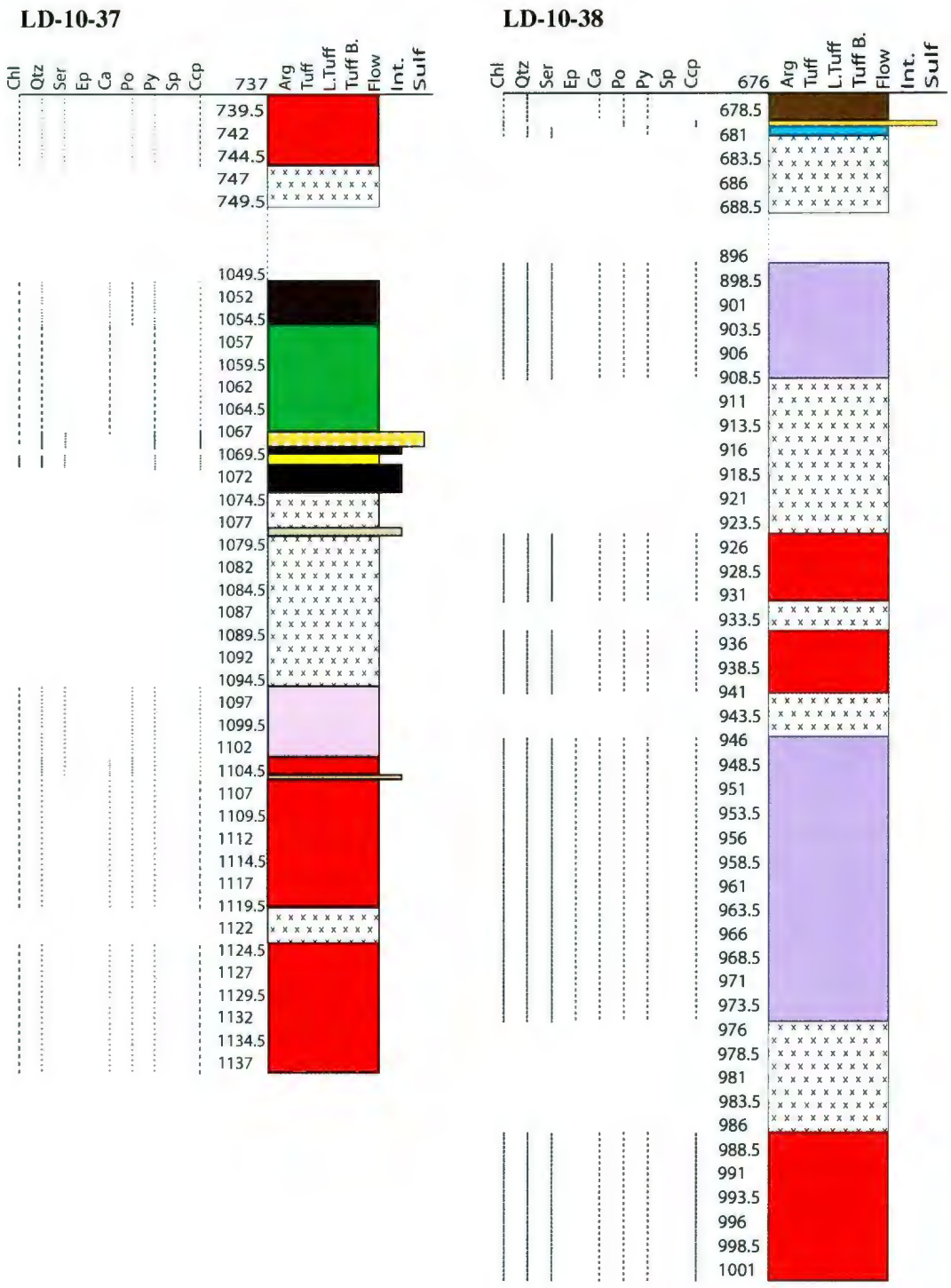

Graphic Logs A.1.2 cont: Digitized graphic logs for Little Deer.

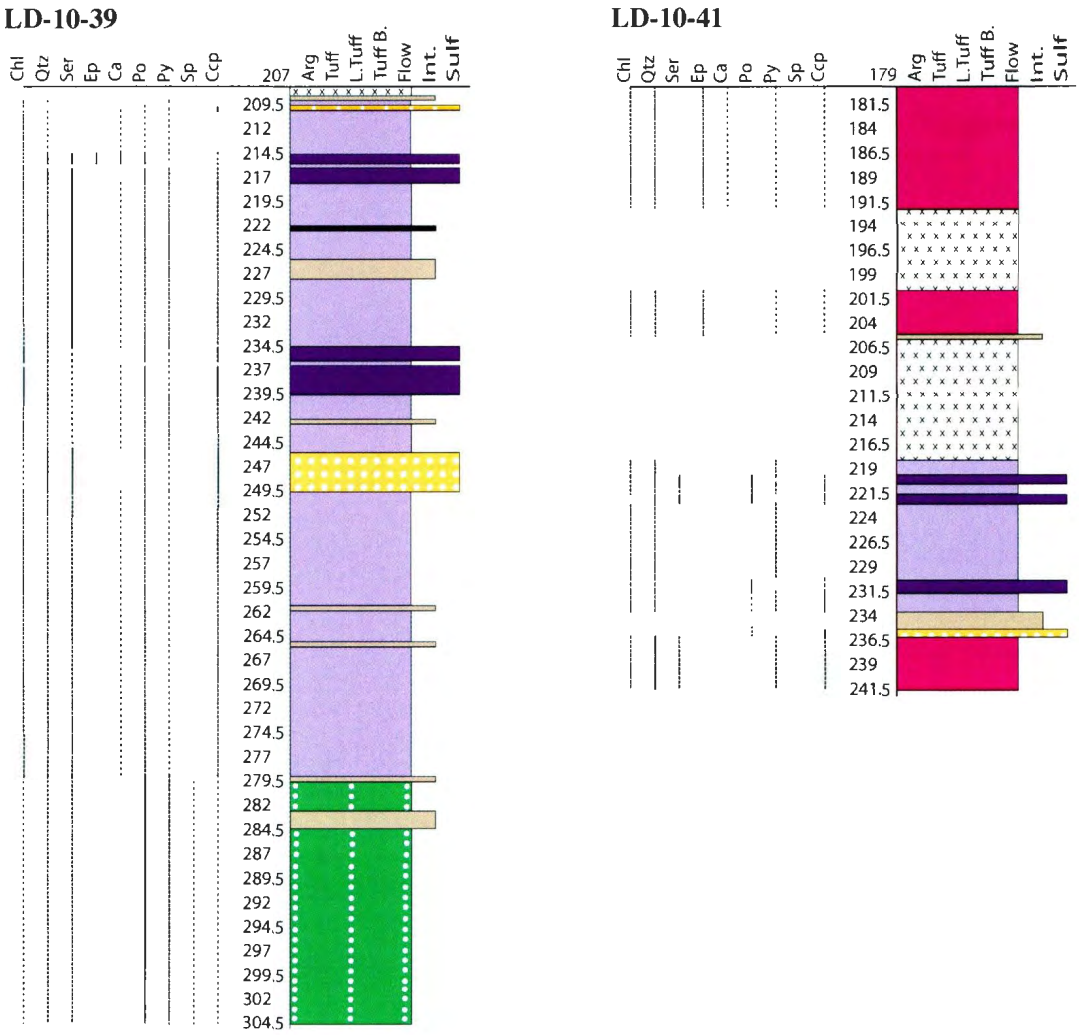

Graphic Logs A.1.2 cont: Digitized graphic logs for Little Deer.

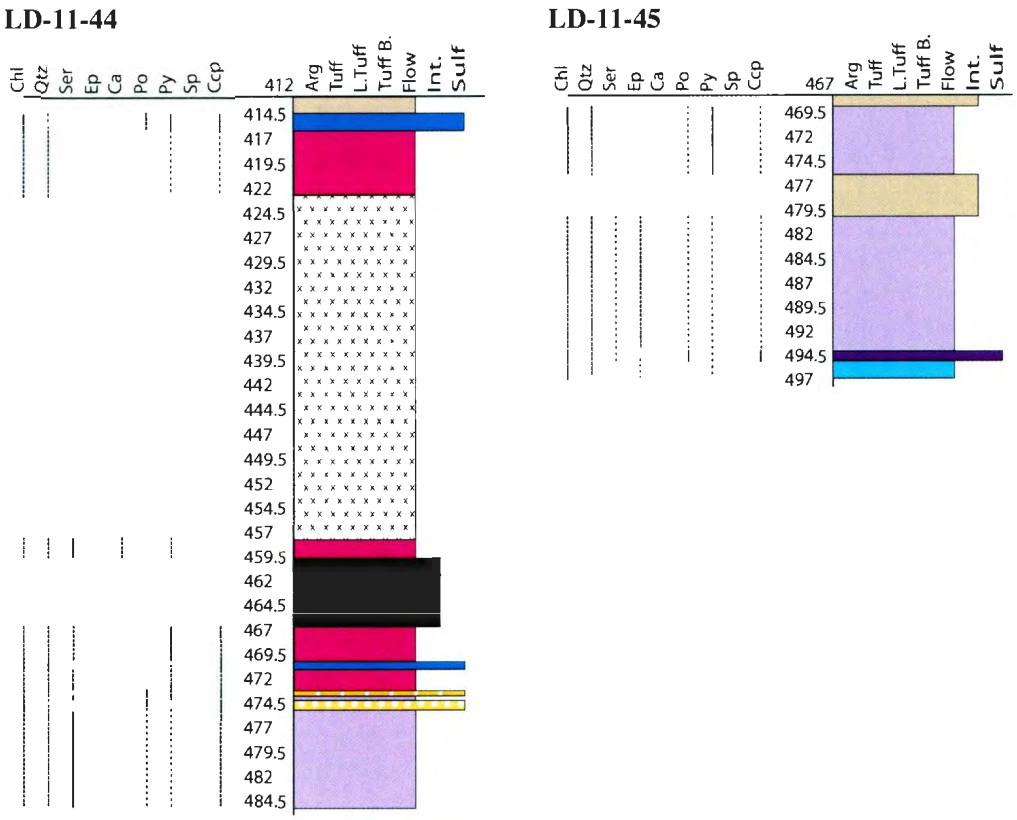

Graphic Logs A.1.2 cont: Digitized graphic logs for Little Deer.

[A.2] Conversion Calculations for Microprobe Results

Electron microprobe analysis (EPMA) results were recorded as atomic percent (at.%) and subsequently converted into weight percent (wt%) and parts per million (ppm). This procedure is detailed below using the element 'Fe' as an example, and highlighted in Table A.1.

- Table A.1: Column (1) lists at. % values for Fe; only values that exceed the minimum detection limit (MDL) are considered for calculation.
- Column (2) displays the atomic weight of the considered element; in this example the atomic weight of Fe (55.84) is used.
- Column (3) values are derived from multiplying columns (1) and (2).
- Column (4) displays the Fe wt% for each analysis. Weight % is calculated by dividing column (3) values by the sum of all column (3) values for each sample, i.e. $X_{Fe} + X_S + X_{Cu} + X_{Zn}$ etc. The result is then multiplied by 100 to obtain wt%.
- Column (5) displays Fe values in ppm. These values are obtained by multiplying column (4) values by 10,000.

Table A.2
The procedure for calculating weight percent (wt. %) and parts per million (ppm) from atomic percents (obtained from microprobe analysis) is highlighted by the data obtained for chalcopyrite-dominated stringer samples.

Sample	(1) Fe Atomic Percents (At. %)	(2) Atomic weight	(3) $X_{(Fe)}$	(4) Fe wt%	(5) Fe ppm
150	46.54	55.84	2599	60.15	601460
152	46.59	55.84	2602	60.19	601874
154	46.74	55.84	2610	60.36	603635
156	46.47	55.84	2595	60.08	600772
158	46.40	55.84	2591	59.99	599865
160	46.52	55.84	2598	60.13	601293

[A.3] Mineral Formula Calculations for Microprobe Results

The procedure for calculating the mineral formula for each microprobe analysis on chalcopyrite, pyrrhotite, pyrite, sphalerite and cobaltite is described below and highlighted using Table A.2. The example below shows the mineral formula calculation of a chalcopyrite from a chalcopyrite-dominated stringer facies but is applicable, and can be modified, for other sulfide phases. Only elemental values that exceed the MDL are considered when calculating mineral formulae.

- Table A.2: Column (1) lists the weight percentages of each element above the MDL. Weight percentages are calculated from the original atomic percent value obtained from the microprobe (Section A.2; Table A.1).
- Column (2) lists the elemental molecular weight for each element above the MDL.
- Column (3) lists the molecular proportions of each analysis. This value is derived by dividing column (1) by column (2).
- Column (4) is the total sum of all the molecular proportions for each analysis.
- Column (5) lists the mineral formula (before recasting) for Cu, Fe and S. These values are calculated by dividing column (1) by column (4) and multiplying by the number of atoms in the sulfide formula (i.e., for chalcopyrite ($CuFeS_2$) = 4 atoms).
- Column (6) is calculated by dividing the number of sulphur atoms in the ideal chalcopyrite sulfide formula (i.e., two sulfur for $CuFe\mathbf{S_2}$) by the sulphur values listed in column (5). This is done for each sample

and ensures that the final chalcopyrite mineral formulae (column 7) will end with a fixed number of sulphur atoms (i.e., 2).

- Column (7) lists the final mineral formula for each chalcopyrite sample analysed. These values were derived by multiplying $MF_{(Cu)}$ and $MF_{(Fe)}$ values in column (5) by the corresponding (re-cast) sulfur value in column (6). As an example, for sample #155 the final chalcopyrite mineral formula is: $Cu_{0.99}Fe_{0.98}S_{2.00}$.

The above procedure is done for each sulfide phase analysed making it possible to determine whether mineral formulae are stoichiometric or non-stoichiometric. Mineral formula results for each sulfide (chalcopyrite, pyrrhotite, pyrite, sphalerite and cobaltite) are presented in Tables 2.5 – 2.9.

Table A.3

The procedure for calculating the chemical mineral formula for sulfide minerals from microprobe analyses. The example shown is for chalcopyrite from chalcopyrite-dominated stringer samples. Abbreviations: wt%: weight percent; EMW: Elemental Molecular Weight; MP: Molecular Proportions; $MP_{(total)}$: Molecular Proportions Total and MF: Mineral Formula

	(1)	(2)	(3)	(1)	(2)	(3)	(1)	(2)	(3)	(4)		(5)		(6)	(7)	
Sample	**Fe wt%**	**EMW**	**MP**	**S wt%**	**EMW**	**MP**	**Cu wt%**	**EMW**	**MP**	**$MP_{(total)}$**	**$MF_{(Cu)}$**	**$MF_{(Fe)}$**	**$MF_{(S)}$**	**Recast for 2 S atoms**	**Recast Cu**	**Recast Fe**
151	30.03	55.84	0.54	35.17	32.06	1.10	34.43	63.55	0.54	2.18	0.99	0.99	2.01	0.99	0.99	0.98
153	29.94	55.84	0.54	35.27	32.06	1.10	34.47	63.55	0.54	2.18	0.99	0.98	2.02	0.99	0.99	0.97
155	29.91	55.84	0.54	35.26	32.06	1.10	34.40	63.55	0.54	2.18	0.99	0.98	2.02	0.99	0.98	0.97
157	29.89	55.84	0.54	35.27	32.06	1.10	34.54	63.55	0.54	2.18	1.00	0.98	2.02	0.99	0.99	0.97
159	30.16	55.84	0.54	35.10	32.06	1.09	34.36	63.55	0.54	2.18	0.99	0.99	2.01	1.00	0.99	0.99
161	29.98	55.84	0.54	35.07	32.06	1.09	34.50	63.55	0.54	2.18	1.00	0.99	2.01	1.00	0.99	0.98

[A.4] SIMS Analytical Methods

This section is from Layne (2012) unpublished.

[A.4.1] Sample Preparation

Small slabs of sulfide-bearing rock were embedded in epoxy in 1 inch diameter aluminum retaining rings and prepared as simple flat polished mounts. After lapidary preparation, all samples were sputter coated with 300 Å of Au, to mitigate charging under primary ion bombardment.

[A.4.2] Instrumentation

All analyses were performed using the Cameca IMS 4f Secondary Ion Mass Spectrometer at the MAF-IIC Microanalysis Facility of Memorial University. This instrument has been updated with additional source lensing in the primary column, enhancing the ability to deliver finely focused beams of Cs^+ for analyses that require both high precision and high spatial resolution. It has also been equipped with modernized ion detection systems that augment performance for stable isotope determinations.

[A.4.3] Analytical Parameters

$\delta^{34}S$ determinations were performed by bombarding the sample with a primary ion microbeam of 600–850 pA of Cs^+, accelerated through a 10 keV potential, and focused into a 5–15 μm diameter spot. To exclude exotic material in the polished surface from analysis, each spot was first pre-sputtered for 180 s with a 25 μm square raster applied to the beam. Depending on the minimum diameter of the critically focused primary beam during each session, a smaller square raster (5μm to 15μm) was applied to the beam during analysis, to improve the homogeneity of primary ion delivery, while maintaining lateral resolution at better than 20μm.

Negatively charged sputtered secondary ions were accelerated into the mass spectrometer of the instrument through a potential of 4.5 keV.

The instrument was operated with a medium Contrast Aperture (150 μm), and Entrance and Exit Slits paired to give flat topped peaks at a mass resolving power (MRP) of 2975 (10% peak height definition) - sufficient to discriminate $^{33}SH^-$ (and $^{32}SH_2^-$) from $^{34}S^-$. In addition, a sample offset voltage of -60eV and Energy Window of 40eV width were deployed to purposely reduce transmission, enabling a higher primary beam current (and concomitantly faster sputter rate). This permitted faster pre-sputtering of the sample and better exclusion of exotic surface material, while maintaining count rates on $^{32}S^-$ below 900,000 cps.

Since absolute transmission is not an issue for these determinations, the simple 150 μm Transfer Lens mode was used, along with a large Field Aperture (1800 μm), giving an approximately 125 μm field of view in the mass spectrometer, and enabling easy monitoring of spot and sample centering.

Signals for $^{32}S^-$, $^{34}S^-$ and a background position at 31.67 Da were obtained by cyclical magnetic peak switching. Standard counting times and peak sequence used were; 0.5 s at the background position, 2.0 s on $^{32}S^-$, and 6.0 s on $^{34}S^-$. Waiting times of 0.25 s were inserted before each peak counting position to allow for magnet settling. A typical analysis consisted of accumulating 80 of these peak cycles, which takes less than 15 min (including pre-sputtering time).

All peak signals were collected with an ETP 133H multiple-dynode electron multiplier (em) and processed through ECL-based pulse-counting electronics with an overall dead time of 12 ns. Background measurements at the nominal mass 31.67 Da were taken during each magnetic switching cycle – and were routinely less than 0.05–

0.1 counts per second. Count rates on $^{32}S^-$ were maintained between 500,000 and 900,000 counts per second by adjusting the primary beam current appropriately for each sulfide phase of interest.

Any change in overall peak intensities with time - which was typically monotonic (and quantitatively minor in its effect on measured $^{34}S/^{32}S$) in a homogeneous sulfide mineral phase - was compensated for using a standard double interpolation ratio algorithm (an approach adopted from TIMS analysis), with each $^{34}S^-$ peak ratioed to the time-corrected interpolation of adjacent $^{32}S^-$ peaks.

Beyond the excellent spatial resolution, a further advantage of SIMS stems from the gradual nature of material removal by sputtering, with each counting interval producing depth-resolved data on the sample. Inclusions of other sulfide phases, in particular, have the potential to produce excursions in the measured $\delta^{34}S$. However, the depth-resolved characteristic of SIMS allows the detection of inclusions, or other heterogeneities within a mineral, simply by monitoring sharp excursions in $I^{32}S^-$ with time. These signal time intervals can then easily be eliminated from the measured data.

[A.4.4] Calibration of Instrumental Fractionation

The production and detection of sputtered secondary ions produces a bias between the actual $^{34}S/^{32}S$ of the sample and that measured by the mass spectrometer – termed Instrumental Mass Fractionation (IMF). IMF in SIMS can generally be considered as a combination of mass discrimination effects at the site of sample sputtering with those in the ion detectors themselves. Other effects, related to the ion optics of the mass spectrometer, are reduced to comparatively insignificant levels in a properly and consistently aligned instrument.

The magnitude of IMF varies substantially between sulfide minerals. For this reason, the $^{34}S/^{32}S$ measured in samples of pyrite, pyrrhotite and chalcopyrite from Little Deer were corrected for IMF by comparison to replicate in run measurements of reference materials UL9B (pyrite; $\delta^{34}S$: 15.8‰), PoW1 (pyrrhotite; $\delta^{34}S$: 2.3‰) and Norilsk (chalcopyrite; $\delta^{34}S$: 8.3‰), respectively.

[A.4.5] Accuracy and Reproducibility

Analyses accumulated in 12 min routinely yield internal precisions on individual $\delta^{34}S$ determinations of better than ±0.2 ‰ (1σ), while producing sputter craters only a few μm deep. These precisions closely approach the optimum possible precision as calculated from Poisson counting statistics.

Overall reproducibility, based on replicate standard analyses, is typically better than ±0.5 ‰ (1σ).